論文 / 著書情報
Article / Book Information

題目(和文)	
Title(English)	Seismic Retrofit for Pile-supported Bridge Abutment Subjected to Liquefaction-induced Lateral Spreading
著者(和文)	SahaPartha
Author(English)	Partha Saha
出典(和文)	学位:博士(学術), 学位授与機関:東京工業大学, 報告番号:甲第11661号, 授与年月日:2020年9月25日, 学位の種別:課程博士, 審査員:髙橋 章浩,北詰 昌樹,竹村 次朗,笠間 清伸,田村 修次
Citation(English)	Degree:Doctor (Academic), Conferring organization: Tokyo Institute of Technology, Report number:甲第11661号, Conferred date:2020/9/25, Degree Type:Course doctor, Examiner:,,,,
学位種別(和文)	博士論文
Type(English)	Doctoral Thesis

Seismic Retrofit for Pile-supported Bridge Abutment Subjected to Liquefaction-induced Lateral Spreading

Saha Partha

DISSERTATION

Submitted in partial fulfillment of the requirements for the degree of

DOCTOR OF PHILOSOPHY

at

TOKYO INSTITUTE OF TECHNOLOGY

2020

Abstract

Liquefaction-induced lateral spreading has caused massive damage to the embankments and the water-front structures, i.e., the bridge abutments in the previous earthquakes. The lateral spreading of the foundation soil is typically responsible for the damage of the embankments and the structures near the water body. This study aims to propose a suitable seismic retrofitting technique for the existing bridge abutment designed according to the old Japanese standard for highway bridges without considering the effects of bridge girder. The ground improvement and ground reinforcement are two commonly used techniques to mitigate liquefaction-induced lateral spreading. In spite of having higher efficiency to mitigate liquefaction, the ground improvement techniques are not feasible for the existing structures. The installation of sheet pile is considered in this study as a potential remedial measure against lateral spreading because of its handiness to implement in the existing structures. The use of sheet pile against lateral spreading is not a unique technology. It has been being used for a long time. However, this study mainly focuses on: a) the ground geometry where the sheet pile can be effectively used, b) the effect of sheet pile width to mitigate the damage of the targeted area, c) the additional reinforcement to improve the performance of sheet pile and d) the efficiency of this sheet pile reinforcement technique to prevent the damages of the abutment due to lateral spreading.

In the beginning, several large-scale shake table tests conducted by public works research institute, Japan are numerically simulated using three-dimensional and two-dimensional finite element analysis. The shake table tests are conducted to study the seismic response of the piled abutment subjected to liquefaction-induced lateral spreading. The piled abutments are designed according to the current and old Japanese design standards for highway bridges. The performance of the fixed-end sheet pile as a seismic retrofit for piled abutment resting in the 10 m thick liquefiable layer is also investigated. The experimental and numerical results reveal that the pile heads are more vulnerable to damage during lateral spreading as it experiences the maximum bending moment. It is also found that installation of a fixed-end sheet pile can reduce the bending moment demand of the existing piles to some extent, although the reduction is not so significant.

The applicability of sheet pile to mitigate lateral spreading of a liquefiable foundation under an embankment is investigated. A series of dynamic centrifuge experiments are used to find out the geometry, i.e., the thickness of the liquefiable layer where the sheet pile can be effectively used. The effect of sheet pile width to reduce the seismic damage of a target area is also investigated.

Several finite element analyses are carried out to determine the favorable embedment depth of sheet pile into the bearing stratum. Finite element analysis is also used to investigate the performance of an anchored sheet pile to mitigate lateral spreading. The experimental results, as well as numerical results, confirm that the sheet pile having sufficient embedment depth can considerably reduce the lateral spreading of the liquefiable foundation. Besides, the experimental results conclude that the extension of the sheet pile width beyond the width of the target area does not provide any additional advantage. Moreover, it is found that the anchorage near the head of the sheet pile significantly increases its efficiency to mitigate lateral spreading.

The efficiency of the sheet pile to mitigate lateral spreading of the foundation soil under an embankment encourages its use as a seismic retrofit for a piled abutment. Two dynamic centrifuge experiments and several two-dimensional finite element analyses are carried out to study the performance of the sheet pile to reduce the damage of piled abutment subjected to lateral spreading. The experimental results show that the old piled abutment, where the piles are mostly slender, has a minor pinning effect to the lateral spreading. The pile head and the interface of the liquefiable and non-liquefiable layer are found vulnerable to be damaged during an earthquake as those locations experience large bending moment. The sheet pile installation reduces the channel ward movement of the abutment up to 40% thus reduces the bending moment of the abutment piles. Besides, the performance of the sheet pile can be improved with the installation of anchorage according to the numerical results. The anchored sheet pile can reduce the horizontal displacement of the abutment up to 50% and the bending moment of the pile head up to 47%. The contribution of the inertia force of the abutment to the bending moment of the pile head is also carefully investigated using finite element analysis. The numerical results show that the contribution of the inertia force of the abutment is about 30% of the total bending moment near the pile head under the described analysis conditions. The effect of the bridge girder significantly affects the seismic response of the abutment. Finite element analysis is used to investigate the effect of the bridge girder. The existence of the bridge girder has a positive effect on reducing the bending moment of piles. The bridge girder reduces the bending moment (nearly 57%) of the pile by sharing a considerable amount of lateral load from the backfill soil. However, the collision between the abutment and the girder may cause damage to the abutment or the unseating of the bridge girder.

Acknowledgements

I would like to express my sincere thanks and gratitude to a number of individuals without whom this study would not have been completed. First and foremost, my honorable supervisor Prof. Akihiro Takahashi. His adroit guidance kept me on the right track throughout this journey. I have always received the best suggestions from him not only in my academic research but also in my personal life. He was more than a supervisor to me.

I am grateful to the committee members, Prof. Masaki Kitazume, Asso. Prof. Jiro Takemura, Asso. Prof. Kiyonobu Kasama and Asso. Prof. Shuji Tamura, for their valuable comments and suggestions to enrich my dissertation.

I do not want to miss the opportunity to say thanks to Mr Sakae Seki. He is the person without whom the experiments would not have been completed successfully. His valuable suggestions helped me a lot to design the experimental models. I am also grateful to Dr Kazuki Horikoshi for his continuous support during this period.

I am thankful to all my lab mates and friends, especially Jenisha, Wang, Vijay, Gobi, Ritesh and Max. We had a lot of wonderful memories. I am fortunate to have such a friend like them. They made this difficult PhD journey convenient and enjoyable.

I am indebted to the Ministry of Education, Culture, Sports, Science and Technology (MEXT) for the financial support provided throughout my study in Japan.

Last but not least, I am grateful to my parents and family members. I am here today only because of their inspiration. They were always beside me during all the ups and downs in my life. I acknowledge my wife, Jhuma, who has always inspired me and given me the mental strength to go through this hard time.

[This page intentionally left blank]

Table of contents

[This page intentionally left blank]

List of figures

[This page intentionally left blank]

List of tables

[This page intentionally left blank]

Chapter 1

Introduction

1.1 Liquefaction hazard

Liquefaction, in general, can be defined as the phenomena of saturated cohesionless soil that involves the ground deformation associated with the generation of excess pore water pressure under undrained cyclic loading. When saturated cohesionless soil is subjected to cyclic shearing under undrained condition, the pore water pressure is gradually increased because of the densification tendency of that soil. The excess pore water pressure may lead to significant degradation of soil strength and stiffness that triggers the ground deformation. Liquefaction of saturated cohesionless soil resulting from cyclic shearing is broadly divided into two groups: flow liquefaction and cyclic mobility. A flow liquefaction takes place when the static shear stress required for the static equilibrium of a soil mass is greater than its shear strength. A large deformation may be caused due to the flow liquefaction. In contrast to flow liquefaction, lateral spreading, which is a form of cyclic mobility, develops incrementally during earthquake shaking. The deformations produced by lateral spreading are driven by both cyclic and static shear stress. Moreover, this deformation can occur on very gently sloping ground or on a virtually flat ground adjacent to the water bodies (Kramer, 1996). Lateral spreading on gently sloping ground is generally the most pervasive and damaging type of liquefaction-induced ground failure generated by earthquakes (National Research Council, 1985). Lateral spreading is particularly damaging if non-liquefied layer rides on top of the liquefied soil (Finn & Fujita, 2002).

Severe damage to different infrastructures including buildings, bridges, and transportation facilities have been reported during the past earthquakes due to liquefaction or liquefaction-induced lateral spreading. It caused huge economic losses as well as unlimited casualties of human lives. Many infrastructures supported by deep foundations were damaged due to the loss of bearing capacity and insufficient bending stiffness of piled foundations during the 1964 Niigata and the 1995 Kobe Earthquakes (Pamuk, Gallagher, & Zimmie, 2007). Pile foundations, particularly for ordinary bridges, have often been designed in the past for vertical and lateral static load only. A performance-based design approach was focused on observing the bridge failures during the 1989 Loma Prieta and the 1994 Northridge Earthquakes. A clear demonstration of structural damages of the pile due to liquefaction during the 1964 Alaskan Earthquake (Bartlett &

Youd, 1992) and again more recently during the 1995 Kobe Earthquakes emphasized a design of resilient pile against lateral spreading. Thus, the design and construction of any megastructure like bridges in this kind of problematic soils (liquefiable soils) receive the attention of researchers.

Besides, a large number of earthen embankments and river dykes were damaged in the previous earthquakes in Japan. A total length of 9290 m of river dykes was damaged over 32 sites located along 6 different rivers during the 1995 Kobe Earthquake (Matsuo, 1996). The Tohoku Earthquake in 2011 with a magnitude of 9.0 severely damaged the embankments and related structure at 2115 sites over the Tohoku and Kanto region (Oka, Tsai, Kimoto, & Kato, 2012). Most recently the Kumamoto Earthquake in 2016, around 500 river dykes were reported to be damaged in the Kumamoto prefecture. The magnitude of the earthquake was recorded at 7.0 in JMA seismic intensity (Mukunoki et al., 2016). All the aforementioned statistics reveal the severe damage of the earthen embankments during the previous earthquakes in Japan. Most of the post-earthquake reconnaissance surveys claim that the liquefaction or the liquefaction-induced lateral spreading of the foundation soil is primarily responsible for the extensive failure of the embankments.

1.2 Bridge failure associated with lateral spreading

Two successive mega earthquakes at two different parts of the world, which were March 1964, Alaskan Earthquake with a moment magnitude of 9.2 (Hansen et al., 1966) and June 1964, Niigata Earthquake with a moment magnitude of 7.5 (Amiri, 2008), brought the catastrophe of lateral spreading into the attention to engineers. Extensive damage to bridge structures due to liquefaction-induced lateral spreading has been reported in both of these two cases. During lateral spreading, the intact surficial soils above the liquefiable layer are displaced toward the natural topographical depression. Such displacement pushes the retaining structure like bridge abutments along with its supporting piles riverward and causes extension damage near the banks and compression damage in the center of the channels (Bartlett, 2014). The Tohoku earthquake (M 9.0) in 2011, which is considered as the most powerful earthquake ever recorded in the history of Japan, caused massive damage to the structures and transportation facilities. A large number of bridges have been reported to experience a moderate to extensive deterioration during this earthquake (Kawashima & Buckle, 2013). However, any strong evidence of liquefaction-induced damages of bridge facilities has not been reported for this earthquake.

Some case histories related to the damages of the bridge foundations during previous earthquakes have been presented in the following sections. Through the observation of the previous damage pattern, a baseline of the performance of structural elements can be established. Simultaneously the key factors that instigate the failure of the structural foundations can be roughly identified.

1.2.1 Bridges damaged during the 1964 Alaskan Earthquake

On March 27, 1964, a great earthquake with a moment magnitude of 9.2 was triggered in the Prince William Sound region of Alaska, which is known as Good Friday or Great Alaskan Earthquake. This earthquake is the most powerful earthquake in the history of the United States and the second largest earthquake ever recorded, next to the M 9.5 magnitude earthquake in Chile in 1960. The epicenter of this earthquake was located about 10 km east of the mouth of College Fiord, 90 km west of Valdez and 120 km east of Anchorage. Approximately 4.5 minutes lasted earthquake caused huge damage to the public property with an estimated cost of 311 million USD (1964 value) (Hansen et al., 1966). The affected area by the earthquake and the epicenters of the previous active volcanos and the Aleutian Trench is shown in Fig. 1.1.

Lateral spread resulting from this earthquake caused severe damage to Alaskan Highway and Railroad in southern Alaska mainly due to the differential movement of channel and floodplain deposits. It is estimated that lateral spread caused 80 million USD (1964 value) damage to the 266 bridges and numerous sections of the embankment along Alaska Railroad and Highway (McCulloch & Bonilla, 1970; Kachadoorian, 1968). Lateral spread displacement usually took place along the line with the longitudinal axis of the bridge in the direction perpendicular to the channel. During lateral spreading, the liquefied soils produce a stream ward movement. Sometimes this channel ward movement of the adjacent banks is so severe that it reduces the width of the channel as much as 2 m to 3 m. The channel ward movement of the soil behind the abutment pushes it towards the channel consequently, it produces a tremendous compressive force to the superstructure. For railroad bridges, compressive forces exerted by the abutment caused arching, buckling and jackknifing of the superstructure thus led a partial or complete collapse of the bridges. The most damaged structures were the simply supported bridges with concrete decks because of the differential displacement between the supporting piers (Bartlett, 2014). Simultaneously, the horizontal movement was also accompanied by liquefaction-induced settlement in the abutment area and by a swelling up of liquefied sediments within the center of the channels (McCulloch & Bonilla, 1970). A typical generalized form of soil movement is shown in Fig. 1.2.

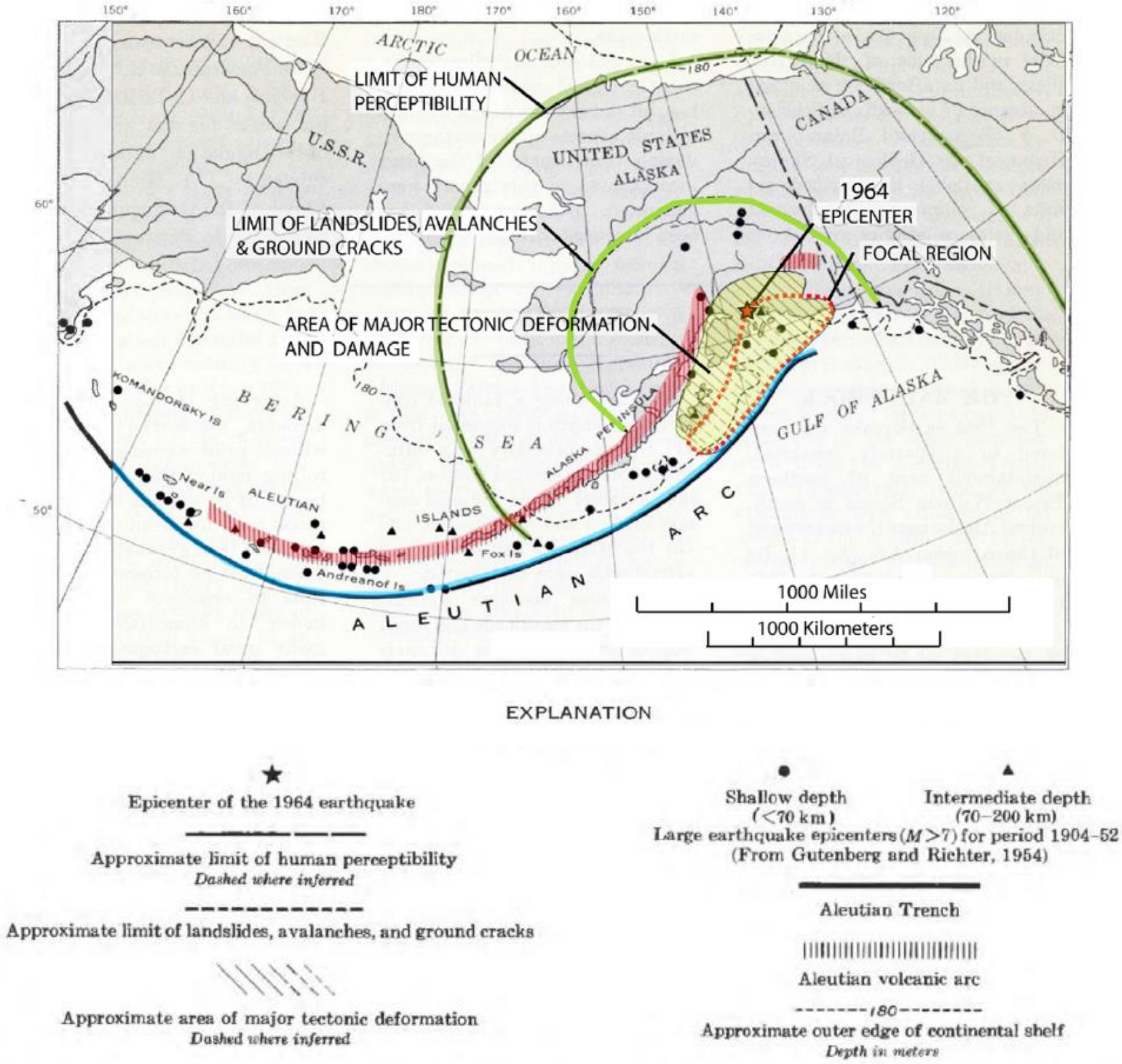

Fig. 1.1: Maps of Alaska and adjacent areas indicating the location of the 1964 earthquake, the area affected by the earthquake, epicenters of the previous earthquakes, active volcanism and the Aleutian Trench (National Research Council (US). Committee on the Alaska Earthquake, 1972).

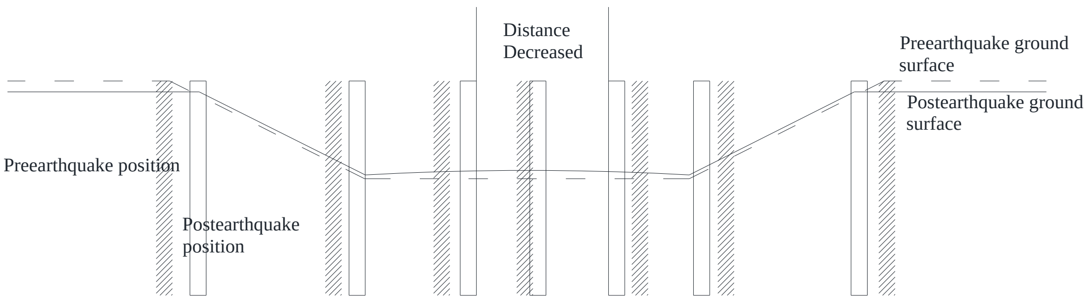

Fig. 1.2: Generalized diagram of typical displacement due to lateral spreading (after McCulloch and Bonilla, 1970).

The abutment of a steel deck girder highway bridge was severely damaged due to the channel-ward movement of the river bank, as shown in Fig. 1.3. The steel deck was strong enough to resist the compressive forces imposed due to the channel ward movement of the abutment. Consequently, the abutment was broken down from its lower part.

Fig. 1.3: Damage of abutment due to lateral spreading (USGS).

A 203 m long steel girder bridge located at milepost 147.5 on the secondary channel of Matanuska River also underwent severe lateral spreading. The bridge was supported on concrete piers. Like other bridges in this area, the abutment and piers of this bridge were displaced about 0.3 m towards the channel. McCulloch and Bonilla (1970) reported the following damages of this bridge. "*Piers and abutments were jammed stream ward against the central spans. Piers and abutments were also displaced horizontally; the north abutment and pier shifted about 1 foot west (downstream) and the third pier (from the north) moved about 1 foot south toward the channel.*"

At that period, the Alaska Department of Highways was constructing four new highway bridges on Snow River to replace the existing old bridges made of asphalted timber plank deck supported by the concrete abutment and timber piles. All the existing bridges were severely damaged due to the lateral ground displacement and differential vertical settlement. The bridge decks were buckled due to a tremendous compressive load. Sometimes the decks were separated from the pile caps. However, the lateral movement of the newly constructed bridge piers drew the attention, as shown in Fig. 1.4. One of the four free-standing piers was moved approximately 2.4 m apart from its original position towards the nearby Kenai Lake due to lateral spreading. Each of these four piers was supported by 21 concrete-filled steel tube piles extending up to the depth of about 90 feet (27.0 m) below the stream bed level. The pier was subjected to a tilt of approximately 15 deg.

The longitudinal slope of Snow River was 0.15% (Bartlett & Youd, 1992) suggesting that a relatively large ground displacement along a comparatively gentle slope. This kind of translational movement might take place because of the liquefaction at the bottom of the piles or the development of plastic hinge at some depth below the ground surface.

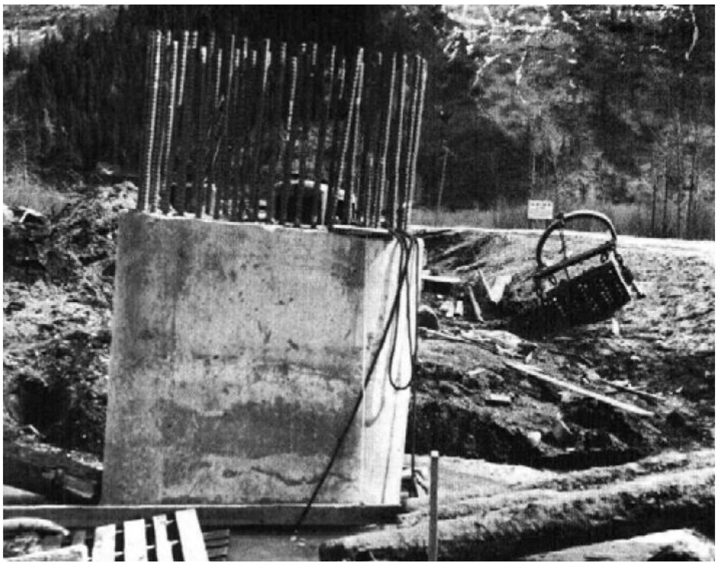

Fig. 1.4: Displacement of highway bridge pier supported on deeply driven steel piles at Snow River (McCulloch and Bonilla, 1970).

1.2.2 Lateral spreading during the 1964 Niigata Earthquake

Niigata Earthquake was one of the two destructive earthquakes in 1964 having a magnitude of 7.5 in the moment magnitude scale. The epicenter was located 50 km south of Niigata city. The earthquake caused extensive damages to Niigata city in spite of the epicenter being located quite far from it. The damages include the destruction of buildings, bridges, and other transportation facilities. Approximately 3534 buildings were reported to be destroyed and another 11000 houses were damaged.

Investigation on the damages during the 1964 Niigata Earthquake reveals the adverse influence of poor sub-soils. In fact, the damages were more due to the perturbation of the soil than the direct effect of ground shaking itself (Hamada, Yasuda, Isoyama, & Emoto, 1986). The lower part of the town was built on top of a thick layer of recent sedimentation. This kind of recently formed layers is very much susceptible to liquefaction and consequently several modern multistoried buildings at that time collapsed because of the loss of support from the sub-soil. During the earthquake, a

10 m thick layer of soil was liquefied and moved towards the Shinano River and caused a complete collapse of several bridges.

The collapse of Showa Bridge was one of the worst incidents during the 1964 Niigata Earthquake. Five simply supported spans of about 28 m long in between the piers P-2 and P-7 fell into the river, as shown in Fig. 1.5. There was an obvious collision between the girders themselves and between the girders and the abutment on the left bank. The bridge pier foundations on the left bank moved towards the river channel (Amiri, 2008).

Fig. 1.5: Collapse of Showa Bridge during the 1964 Niigata Earthquake.

A significant rotation took place at the interface between the liquefied layer and the base soil (at a depth of about 16 m) along the pile underneath the pier P-4, as shown in Fig. 1.6. It is also evident that the bridge didn't collapse due to the inertia loading since the bridge collapsed after the earthquake event. Therefore, it is obvious that the failure mechanism was primarily instigated by the channel-ward movement of piers and subsequent rotation of the piles. Although some other researchers explained the buckling of piles as the leading cause of failure of the bridge (Bhattacharya, Madabhushi, & Bolton, 2004). It is to be noted that buckling of a slender pile may take place because of loosening the lateral confinement during liquefaction.

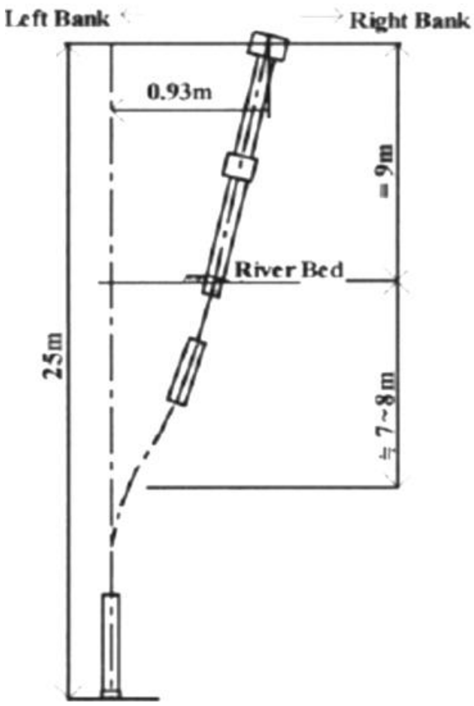

Fig. 1.6: Deflection of steel pile under the pier P-4 of Showa Bridge (Hamada et al., 1986).

Unlikely the nearby Showa Bridge, the abutment and first two piers of Yachiyo Bridge suffered severe damages due to lateral spreading, as shown in Fig. 1.7. The permanent displacement of the river bank towards the channel was approximately 4.6 m. The second pier on the left bank was broken from its lower part because of the forward movement instigating the collision between the pier and the comparatively rigid girder of the bridge. The permanent horizontal deformation between the top of this pier and the broken lower part was approximately 1.1 m. A similar kind of damages was also observed on the opposite bank of the river.

Fig. 1.7: Damages of Yachiyo Bridge during the 1964 Niigata Earthquake (Hamada et al., 1986).

1.2.3 Failure of Landing Road Bridge during the 1987 Edgecumbe Earthquake

The 1987 Edgecumbe Earthquake was one of the most damaging earthquakes that New Zealand has experienced in recent decades. The magnitude of the earthquake was 6.3 in the moment magnitude scale. Almost 50% of the houses in Edgecumbe area were damaged due to the earthquake. Since the hypocenter of the earthquake is too shallow, approximately 8 km, the earthquake was felt over a large area. Liquefaction-induced lateral spreading also took place. Consequently, at least 6 bridges, ranging from single span to the 240 m long Landing Road Bridge, have been reported to be damaged significantly.

The Landing Road Bridge was constructed across the Whakatane River during 1962. It consisted of 13 spans of two-lane concrete decks having a length of 18.3 m each and two footpaths (Keenan, 1996). The superstructure is supported by a number of piers and abutments, forming the whole structure sufficiently stiff and monolithic. The substructure comprised of concrete pier having a similar width of the superstructure supported by eight numbers of 406 mm square racked prestressed piles. The abutment was also supported by eight number of 406 mm square racked prestressed piles. Five of them were placed near the river and another three were in the embankment approach. During the earthquake, liquefaction was reported to cause a lateral movement of 1.5 m inward the channel.

Apparently, the response of the bridge superstructure during the earthquake was quite fine except for some buckling in a pair of concrete footpath slabs (Keenan, 1996). This buckling may be instigated by the compressive force along the longitudinal axis of the bridge. However, excavation up to one meter near the northern abutment showed the racked piles on the riverside were cracked and the cracks were extended up to 75% of the width of the pile. Landward soil near the left bank pier had mounted up whereas, a gap of up to 600 mm was formed on the riverside, which is the clear evidence of passive failure.

The estimated force required to initiate the failure of the piles was almost at the same order of magnitude to that of the rough estimation of passive forces exerted by the surficial soil crust (Keenan, 1996). Moreover, since the piers remained nearly vertical even after the earthquake, Keenan reported that the piles and piers didn't go through the complete collapse mechanism but, the cracks at the top of the pile initiated the development of potential plastic hinge. The most vulnerable points were the top of the piles located at the riverside row. The probable failure pattern proposed by Keenan is shown in Fig. 1.8.

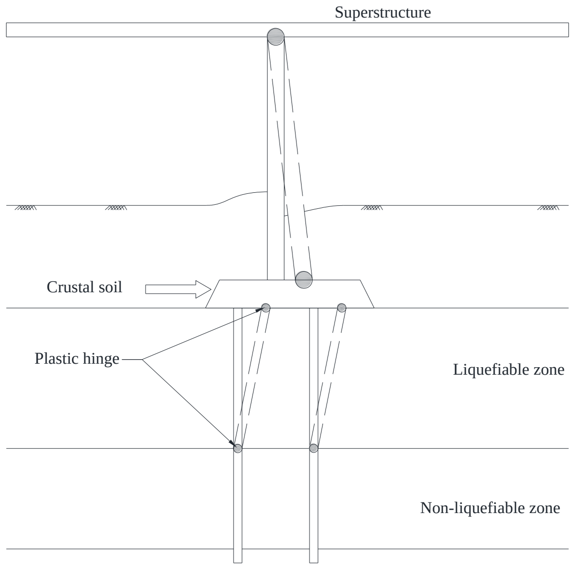

Fig. 1.8: Probable failure mechanism of Landing Road Bridge.

1.2.4 Damages during the 1995 Kobe Earthquake

The 1995 Kobe Earthquake is one of the worst earthquake incidents in the history of Japan in terms of economic loss and loss of human lives as well. Extensive soil liquefaction took place in several artificial islands made of weathered granite called “Masado.” Although masado had been considered to have high liquefaction resistance, unexpectedly, severe liquefaction-induced damages took place in those islands and surrounding cities. The damages include ground subsidence, ground fissure, the formation of sand boils, seaward movements of quay wall, etc. Ejection of liquefied material continued on Port Island nearly about one hour after the earthquake (Shibata, Oka, & Ozawa, 1996).

A large number of buildings and bridges were located within this liquefied zone, thus, suffered from extensive damages of foundations especially pile-supported foundation during lateral spreading. A detailed investigation was conducted to inspect the extent of the failure and its mechanism. The development of cracks along the depth of piles in the affected zone was investigated by lowering a borehole video camera. Characteristics failure of piles under Pier 211 of Uozakihama Bridge is shown in Fig. 1.9. Likewise, the other piles described in the previous sections, the pile head and interface of liquefied and non-liquefied layers have been found to be vulnerable to develop cracks.

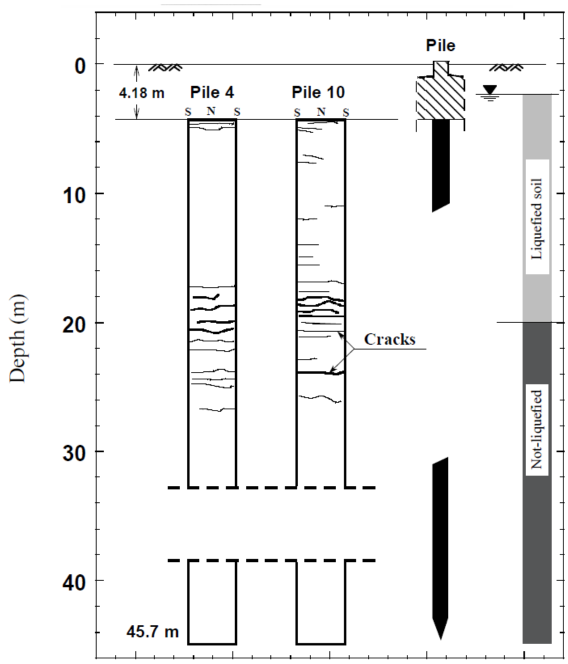

Fig. 1.9: Development of cracks along the pile under Pier 211 of Uozakihama Bridge (Amiri, 2008).

1.2.5 Damage of modern bridges on slender piles after the Canterbury Earthquakes

The region in and around Christchurch comprising of Christchurch City, Selwyn and Waimakariri Districts suffered from two significant earthquake events on 4th September 2010 and 22nd February 2011 with a magnitude of 7.2 and 6.3, respectively. Most of the structures severely damaged during those earthquakes were older buildings including notable landmarks, simply supported bridges including several historic bridges and few modern bridges designed with slender piles. The majority of the earthquake damage to bridges was caused by the liquefaction-induced lateral spreading and settlement, and to a lesser extent because of seismic inertia loads on the structures (Waldin, Jennings, & Routledge, 2012).

A number of historic bridges are situated in Christchurch which was constructed at the beginning of the last century. Antigua St Footbridge and Colombo St Bridge were two such historical bridges built in 1901 and 1902, respectively. Both of these two bridges were supported on non-piled concrete abutments constructed over a layer of liquefiable soils overlaid with shallow river gravel. The northern abutment of Colombo St Bridge suffered from a considerable rotation due to lateral spreading. Similarly, the unreinforced abutments of Antigua St. Footbridge underwent significant cracking and rotation. Most of the simply supported bridges in that region showed better performance against the seismic effect except few like the Avondale Bridge and the Fitzgerald

Twin Bridge. These two bridges were constructed in 1961 and 1964, respectively, and the abutments and piers are supported by the prestressed concrete piles. However, the bridges suffered significant rotation because of the formation of the plastic hinge at piles immediately below the abutment.

Although, most of the severely damaged bridges were comparatively older while the effect of liquefaction/lateral spreading was not considered properly during its design. However, failure of some modern bridges particularly Porritt Park Footbridge (Fig. 1.10) drew the attention because of its severe rotation at its both abutments. This bridge was constructed on closely spaced slender and flexible piles which might act as a pseudo wall and subjected to the tremendous lateral forces from the liquefied soil behind it (Waldin et al., 2012).

Fig. 1.10: Rotation of abutment of Porritt Park Footbridge (Waldin et al., 2012).

1.3 Physical modeling to observe the pile behavior in liquefied soil

Physical modeling provides an important means of getting an insight into the response of the ground as well as the structural elements for example piles inside the soil during liquefaction. In physical modeling, a scaled-down model or sometimes the complete prototype is investigated to achieve the desired goal. The prime criterion for obtaining more accurate results from a model experiment is to follow the appropriate similarity rule for choosing model dimension and material parameters. Controlling the proper research condition, almost the exact response of any particular element can be achievable. The attractive feature of a model experiment is that the properties of the model ground and structural elements can be controlled in a very precise way thus the influence of any particular properties of soils or structural elements can be distinctly inspected. However, an experiment can never capture all the physical phenomenon of real-life structures, rather it is used as a useful tool to understand the phenomena.

From the discussions in the previous section, it is evident that the permanent lateral deformation or lateral spreading of liquefied soil is the primary cause of the distress of piles during an earthquake. Moreover, the movement of the non-liquefiable crust over the liquefiable soil governs the damages to the piles (Hamada, 2000). A large number of physical model tests have been conducted in the last few decades to determine the response of piles or pile groups against lateral spreading. Experiments comprise both 1g shake table test and centrifuge tests even several prototype tests to simulate the response of pile under different geographical conditions and pile types. A brief description of some of the previous research works and their findings is presented in the following sections.

1.3.1 Upslope resistance of liquefiable soil

Brandenberg et al. (2005) presented an uncommon behavior of liquefied soil in this paper. A series of centrifuge tests were performed on 9 m radius centrifuge at the University of California Davis in order to study the behavior of a single pile and pile group subjected to lateral spreading. Pile diameter ranges from 0.36 m to 1.45 m for single piles and 0.73 m to 1.17 m for group piles. Each experiment was conducted under a series of realistic ground motions with peak acceleration varying from 0.13 g to 1.00 g. The crustal layer, made of clay overlying a loose liquefiable soil layer, was used to imitate the non-liquefiable surface layer in real-life structure. The experimental setup is shown in Fig. 1.11.

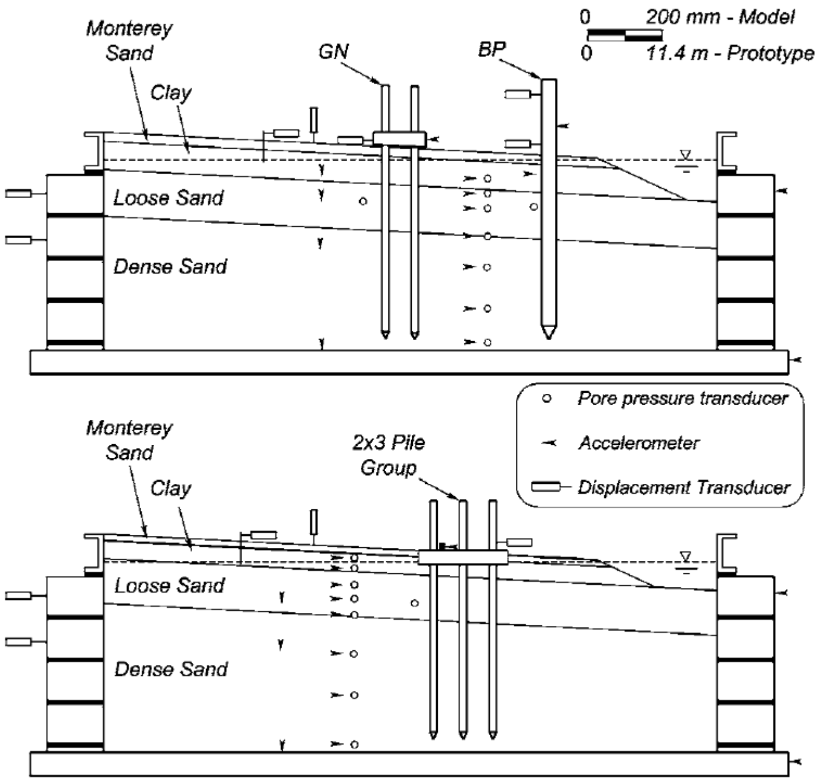

Fig. 1.11: Cross-sectional view of the experimental setup (Brandenberg et al., 2005).

Densification of the loose sand layer because of post-shaking consolidation and the cyclic degradation of the stress-strain behavior was reported due to the application of the series of earthquake events. It was reported that the relative density of the loose sand layer was increased roughly to 10% on average. This densification process was expected to increase the liquefaction resistance of the sand layer however, the liquefied state was observed to continue throughout the series of ground shaking. It verifies the recurrence of liquefaction of the same soil layer even after the prior densification during the past earthquake events.

Lateral resistance of the liquefied soil in the upslope direction was also observed which is beyond the general concept of liquefaction. It was noted that the peak bending moment always coincides with the peak downslope loading from the clay crust however, at that instant the liquefiable soil layer provided lateral resistance against the downslope movement of the pile. This phenomenon of liquefied sand was explained by the phase transformation behavior of liquefiable sand. The loose sand was temporarily stiffened and the pore pressure ratio was dropped due to the dilatancy after some straining. Thus, it prevents the incremental downslope displacement of the pile guided by the progressively increasing lateral load from the clay crust. The whole phenomena are depicted in Fig. 1.12. Moreover, the authors emphasized the consideration of the side and the base friction between the embedded pile caps and the crust which found to contribute significantly to the total load imposed on the foundation.

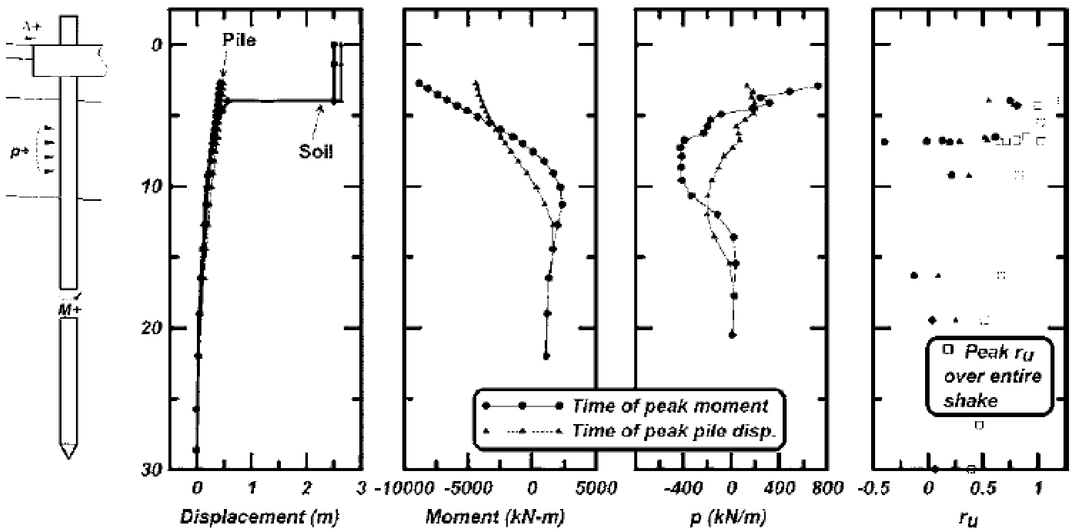

Fig. 1.12: Snapshots of displacement, moment, lateral load on pile, and pore pressure ratio at the time of peak bending moment and peak pile cap displacement (Brandenberg et al., 2005).

1.3.2 Response of a group of piles in extremely loose sand

Haeri et al. (2012) presented an interesting behavior of piles subjected to lateral spreading in extremely loose soil. It was described that the ground along with the pile started the downslope movement once the soils get liquefied just after the beginning of the shaking. However, unlike the free field condition where the movement of soil was continued until the end of shaking, the pile bounced back gradually after reaching the maximum displacement a few seconds after the beginning of lateral spreading. This procedure was continued throughout the shaking and had a residual displacement at the end of shaking, as shown in Fig. 1.13. This kind of response of the pile was explained by the significant degradation of soil stiffness because of liquefaction. The strength of the soil was reduced up to such level that it became too weak to prevent the backward movement of the piles.

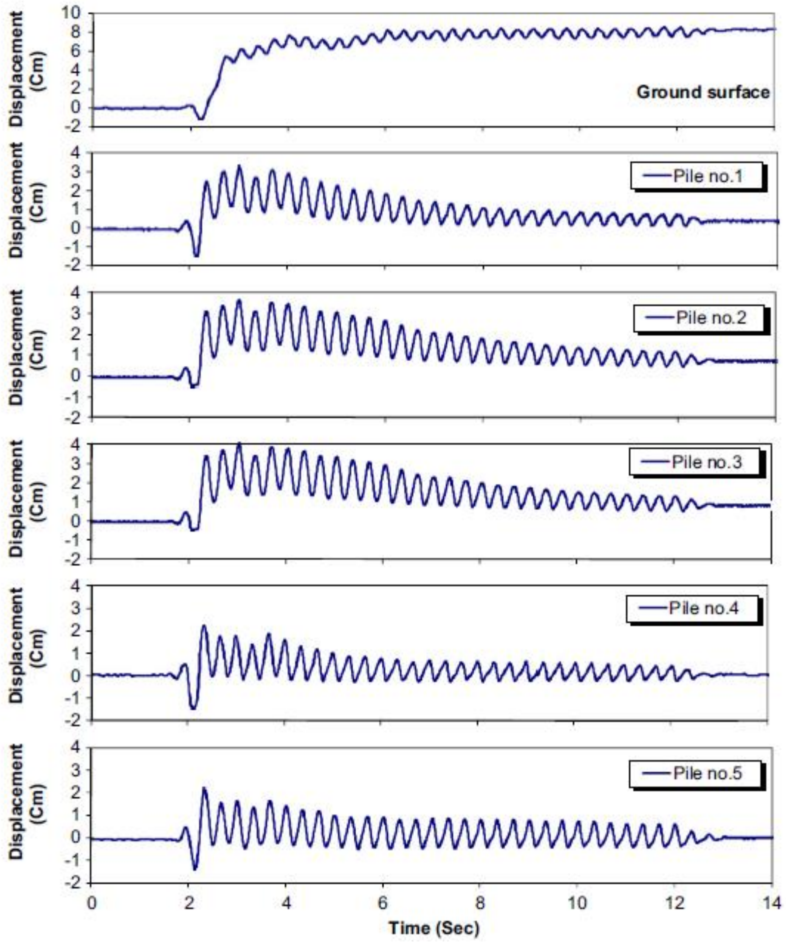

Fig. 1.13: Time histories of ground surface displacement and lateral displacement of pile (Haeri et al., 2012).

1.3.3 Behavior of pile group adjacent to the earth retaining structure

A large scale shake table (E-defense) test, described by Motamed et al. (2013) represented the behavior of a pile group located adjacent to a gravity-type quay wall during lateral spreading. Extensive liquefaction-induced lateral spreading was observed which caused the lateral movement of the quay wall of about 2.2 m. The model was built in a large container with a dimension of 16 m long, 5 m wide and 4 m in height. A sand layer with a relative density of 60% was prepared as a liquefiable layer overlain by a non-liquefiable dense sand layer having a relative density of 90%. The deep foundation was modeled with a pile group consisting of six piles. The experimental results illustrated that the rear row piles (closer to the quay wall) sustained larger lateral loads thus underwent significant damages in comparison with the piles at the front row. He mentioned that the rear row piles might have subjected to the excessive axial forces imposed by the tilted superstructure which caused the extensive damages to those piles. The displacement of the liquefied soils and the failure pattern of piles are depicted in Fig. 1.14.

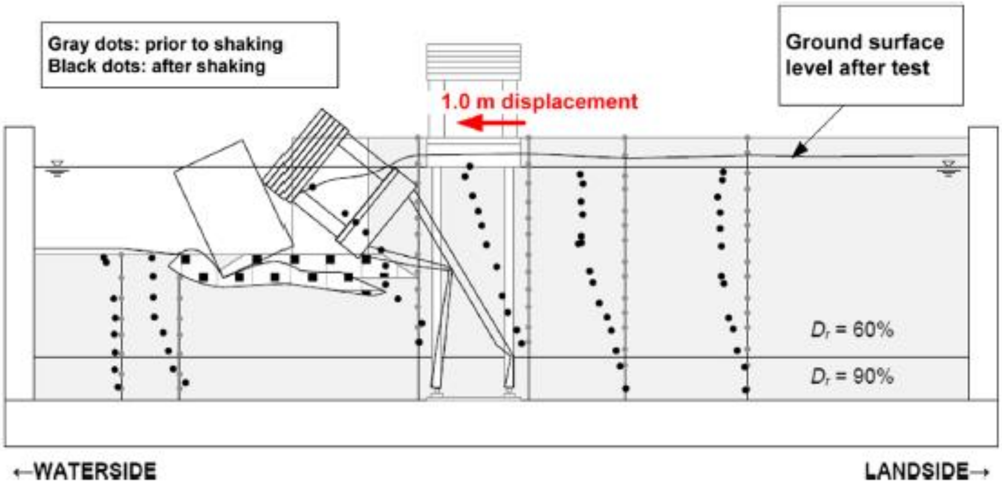

Fig. 1.14: Residual displacements of soil and the typical failure of pile groups (Motamed et al., 2013).

Liquefaction-induced lateral pressure on pile surface prior to its structural failure was compared with the Japan Road Association (JRA) and Japan Sewage Work Association (JSWA) design specification for pile against lateral spreading, as shown in Fig. 1.15. They mentioned that the failure of the structure took place before the complete mobilization of the lateral spread. Therefore, no particular conclusion was made. However, the author believes the force-based method is quite useful in the preliminary analysis.

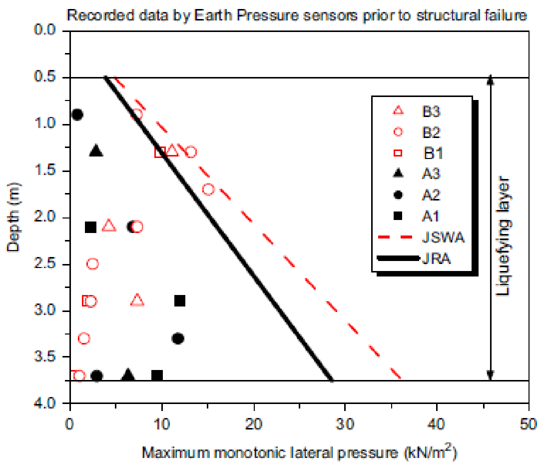

Fig. 1.15: Distribution of maximum monotonic lateral pressure along depth prior to the structural failure of piles and comparison with recommended values by design guidelines (Motamed et al. 2013).

1.3.4 Response of single pile behind a quay wall.

A shake table test described in Su et al. (2016) is performed to determine the response of a single pile behind a quay wall subjected to lateral spreading. The model ground was prepared inside a large laminar container having a dimension of 3.5 m long, 2.2m wide and 1.7m in height. A steel pipe with a diameter of 0.088m is used as a pile. The pile tip is inserted into a socket attached to the base of the container to imitate the fixed end condition.

Attenuation of acceleration amplitude in the soil is reported in this paper while the soils get liquefied. Moreover, the propensity of the stiff pile to bounce back slightly is also reported. The paper also describes the applicability of force-based simplified design approach for pile subjected to lateral spreading. A Beam on Non-linear Winkler Foundation model is proposed and recommended that the proposed BNWF can predict the observed pile in a better way compared to the simple soil pressure-based approach.

1.4 Motivation of this research

Several experimental and numerical studies have been conducted to study the response of pile or group of piles subjected to lateral spreading. Post-earthquake survey and experimental studies show that the locations near the pile head in the cases of group piles and the interface of liquefiable and non-liquefiable soil layers usually experience the maximum bending moment. However, the locations and the magnitude of the bending moment might be influenced by several factors, for example, the types of the pile and its arrangements in a pile group, type of superstructure, and the geometry of the ground. Although, a number of researches exist on the pile response in liquefied soil, but a very few researches at least in the knowledge of the author have been observed to study the behavior of pile-supported bridge abutment. The load distribution pattern of bridge abutment is quite different from the other types of foundation. The vertical wall of the abutment though supports the loads coming from the bridge deck at the same time, it retains the earth of the approach embankment. Thus, the vertical wall transfers a considerably large amount of lateral load as well as the bending moment to the supporting piles. A large number of the bridge structures are damaged during lateral spreading accompanied by the collapse of the abutments. Therefore, it is essential to get an insight into the seismic response of pile-supported bridge abutment and find a viable remedial measure against lateral spreading to prevent the failure of the existing bridge abutments.

Remedial measures against the liquefaction or liquefaction-induced lateral spreading are primarily classified into two types; a) ground improvement and b) reinforcement. Ground improvement techniques consisting of ground densification or chemical ground stabilization, prevent the occurrence of liquefaction thus prevent the failure of the surrounding structures. However, the ground improvement techniques are not very effective for the existing structures which will be described in the next chapters. Besides, the reinforcement technique includes the retrofitting of the structure itself to make it earthquake resilient and the ground reinforcement to mitigate excessive ground movement. Retrofitting is a very efficient and cost-effective technique for the existing superstructures. However, the retrofitting technique is quite difficult to implement for the existing underground structures like pile. Therefore, the installation of the sheet pile, an indirect reinforcement technique, is used in this study to mitigate the lateral spreading of the liquefied ground.

In addition to the experimental studies, the numerical analysis plays an important role especially when the physical modeling, for example, large scale model/prototype tests are not feasible. Numerical analysis is an essential tool to get reliable information about the seismic response of the ground and the surrounding structures. Moreover, a validated numerical model can be the source of a vast amount of information which is not possible to get through the experimental results. Therefore, the centrifuge modeling as well as finite element analysis is used in this study to find a viable seismic retrofit for existing piled abutment.

1.5 Objectives of this study

Displacement, triggered by lateral spreading, may range from few centimeters to several meters. The ground moves towards the down-slope or the free face, such as a river channel. Because of the development of excess pore water pressure, the foundation soils lose its strength which triggers the channel-ward movement of the non-liquefied surface layer. Simultaneously the soils in the riverside also lose its resistance thus the bridge abutment is subjected to a large displacement at the free face. This channel-ward movement of the abutment may lead the bridge deck in front of it to buckle vertically or may cause unseating from the support. Moreover, the liquefied soils move towards the channel and damage the foundation of the abutments. Therefore, the abutment foundations are always vulnerable to be damaged severely during lateral spreading. Relatively slender pile foundations were found to either shear at a depth or develop plastic hinge during the previous massive earthquakes while a large foundation underwent channel-ward rotation and translation (Bartlett, 2014). The mitigation of the lateral spreading of the foundation soils under the embankment can potentially prevent the failure of the abutment of a river spanning bridge. This study focuses on preventing seismic damage to the existing bridge abutment. The installation of sheet pile is considered here as a potential remedial measure against liquefaction induced lateral spreading to avoid the difficulties of applying traditional ground improvement techniques. Several factors can influence the efficiency of sheet pile as a seismic retrofit, i.e., the thickness of the liquefiable layer, embedment depth into the bearing strata, and the width of the sheet pile, etc.

Therefore, this study focuses to find out:

a) The favorable ground geometry where the sheet pile can be effectively used.

b) The effect of sheet pile width to mitigate the damage of the targeted area.

c) The additional reinforcement to improve the performance of the sheet pile.

d) The efficiency of this sheet pile reinforcement technique to prevent the damages of the abutment due to lateral spreading.

1.6 Outline of dissertation

This dissertation consists of five additional chapters. A brief description of each chapter is given below.

Chapter 2: Seismic response of the piled abutment subjected to liquefaction-induced lateral spreading

This chapter describes the seismic response of the bridge abutment. The numerical simulation of the large-scale shake table tests by using two-dimensional and three-dimensional finite element analysis is described here. Two types of the model abutment are used in theses analyses. One is designed according to the current Japanese design standard for highway bridges and the other is designed based on the old design standard.

Chapter 3: Performance of sheet pile to mitigate liquefaction-induced lateral spreading of loose soil layer under the embankment

This chapter describes the experimental results of five dynamic centrifuge experiments. The experiments are conducted to investigate the performance of the sheet pile to mitigate liquefaction-induced lateral spreading of various thicknesses of liquefiable foundation under an embankment.

Chapter 4: Effect of thickness of liquefiable layer and embedment depth on the performance of sheet pile as a seismic retrofit.

This chapter explains the results of two-dimensional finite element analysis. Several numerical analyses are conducted to observe the effect of thickness of the liquefiable layer and embedment depth of the sheet pile. The performance of the anchored sheet pile to mitigate lateral spreading is also investigated.

Chapter 5: Performance of sheet pile as a seismic retrofit for piled abutment subjected to lateral spreading

The results of two dynamic centrifuge experiments are described in this chapter. The centrifuge experiments consist of a bridge abutment reinforced with a sheet pile. The response of piled abutment is also investigated by two-dimensional finite element analysis. The results between the reinforced and unreinforced abutment are compared. This chapter also describes the effect of bridge girder on the bridge abutment. Finally, this chapter describes the performance of the anchored sheet pile to prevent the damage of the bridge abutment subjected to lateral spreading.

Chapter 6: Conclusion and recommendations

This chapter summarizes the important research findings and recommends some scopes of future study.

[This page intentionally left blank]

Chapter 2

Seismic response of the piled abutment subjected to liquefaction-induced lateral spreading

2.1 Introduction

Finite element analysis is frequently used nowadays to determine the response of the liquefied ground and its effects on the surrounding structures. Two-dimensional finite element analysis is more popular because of its less computational demand. However, three-dimensional finite element analysis can incorporate the precise depiction of the size, shape and geometry of the model ground and the structures. Two-dimensional and three-dimensional finite element analysis of piled abutment resting on a liquefiable layer are carried out and described in this chapter to show the seismic response under different geometric and structural conditions. The numerical results are compared with the large-scale shake table test performed in the Public Works Research Institute (PWRI). Both the experiment and the numerical simulation are conducted on the model abutments designed based on current Japanese standard for highway bridges (Japan Road Association, 2002) as well as the bridge abutment designed based on the old Japanese standard (Japan Road Association, 1964). The Tohoku Earthquake, 2011 is applied as an input ground motion.

2.2 Experimental setup

Bridge abutments including the approach embankments are designed and modeled with a scale of 1:10 in these experiments. Two different configurations of model abutments are incorporated in these experiments. In Experiment-1, the model abutment is designed according to the current Japanese design standards for highway bridges and in Experiment-2 and 3, the model abutments are designed based on the old Japanese design standards. The detailed description of both model abutments is given in section 2.2.1. A 6 m × 3 m × 2 m steel container is used to prepare the model ground. The base of the container is fixed to the shaking table. In order to examine the effect of the shape of the embankment, two different configurations of the approach embankment are made. In Experiment-1 and 2 the widths of the embankment are kept 3.0 m which are equal to the width of the model container whereas, in Experiment-3, a limited extent of the embankment is considered. In Experiment-3, the top width of the approach embankment is equal to the width of the abutment having a side slope of 1:2 both in transverse and longitudinal directions. The plan and cross-sectional views of the experimental setups are shown in Fig. 2.1 to 2.3. A lifted water tank is used to saturate the foundation soil and the flow of the water from the base of the container is continued until the constant head of water is reached in the standpipe.

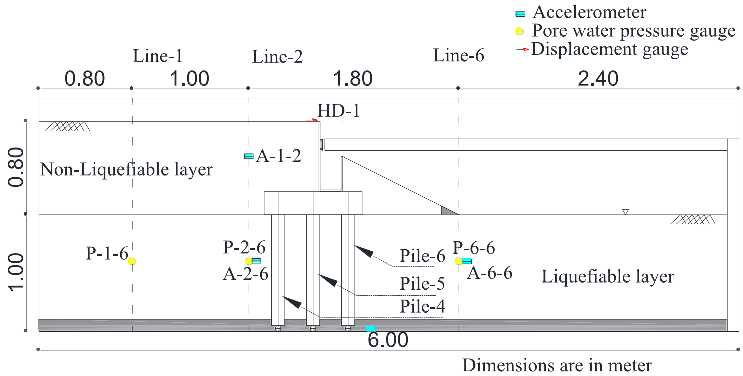

Fig. 2.1: Longitudinal section of the experimental setup of Experiment-1.

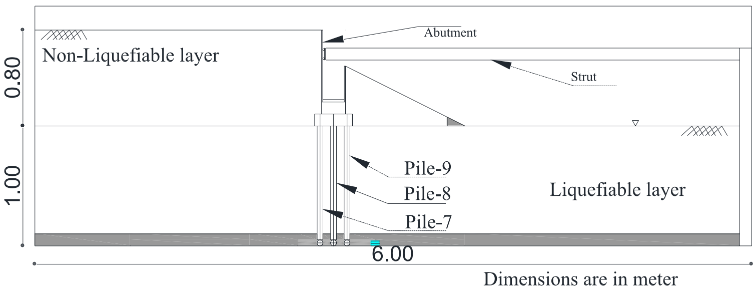

Fig. 2.2: Longitudinal section of the experimental setup of Experiments-2 and 3.

2.2.1 Description of the model abutment

The model abutment in Experiment-1 is supported by a 3 × 4 pile group. The piles are hinged at its tip to the container to prevent the translational movement of the pile group. The head of the piles is rigidly attached to the footing of the abutment. The half-width of the bridge abutment is modeled to take advantage of symmetry. Because of that reason, only six piles are visible in the plan view. The piles are designed with a 1.10 m long steel (SS400) bar having a cross-sectional dimension of 31 mm × 25 mm in order to adjust to the bending stiffness of the pile design based on the current design standard. In fact, the old standard allows the closely spaced flexible piles, whereas, the current standard recommends using comparatively stiff piles with wider spacing. A series of circular rings having an outer diameter of 114.3 mm are attached to the pile along its length to impose the effect of the volume of the piles. The longitudinal section and the plan view of the Experiment-1 are shown in Figs. 2.1 and 2.3 (a), respectively.

A strut, rigidly fastened to the experiment container, is placed in front of the abutment to simulate the strut effect of the bridge girder. The current Japanese design standard for highway bridges recommends using a comparatively large gap between the face of the abutment to the edge of the bridge girder. The gap between the strut and the abutment in Experiment-1 is kept 20 mm to avoid the frequent collision. The physical properties of the piles are summarized in Table 2-1.

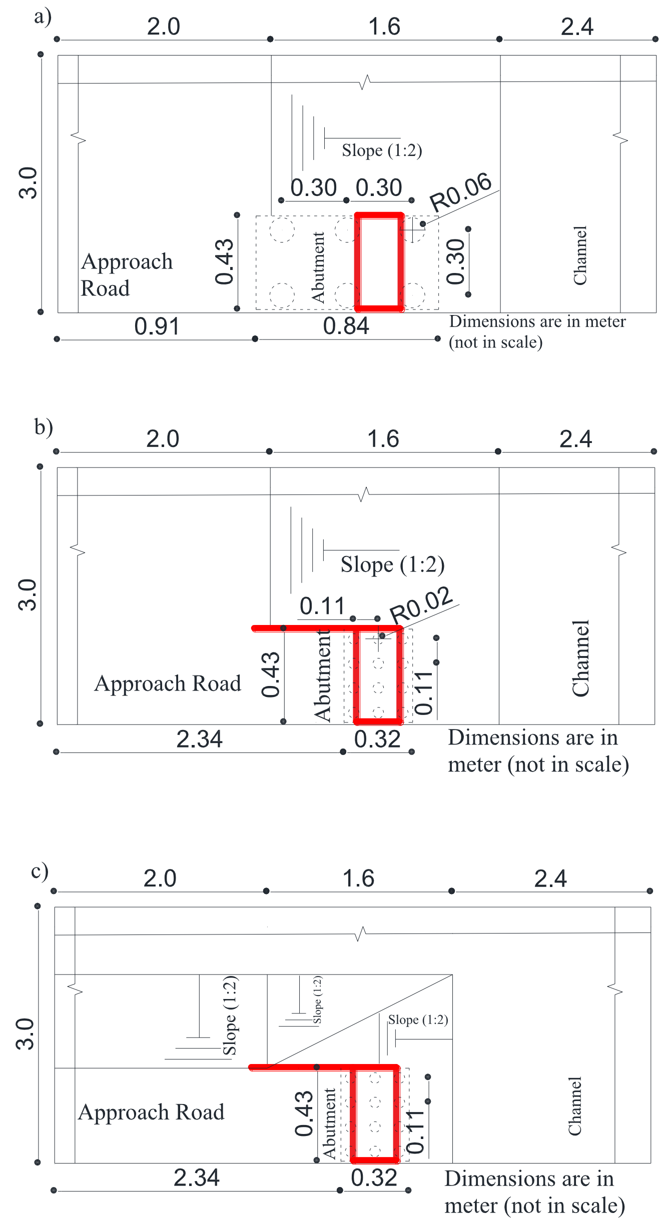

Fig. 2.3: Plan view of experimental setups of (a) Experiment-1, (b) Experiment-2, and (c) Experiment-3.

The model is subjected to the 2011 Tohoku Earthquake ground motion applied with an appropriate similitude law (Muir Wood 2004). Similarly, two other experiments are conducted to examine the response of the bridge abutment designed based on the old Japanese standard. Based on the old Japanese standard, the abutment is supported by a 3 × 8 pile group. The specifications of the pile are described in Table 2-2. In Experiment-3, the width of the embankment is limited to the equal width of the abutment and in Experiments-1 and 2 the width is considered to be semi-infinite. To observe the strut effect of the bridge girder the gap between the strut and bridge abutment in Experiments-2 and 3 is kept smaller, which is only 5 mm.

2.2.2 Preparation of the model ground

As it is mentioned earlier, the model ground is built inside a large container having dimensions of 6 m × 3 m × 2 m in length, width, and height, respectively. Silica Sand No. 6 with a relative density of 50% is used to make the embankment as well as the foundation soil which is placed over a drainage layer with a thickness of 100 mm. The dry deposition method is used to prepare the model ground and then compacted by tamping to reach up to the desired level of compaction. The foundation soil up to the base of the pile cap is kept saturated to ensure liquefaction of that soil during shaking. The physical properties of Silica Sand No. 6 are listed in Table 2-3.

Table 2-1: Specifications of piles in Experiment-1.

Element type	Properties
Pile upholding (each pile)	
Dimensions (mm)	1105×31×25
Modulus of elasticity (N/m^2)	2×10^{11}
Mass (kg)	6.72
Circular ring (each pile)	
Outer diameter (mm)	114.3
Inner diameter (mm)	112.3
Height (mm)	810
Material type	Steel (SUS304)
Mass (kg)	4.50

Table 2-2: Specifications of piles in Experiments-2 and 3

Element type	Properties
Pile upholding (each pile)	
Dimensions (mm)	1102×19×8
Modulus of elasticity (N/m^2)	2×10^{11}
Mass (kg)	1.31
Circular ring (each pile)	
Outer diameter (mm)	48.6
Inner diameter (mm)	46.6
Height (mm)	864
Material type	Steel (SUS304)
Mass (kg)	2.0

Table 2-3: Physical properties of Silica Sand No. 6.

Physical properties	Silica Sand No. 6
Specific gravity, G_s	2.647
Relative density, D_r (%)	50
Void ratio, e_o	0.804
Maximum void ratio, e_{max}	1.014
Minimum void ratio, e_{min}	0.594
Uniformity coefficient, U_c	2.08
Permeability (m/s)	5.15×10^{-4}

2.3 Finite element model

In this study, a finite element code developed by Takahashi (2002) is used to simulate the shake table test results described in the previous section. A fully coupled u-p formulation is used in this finite element code. The governing equation of an infinitesimal soil element considering the moment balance relation of the solid-fluid matrix can be expressed as Eq. 2.1.

$$L^T\sigma-\rho\ddot{u}+\rho b=0 \qquad (2.1)$$

Where $\ddot{u}$ represents the acceleration of the solid matrix, $\rho = [(1-n)\ \rho_s + n\ \rho_f]$ is the total density, n is the porosity of the porous material, ρ_s is the density of the solid particle, ρ_f is the density of the water, and b is the body force, σ is the stress tensor representing the total stress, and L is the differential operator. Combining the flow conservation equation, moment balance of fluid and generalized Darcy's seepage law, the governing equation for pore fluid can be written as Eq. 2.2.

$$\frac{k}{\rho_f g}\nabla^T(\nabla p+\rho_f b)+m^T\dot{\varepsilon}-\frac{n\dot{p}}{K_f}=0 \qquad (2.2)$$

Where k is the hydraulic conductivity, ∇ is a differential operator, p is the pore pressure, ε is the strain, m = $[1\ 1\ 1\ 0\ 0\ 0]^T$ for three-dimensional cases and $[1\ 1\ 0\ 0]^T$ for two-dimensional cases, n is the porosity, and k_f is the bulk moduli of pore fluid. Eq. 2.1 and Eq. 2.2 together with the constitutive equation, define the behavior of porous solids and pore water pressure.

2.3.1 Finite element mesh

The finite element meshes used in these numerical analyses for Experiment-1, Experiment-2, and Experiment-3 are designated with Model-1, Model-2, and Model-3, respectively, as shown in Fig. 2.4. The soil materials, the footing, and the stem of the abutment are modeled as 8-nodes brick elements whereas, the piles are modeled as elastic beam elements. The whole domain is divided into a number of uniform meshes except near the structural elements, where comparatively finer meshes are used to arrange the structural members. The 0.2 m × 0.2 m × 0.2 m brick elements are used to model most of the domain of the liquefiable layer and the 0.2 m × 0.2 m × 0.1 m brick elements are used in the case of non-liquefiable approach embankment. Smaller brick elements for approach embankment are used to accommodate the 1:2 slope of the embankment.

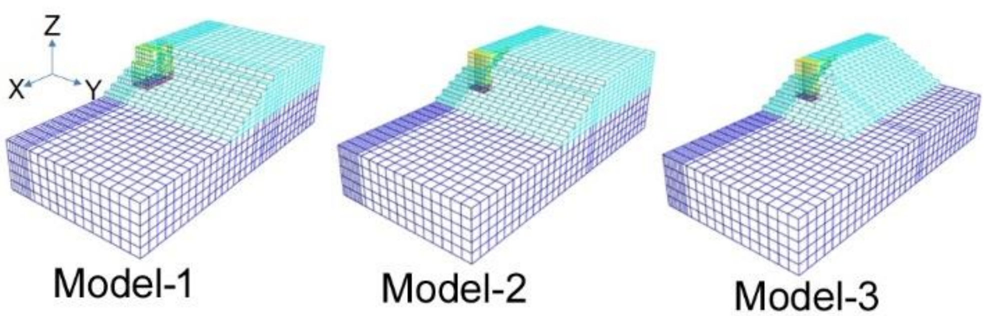

Fig. 2.4: Finite element meshes for Model-1, Model-2, and Model-3.

2.3.2 Material Parameters

The soil elements are modeled as an elastoplastic material and a constitutive model proposed by Asaoka et al. (2002) is used to predict the cyclic behavior of sand. This model is an advanced constitutive model that can consider the decay of the internal structure of the soils. The difference between clay and sand can be distinguished by considering super-loading surfaces together with rotational hardening in the modified cam-clay model. Fourteen parameters are required to formulate the soil model out of which κ and λ are the tangent of the swelling and the virgin compression line and can be determined from the consolidation test. e_o, ν, and G_s are the initial void ratio, Poisson's ratio and the specific gravity of the soil, which can be determined from element tests. All other parameters are determined by trial and error so that the numerical liquefaction resistance curve closely fits the experimental one. Two sets of parameters are used in these analyses, namely highly liquefiable soil (HLS) parameters and low liquefiable soil (LLS) parameters. The soil parameters are listed in Table 2-4. HLS parameters are used in three-dimensional finite element analysis to show the response of the ground and abutment in highly liquefiable soil. However, the HLS and LLS parameters are both used in two-dimensional analysis which is described in the last part of this chapter.

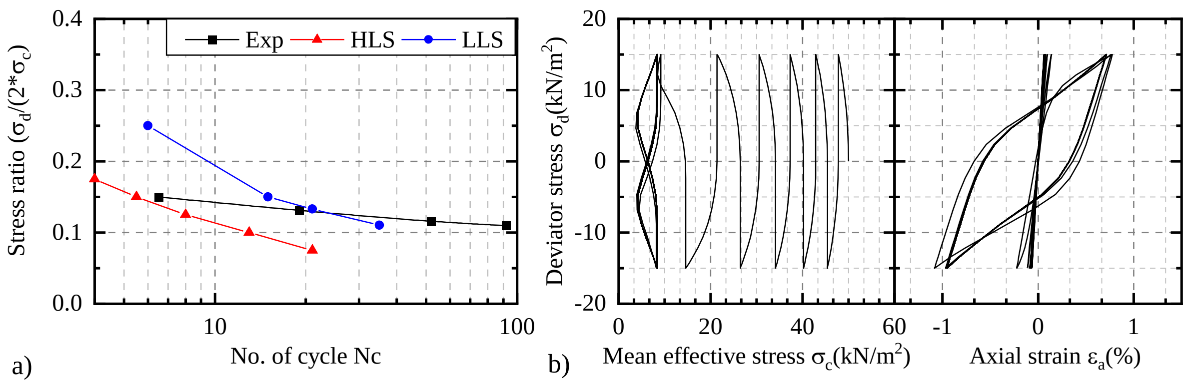

Fig. 2.5: a) Comparison of experimental and numerical liquefaction resistance curve and b) typical stress path and stress-strain curve under cyclic loading for HLS.

The comparison of the experimental numerical liquefaction resistance curve, the typical stress path (using HLS parameters), and stress-strain curve (using HLS parameters) under cyclic loading are presented in Fig. 2.5. The abutment and the piles are modeled as elastic solid elements and beam elements, respectively. In reality, the piles sometimes go under significant rotation due to the development of a plastic hinge. However, the objective of this study is to examine the location of the peak bending moment and its magnitude. Therefore, the consideration of the piles as an elastic element does not have a significant effect on the overall response of the abutment. The parameters are summarized in Table 2-5.

Table 2-4: Soil parameters for numerical analysis.

Parameters	HLS parameters	LLS parameters
κ	0.004	0.04
λ	0.05	0.05
G_s	2.65	2.65
e_o	0.804	0.804
ν	0.33	0.33
φ	35°	38°
φ_d	38°	35°
b_r	3.0	5.0
m	0.1	2.75
a	2.7	1.0
R	1.0	0.85
R_o^*	0.25	1.0
K_o	1.0	1.0
k (m/s)	5.14×10^{-04}	5.14×10^{-04}

Table 2-5: Material parameters for structural elements.

Element type	Parameters	Experiment-1	Experiment-2 and 3
Vertical wall	ρ (Mg/m^3)	1.02	1.59
	E (N/m^2)	2.10×10^{11}	2.10×10^{11}
	ν	0.26	0.26
Footing	ρ (Mg/m^3)	0.29	2.10
	E (N/m^2)	2.10×10^{11}	2.10×10^{11}
	ν	0.26	0.26
Pile	EI (N-m^2)	8.46×10^{3}	1.70×10^{3}
	EA (N)	1.62×10^{8}	31.92×10^{6}

2.3.3 Input ground motion

Acceleration time history recorded by an accelerometer that is attached to the base of the container during the experiment is used in this analysis as an input ground motion. The recorded data may contain background noise from different sources. Most of the noises are non-seismic and remain in the range of low or high frequency (Kramer, 1996). This kind of high-frequency or low-frequency acceleration data which is beyond the engineering interest needs to be isolated from the recorded data. Another correction is also introduced to avoid the permanent displacement at the end of motion is commonly known as baseline correction. A computer-based software (Seismosignal-2016) is used for baseline correction and to obtain a bandpass filtered (frequencies in between 0.1 Hz to 25 Hz) ground motion data. The input ground motion for Model-1 (Experiment-1) is shown in Fig. 2.6.

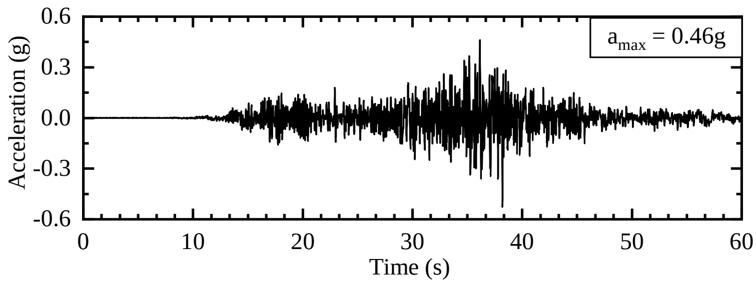

Fig. 2.6: Input ground motion for Model-1 (Tohoku Earthquake).

2.4 Comparison of numerical and experimental results in Model-1

The obtained ground response in numerical analysis is much more catastrophic than it is observed in the experiment. The model ground in numerical analysis is subjected to a significant lateral spreading and goes under a large surface settlement. The deformed shape, and horizontal displacement (x-direction) and vertical settlement (z-direction) at the shoulder (point "S" marked in Fig. 2.7) of the embankment are depicted in Figs. 2.7 and 2.8, respectively.

Figure 2.8 shows a considerably large horizontal displacement of the embankment which reaches nearly about 300 mm, while the maximum horizontal displacement was 20 mm in Experiment-1. It signifies the simulated displacement is approximately 3.0 m in the prototype. Although this is apparently large, this kind of excessive lateral spreading was observed in past earthquakes. For example, during the 1990 Luzon earthquake in the Philippines, the right bank of Pantal River near Magsaysay Bridge which was underlain by sand deposits, was subjected to a liquefaction-induced lateral flow of about 5.0 m (Amiri, 2008).

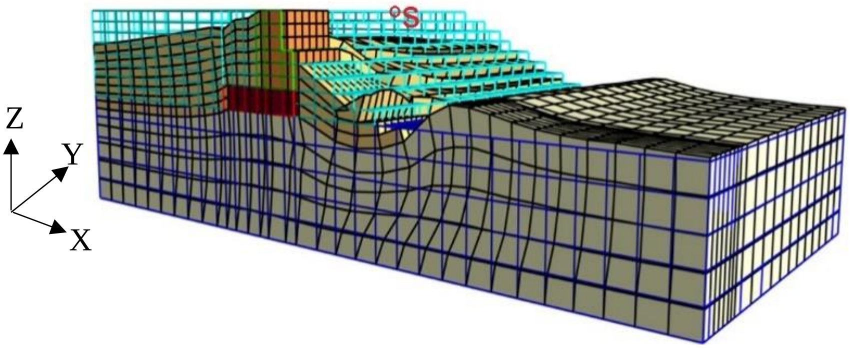

Fig. 2.7: Deformed shape of the ground in Model-1 (HLS parameters).

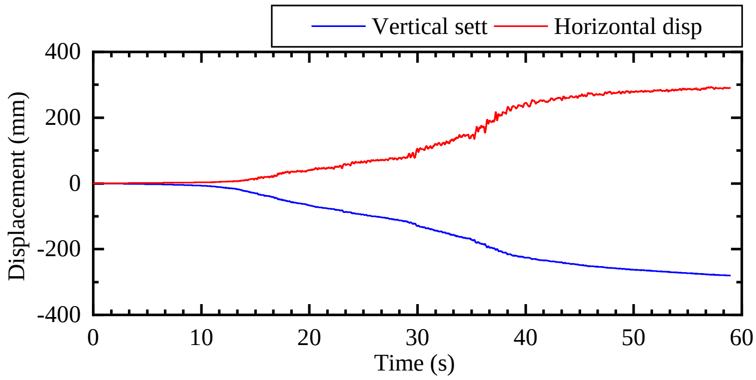

Fig. 2.8: Computed horizontal displacement and vertical settlement of point "S" marked in Fig. 2.7 (HLS parameters).

2.4.1 Evolution of excess pore water pressure

The distribution of computed pore pressure ratio, which is expressed as the pore water pressure divided by the initial vertical effective stress, throughout the model ground is illustrated in Fig. 2.9. While the pore pressure ratio reaches to the unit value, the corresponding soil mass is considered to be liquefied. According to the illustration, almost all parts of the foundation soil both underneath the embankment and inside the channel get liquefied. The comparison of computed and experimental results of excess pore water pressure at three different locations underneath the embankment and inside the channel is shown in Fig. 2.10. The numerical results represented by red lines in the illustration show a quick development of excess pore water pressure. Almost all the cases, there is a sharp increase in excess pore water pressure after 10 s of shaking whereas, in experimental results, the generation of major excess pore water pressure starts after 30 s of shaking. Besides, the magnitude of excess pore water pressure, especially underneath the embankment is considerably large in comparison with the experimental results. Inside the channel, the magnitude of the maximum computed pore water pressure is almost equal to the experimental values. It is evident from Figs. 2.9 and 2.10 that the experimental excess pore water pressure underneath the embankment was not large enough to make the soil liquefied. However, the foundation soil inside the channel gets liquefied during the experiment as well as in numerical analysis.

The degree of saturation of the model ground plays an important role in the occurrence of liquefaction. Usually, the liquefaction resistance of soil is significantly increased with the decrease in the degree of saturation. In fact, the cyclic behavior of the partially saturated sand resembles the behavior of a densely saturated sand (Yoshimi, Keizo, & Tokimatsu, 1989) that requires a large number of cycles to reach to liquefaction. It implies that the rate of pore water pressure generation is also significantly affected by the degree of saturation. The model ground is saturated in the open air with tap water. The water container is mounted at a certain height and the water is allowed to seep through the bottom of the container to saturate the ground. Fully saturated condition is quite difficult to achieve for such a large model. Therefore, the highly liquefiable soil parameters used in this analysis, along with an improper saturation of the experimental model ground, create a significant inconsistency between the experimental and numerical results.

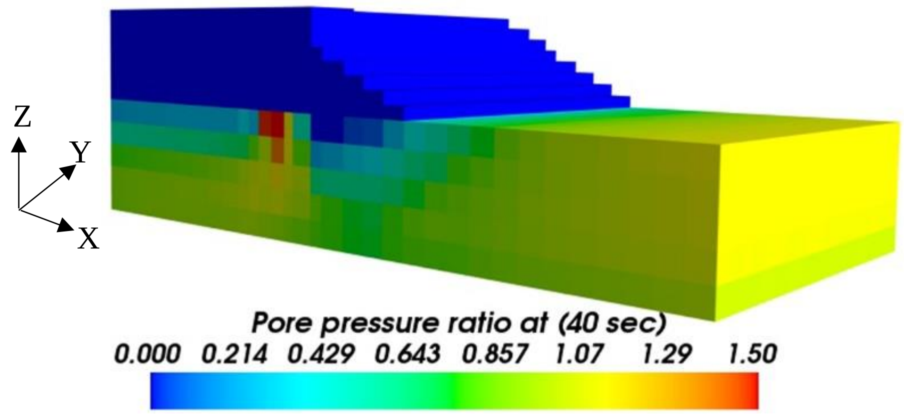

Fig. 2.9: Distribution of pore pressure ratio throughout the model ground (HLS parameters).

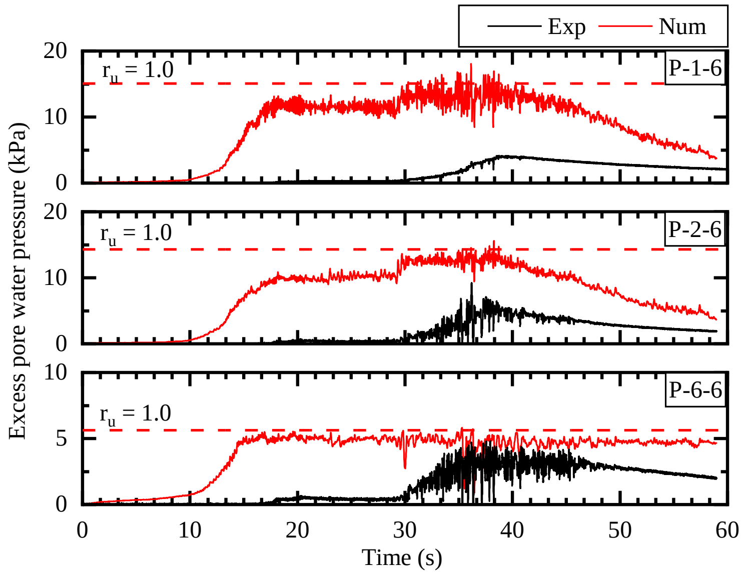

Fig. 2.10: Comparison of computed (HLS parameters) and experimental excess pore water pressure time histories.

2.4.2 Ground response

A comparison of computed and experimental acceleration time histories at three different points, which are inside the backfill, inside the liquefiable layer underneath the embankment, and inside the channel is shown in Fig. 2.11. Although the computed acceleration time history inside the backfill cannot perfectly capture the peaks of the experimental results, the computed results are quite comparable. However, a significant de-amplification in the magnitude of the acceleration is observed inside the liquefiable layer. This phenomenon is frequently observed in the liquefied soil during a real earthquake. Because of the substantial loss of shear strength during liquefaction, the soils lose their capacity to transfer shear wave and consequently, the de-amplification of the acceleration time histories takes place. Figure 2.12 illustrates the computed and measured horizontal displacement at the crest of the abutment. The computed results indicated by the red line show a significant contrast with experimental results. The computed lateral movement is excessively larger than it is observed in the experiment. During lateral spreading, while the foundation soil gets liquefied, the upper crustal layer moves towards the channel, and it pushes the structures. Since the foundation soil in the numerical analysis completely gets liquefied, the abutment is subjected to a comparatively large earth pressure due to the movement of the backfill which causes an excessively large horizontal movement of the abutment.

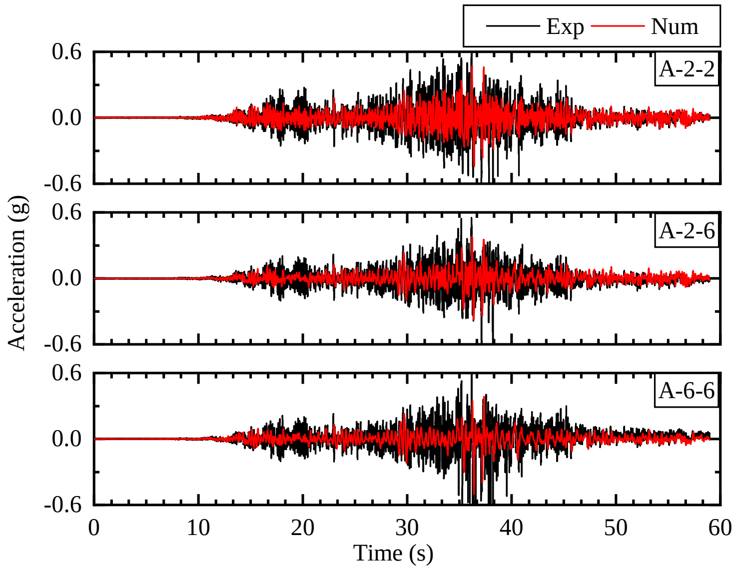

Fig. 2.11: Comparison of computed (HLS parameters) and experimental acceleration time histories.

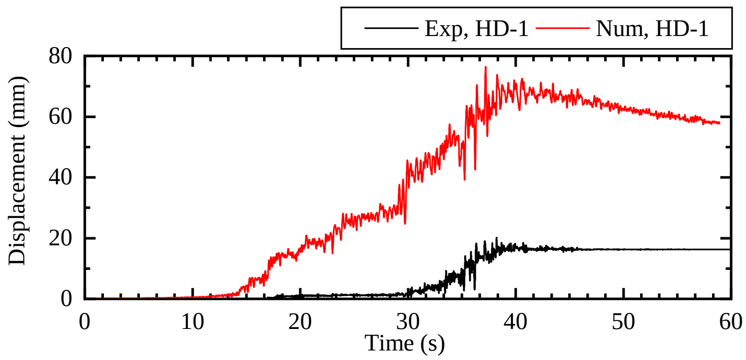

Fig. 2.12: Comparison of the horizontal movement of the abutment (HLS parameters).

Besides, the abutment shows a tendency of backward movement after 40 s and finally reaches a permanent displacement of approximately 60 mm. It is to be mentioned here, that the time histories show an early generation of pore water pressure which triggers the movement of the soil and structural elements earlier in numerical analysis. The tendency of the backward movement of the abutment is probably caused due to the significant loss of shear strength of the foundation soil. During liquefaction, the soils lose their capacity to prevent the backward movement of the stiff piles, eventually, the abutment tends to rebound to its original position.

2.4.3 Bending moment of piles

A comparison of computed and experimental bending moment profiles for Pile-4, Pile-5, and Pile-6 at 37.2 s while the pile heads are experiencing maximum bending moment is shown in Fig. 2.13. The red color solid lines represent the computed bending moment isochrone, whereas, the black dots denote the measured bending moments in the experiment. It is evident that the maximum bending moment both in the experiment and numerical analysis took place near the head of the piles. Although the distributions are similar, the maximum computed bending moment is significantly large in comparison with the experimental values. The response of a pile-supported abutment in liquefied soil is directed by a complex interaction between the piles and the surrounding soil which is influenced by several factors, for example, the amount of relative displacement of the crustal layer, the stiffness of the piles and so forth. Because of the severe liquefaction of the foundation soil, the horizontal movement of the crustal layer far from the structure in the transverse direction is considerably large. This implies that the crustal layer imposes comparatively large passive pressure to the comparatively stiff pile-supported abutment and consequently, the piles are subjected to a large bending moment. The computed bending moment distribution patterns of all the piles, Pile-4, Pile-5, and Pile-6, are almost similar. Another important thing is that the critical bending moment is unlikely to coincide with the principal shocks of the input ground motion. Therefore, the direct consideration of the inertia force of the backfill soil mass due to principal shocks may not provide the true critical bending moment due to lateral spreading.

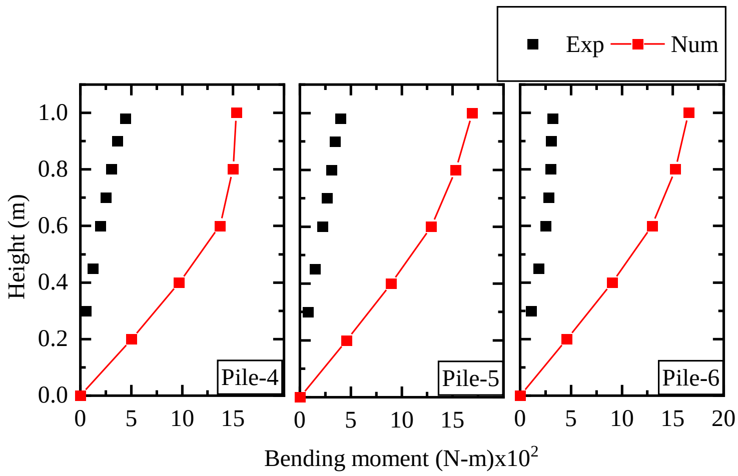

Fig. 2.13: Computed (using HLS parameters) and experimental bending moment profiles of Pile-4, Pile-5, and Pile-6 at 37.2 s when the head of Pile-6 experience maximum bending moment.

2.4.4 Strut effect of bridge girder

In Experiments-2 and 3, a rigidly fastened strut is placed extremely close (only 5 mm) to the face of the abutment to examine the strut effect of the bridge girder. In the experiment, the model abutment is designed based on the old Japanese standard for highway bridge design. Numerically, the effect of the strut is modeled by imposing a constraint on the horizontal movement of the abutment. The Tohoku Earthquake ground motion is also used here as an input ground motion. In order to compare the dynamic response of the abutment, both the Model-1 and Model-2 are analyzed. The comparison of maximum bending moment distribution of piles at 37.2 s in Model-1 and at 38.2 s in Model-2 during Tohoku ground motion data is shown in Fig. 2.14. The strut effect completely changes the bending moment distribution profile. The red color line represents the bending moment profile for Model-2 where there is a constraint in horizontal movement of the abutment. Two different peaks are observed, one exists at the middle height of the pile and the other is near the pile head. A similar response is also observed in experimental results. This kind of bending moment distribution implies a backward rotation of the abutment. In these circumstances, a significant part of the horizontal forces imposed due to lateral spreading is shared by the strut causing a considerable reduction of bending moments along the piles.

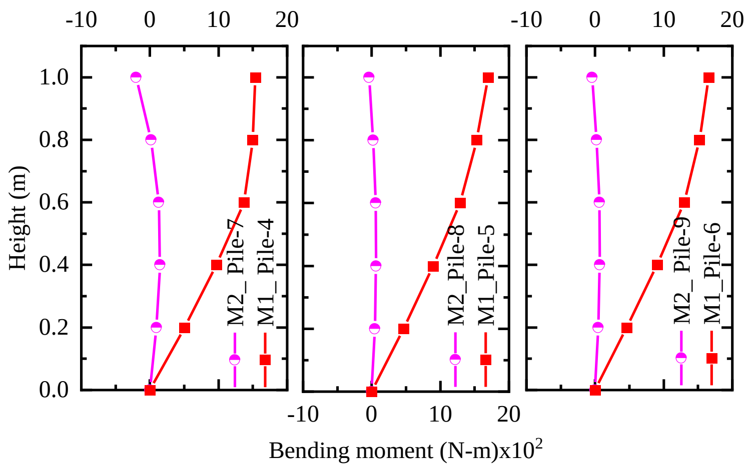

Fig. 2.14: Bending moment distribution of piles in at 37.2 s in Model-1 and at 38.2 s in Model-2 when the heads of Pile-6 in Model-1 and Pile-7 in Model-2 experience maximum bending moment (HLS parameters).

2.4.5 Effect of the width of the embankment

The abutment is subjected to the destabilizing forces from the soil mass inside the probable wedge of failure and the side frictions caused due to the flow of side soils. In order to examine the effect of the width of the embankment in failure mechanism, an abutment model similar to the Model-2 with a finite width of the embankment at its top, which is regarded as Model-3, is analyzed. The response of the model abutment is also studied under the Tohoku Earthquake motion. The comparison of the bending moment profiles is illustrated in Fig. 2.15. The figure represents that the pile-7 in Model-3 is experiencing a smaller bending moment in comparison with the piles in Model-2. Quantitatively almost 25 percent of the maximum bending moment is reduced due to the removal of the extended part of the embankment. The bending moment in all other piles is almost similar. Lateral spread of the embankment in Model-3 in the direction perpendicular to the axis of the embankment may reduce the lateral pressure on the pile-7 thus reduce the bending moment.

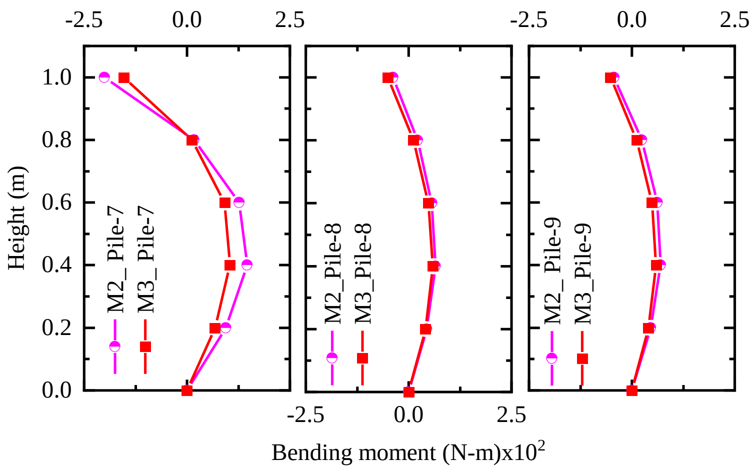

Fig. 2.15: Comparison of the bending moment profile of piles at 38.2 s in Model-2 and Model-3 when pile head (Pile-7) experience maximum bending moment (HLS parameters).

2.5 Effect of sheet pile

A large shake table test (Experiment-4) conducted by PWRI is simulated using two-dimensional finite element analysis. Experiment-4 is conducted by PWRI to observe the efficiency of sheet pile as a seismic retrofit for piled abutment resting on a 10 m thick liquefiable soil in the prototype. The configuration of the model ground and the abutment is similar to the Experiment-2. In addition, a sheet pile is installed in front of the abutment on the channel side to prevent lateral spreading. The plan view and the longitudinal section of the experimental setup are shown in Fig. 2.16. The sheet pile having the equal width of the abutment is placed in front of the abutment on the channel side. The tip of the sheet pile is fixed to the container base. The bending stiffness of the sheet pile is 3.9 $\times 10^{10}$ N.mm^2. The specifications of the piles are listed in Table 2-2.

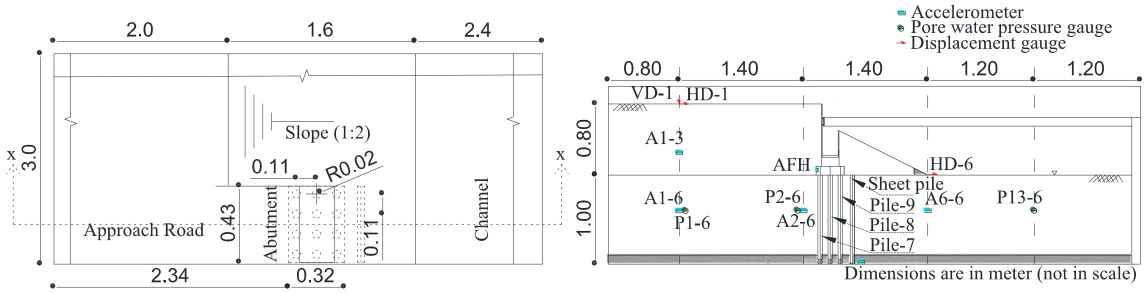

Fig. 2.16: a) Plan view and b) x-x section of Experiment-4.

2.5.1 Finite element model and applied ground motion

Two-dimensional finite element analysis is usually conducted under plane strain condition, which is considered as a limitation of this technique to model a structure having a finite width in the transverse direction. However, because of its less computational demand with reasonable accuracy, two-dimensional finite element analysis is used herein these analyses. It is simplified that the extended part of the embankment width does not have a significant effect on the structural response. Therefore, the width of the embankment is considered as the equal width of the abutment, which imposes a three-dimensional essence in a two-dimensional analysis. The soil is modeled with four-node quadrilateral elements and the piles and sheet piles are modeled with elastic beam elements. A master and slave node technique is used which imposes an identical deformation between the nodes of the structural elements and the corresponding linked nodes of the soil element. The bending stiffness of four piles in a row in the experiment is estimated as the bending stiffness of the representative pile for that row to model the piles in the plane strain condition.

The elasto-plastic constitutive model proposed by Asaoka et al. (2002) is also used in two-dimensional finite element analysis to predict the dynamic behavior of soil elements. Two different sets of parameters are used to define the low liquefiable soil (LLS) and highly liquefiable soil (HLS) as it is mentioned before. The LLS parameters show better agreement with the liquefaction resistance curve of the Silica Sand No. 6, which is used to simulate the shake table experiment. Whereas, the HLS parameters are used to see the response of the similar model under highly liquefiable condition. Besides, the abutment is modeled as four-node elastic solid elements and the piles and the sheet piles are designed as elastic beam elements. It is unlikely the piles behave elastically in reality rather some plastic hinge may develop, which may cause excessive rotation which is beyond the scope of this study. Therefore, all the structural elements in this study are regarded as a perfectly elastic material. The parameters of the structural elements are listed in Table 2-5. The acceleration time histories, recorded at the base of the container during the experiment, are used in this analysis as an input ground motion. The recorded data may contain background noise from different sources. The noises are removed by a bandpass filtered (frequencies in between 0.1 Hz to 25 Hz) using a computer-based software (Seismosignal-2016). The acceleration time histories of the input ground motion are shown in Fig. 2.17.

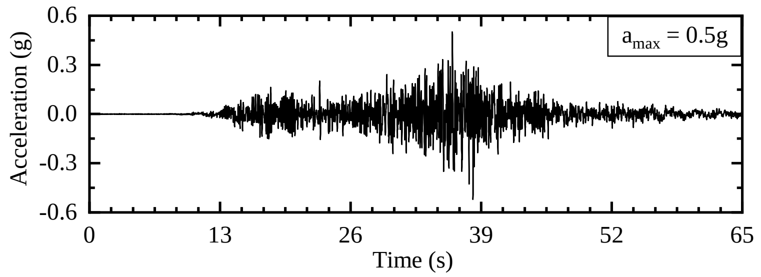

Fig. 2.17: Input ground motion in Experiment-4.

2.5.2 Comparison of experimental numerical results

The calculated deformed shape of the model ground almost at 64.96 s is plotted in the frame of the original shape of the model ground, as shown in Fig. 2.18. The picture presents clear evidence of lateral displacement of the ground towards the channel. Simultaneously, the surface of the embankment is observed to go under considerable settlement. The locations of the embankment near the outer boundary and the vertical wall of the abutment are observed to settle more than the surrounding areas. In these analyses, the periphery of the ground is modeled as a rigid boundary. Besides, the boundary conditions imposed on the abutment wall prevents its horizontal movement at the top. These boundary conditions instigate the pounding between the ground and those relatively rigid boundaries which may cause excessive settlement at that location resulting in a convex shape of the embankment surface. The comparison of the simulated and measured displacement at different locations is illustrated in Fig. 2.19. The graph for the LLS parameters shows good agreement with the experimental results. Whereas, the ground exhibits excessively large deformation in the case of highly liquefiable soil (HLS). It implies that the severity of the lateral spreading significantly depends on the proneness of that soil to be liquefied.

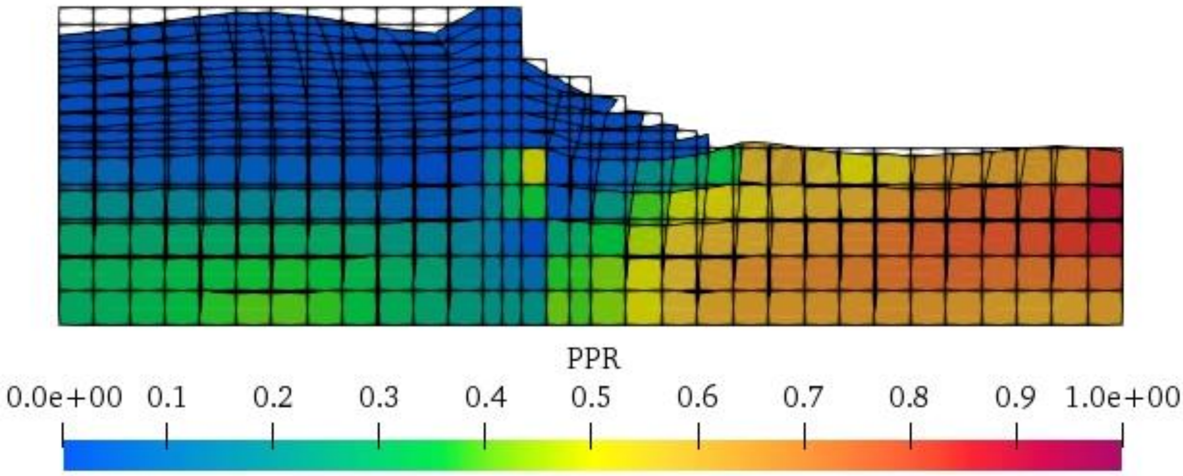

Fig. 2.18: Deformed shape of the model ground at 64.96 s of shaking (LLS parameters).

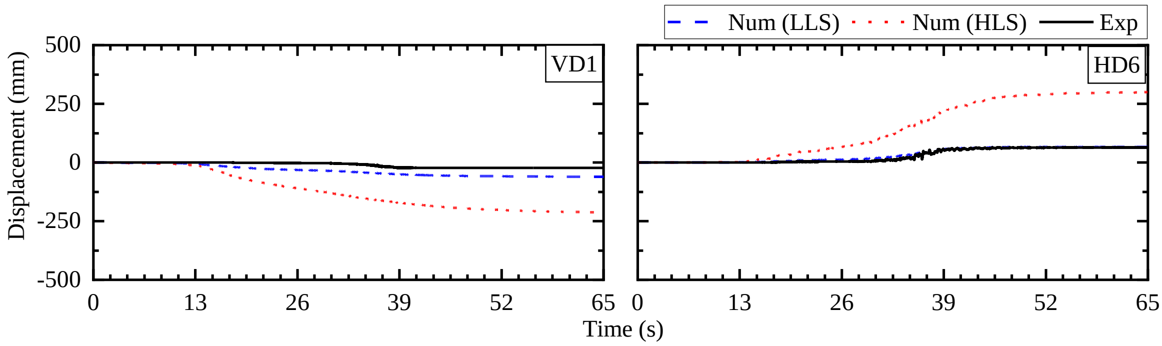

Fig. 2.19: Comparison of simulated and measured displacement of the ground at DV1 and HD6 (Experiment-4).

2.5.3 Evolution of excess pore water pressure

The comparison of simulated and measured pore water pressure generation time histories under the embankment and inside the channel is presented in Fig. 2.20. The graph shows that the excess pore water pressure inside the channel (P13-6) almost reaches up to the initial vertical effective stress denoted by the horizontal straight line (r_u = 1.0) both in experimental and numerical results which represents the liquefied state of the ground inside the channel. However, the simulated excess pore water pressure underneath the embankment, though follow a similar trend as that of the experimental results, is bigger in magnitude. None of the measured and calculated results at that location reaches up to the state of liquefaction under the embankment. Usually, partially saturated soil exhibit delayed generation of pore water pressure and pretends like a dense soil. This kind of phenomenon is observed in the experimental results which demonstrate the degree of saturation is not so high in the experiment. In order to simulate the seismic response of the partially saturated soil, the parameters (LLS) are selected in such a way so that it exhibits higher resistance against liquefaction. The LLS parameters can minimize the magnitude of excess pore water pressure to some extent in comparison with the excess pore water pressure obtained using HLS parameters, as shown in Fig. 2.20. However, the early generation of pore water pressure cannot be avoided.

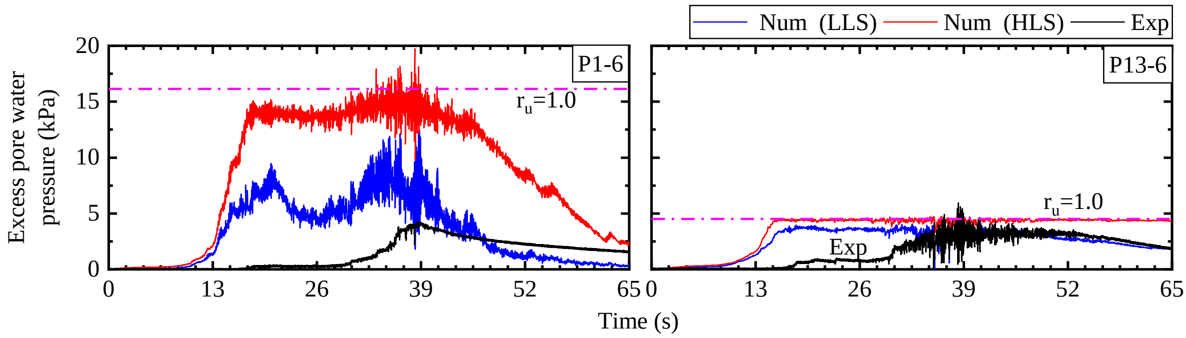

Fig. 2.20: Excess pore water pressure time histories (Experiment-4).

2.5.4 Pile bending moment

Both the experimental and numerical results confirm that the maximum bending moment takes place near the head of the pile and the Pile-7 located at the backfill side is likely to experience the maximum bending moment. The bending moment profiles for Pile-7, Pile-8, and Pile-9 are plotted while the maximum bending moment takes place near the head of Pile-7 and compared with the measured values, as shown in Fig. 2.21. The graph illustrates that the numerical results can reasonably simulate the bending moment of piles along with its distribution pattern. Pile-7 experiences maximum bending moment nearly at 38.21 s in the experiment, whereas it takes place at 38.22 s in the numerical analysis. An increasing trend in bending moment near the head of the pile which is primarily caused by the kinematic earth pressure starts with the generation of excess pore water pressure and stops immediately after the dissipation phase starts (nearly at 39.00 s) underneath the embankment. However, the maximum bending moment takes place immediately before that transition phase with the combination of kinematic and inertial earth pressure. Therefore, the early generation of pore water pressure in the numerical analysis may increase the magnitude of the bending moment however the maximum bending moment takes place nearly at the same time in the experiment and numerical analysis.

2.6 Performance of sheet pile as a seismic retrofit

In order to determine the efficiency of the sheet pile as a seismic retrofit, two additional finite element (FE) models have been analyzed. In the first FE model (Case-1), the sheet pile has been omitted from the model (Case-2) described in the preceding sections, and in another FE model (Case-3), the sheet pile has been extended into the non-liquefiable layer up to the slope surface. The primary purpose of installing sheet pile is to minimize the bending moment demand caused due to lateral spreading. Therefore, the capability of the sheet pile to reduce the bending moment of existing piles of the abutment is regarded as its efficiency in this study. The bending moment profiles of Pile-7, Pile-8, and Pile-9 at 38.2 s are plotted as described in the previous section for all the three cases and compared as illustrated in Fig. 2.22. It is worth-mentioning that LLS parameters have been used in these numerical analyses. The figure shows that the sheet pile can considerably reduce the bending moment although, the extension of the sheet pile inside the non-liquefiable layer does not have significant advantages over the sheet pile in Case-2 where sheet pile is kept up to the liquefiable layer. Although the extension of sheet pile does not have any additional advantages in reducing bending moment, it is advantageous to some other natural disaster, for example flooding or overflow of the river.

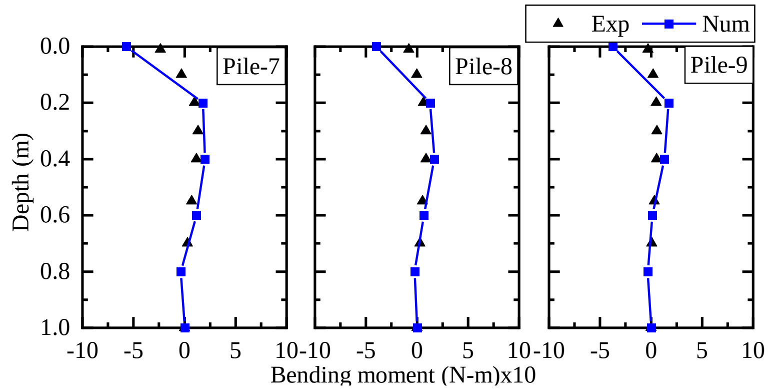

Fig. 2.21: Comparison of measured and simulated bending moment profiles of Pile-7, Pile-8 and Pile-9 at 38.2 s in Experiment-4 (LLS parameters).

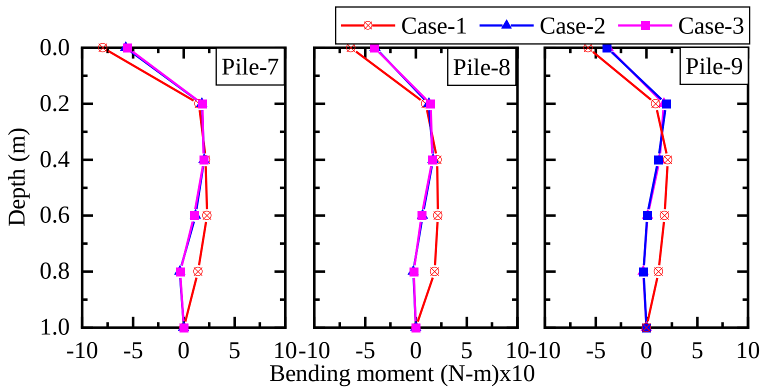

Fig. 2.22: Bending moment profiles of Pile-7, Pile-8 and Pile-9 in Case-1, Case-2, and Case-3 at 38.2 s when the pile head of Pile-7 experiences maximum bending moment (LLS parameters).

2.7 Effect of the stiffness of sheet pile

The severity of liquefaction depends on the state of liquefaction. The highly liquefiable soil is considered to be more hazardous than low liquefiable soil. Therefore, the effect of stiffness of the sheet pile on the response of existing piles resting both in LLS and HLS is described in this section. Besides, the experimental and the analytical results show that the absence of bridge girder during lateral spreading alters the bending moment distribution along the length of the pile. Excessively nonuniform lateral movement of soil may cause unseating of the bridge girder which leads the uninterrupted channel-ward movement of the abutment resulting in the maximum bending moment near the head of the Pile-9 which is located at the front face near the channel. Therefore, the maximum bending moment at the head of both Pile-7 and Pile-9 with the presence and absence of bridge girder is mostly focused in this section. In order to determine the effect of stiffness of sheet pile, several finite element analyses have been conducted with a varying bending stiffness of sheet pile from 0*EI to 5*EI. Where 0*EI implies the FE model without any sheet pile and 5*EI represents the sheet pile stiffness five times of the sheet pile used in the experiment. All the analyses are conducted under both HLS and LLS conditions, and the results are compared in Fig. 2.23. The symbol “wg” and “ng” in the legend of Fig. 2.23 indicates “with girder” and “no girder”, respectively. Maximum bending moment in pile-7 and pile-9 takes place at a different time of the shaking depending on the existence of bridge girder, and the level of liquefaction occurs in the analyses. Analyses results show a sharp reduction in bending moment demand of the existing piles with increased stiffness of sheet pile up to 1.5*EI. The rate of change of bending moment is considerably smaller beyond this range. It implies that the efficiency of sheet pile to prevent lateral spreading does not proportionally increase with the increase of stiffness at the higher range. Therefore, a sheet pile having excessively large bending stiffness is probably less cost-effective in this regard.

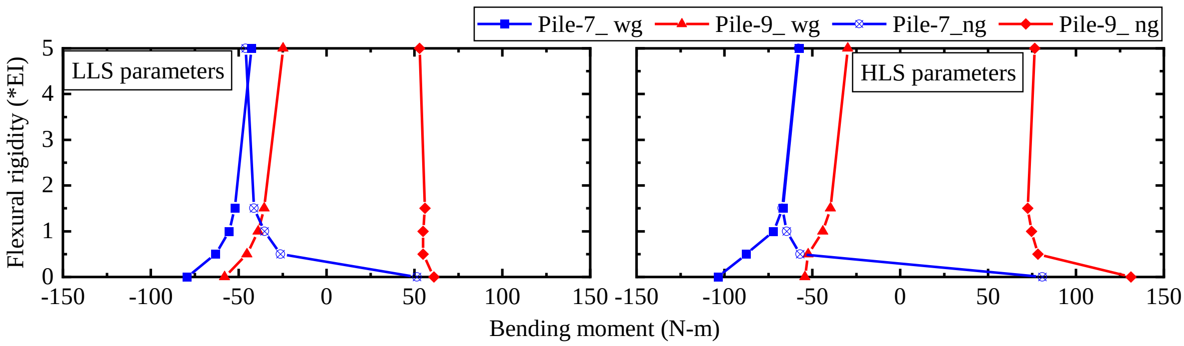

Fig. 2.23: Effect of stiffness of sheet pile to prevent the failure of existing piles.

2.8 Summary

This chapter describes the seismic response of pile-supported bridge abutment. A fully-coupled three-dimensional (3D) finite element analysis is adopted here. A large-scale shake table test of a model abutment designed based on the current Japanese standard is simulated. Another two model abutments designed based on the old Japanese standard with the different geometrical shapes of the embankment are also analyzed to observe the strut effect of bridge girder and the influence of the width of the embankment on the failure mechanism of the bridge abutment. The two-dimensional (2D) finite element analysis is also used here to simulate a shake table to observe the performance of sheet pile as a seismic retrofit. The key findings of this chapter can be summarized as follows;

The 3D finite element analysis can capture the overall response of the bridge abutment subjected to lateral spreading although the magnitudes of the measured parameters for example pore water pressure, horizontal displacement, and bending moment, are smaller than the simulated results.

Accumulation of displacement of both soil and abutment starts with the generation of excess pore water pressure. Significant permanent displacement of soil and as well as structural system toward the channel may take place if the foundation soil gets liquefied.

The maximum bending moment takes place near the head of the piles in all kinds of arrangements. The development of the maximum bending moment in the pile is not necessarily coincided with the arrival of the principal shock. Backward rotation of the abutment is observed due to the strut effect of the bridge girder.

Removal of the extended part of the embankment outside of the approach road may reduce the maximum bending moment up to 25%.

The 2D finite element analysis presents that the installation of sheet pile can considerably reduce the bending moment demand of the existing piles of the abutment during lateral spreading.

The extension of sheet pile inside the non-liquefiable layer of the embankment does not show any additional advantages on the seismic performance of the abutment. However, it is recommended for ease of installation and better maintenance during flooding.

An increase in stiffness of sheet pile increases its efficiency as a seismic retrofit for the piled abutment up to a certain range. However, the efficiency of the sheet pile to prevent lateral spreading does not proportionally increase with the increase of stiffness at a higher range.

[This page intentionally left blank]

Chapter 3

Performance of sheet pile to mitigate liquefaction-induced lateral spreading of loose soil layer under the embankment

3.1 Introduction

Liquefaction-induced lateral spreading causes massive damage to the structures. A large number of earthen structures, for example, river dykes, levees, dam, and road embankments are observed to fail severely during past earthquakes (Yegian, Ghahraman, & Harutiunyan, 1994; Matsuo, 1996; Sasaki et al., 2012). Several experimental and numerical studies have also been conducted to investigate the seismic failure of the embankment and the influence of the liquefiable foundation soils and its non-homogeneity (Kokusho, 1999; Aydingun & Adalier, 2003a; Maharjan & Takahashi, 2014). The post-earthquake survey and the experimental studies reported that the liquefaction of the foundation soils likely causes the seismic damage of the earthen embankment. Therefore, the mitigation of liquefaction-induced lateral spreading of the foundation soil, which could potentially reduce the seismic damage of the embankment, is the focus of this study.

Liquefaction is the phenomenon of saturated sand which causes a significant loss of shear strength of soil due to the generation of excess pore water pressure. Extensive researches have been conducted on the remedial measures against liquefaction-induced damages. The remedial measures are broadly divided into two types; a) prevention of the liquefaction using ground improvement and b) reduction of the ground deformation using reinforcement. The ground improvement techniques, i.e. ground densification, is reported as a potential remedial measure for liquefaction-induced damages in the previous earthquakes (Watanabe, 1966; Ishihara, Kawase, & Nakajima, 1980; Yasuda, Harada, Ishikawa, & Kanemaru, 2012) which is also confirmed in experimental and numerical studies (Liu & Dobry, 1997; Korhan Adalier, Elgamal, & Martin, 1998; Okamura & Matsuo, 2002; Korhan Adalier & Aydingun, 2003). The stone column is another densification technique commonly used for liquefaction mitigation (Korhan Adalier & Elgamal, 2004; Asgari, Oliaei, & Bagheri, 2013). The stone column technique densifies the surrounding soil, and at the same time, it provides vertical drainage for the dissipation of excess pore water pressure. The use of ground densification techniques may not be suitable for the existing structures without interrupting its facilities. The chemical stabilization using colloidal silica may be one of the techniques that can be applied to the existing structures (Conlee, Gallagher, Boulanger, & Kamai, 2012). Centrifuge experiments, as well as the field tests, show that the colloidal silica can mitigate the liquefaction of the ground, thus reducing the associated damages (Conlee et al., 2012; Pamuk et al., 2007; Gallagher, Conlee, & Rollins, 2007). Since the colloidal silica solution in this method is transported through the soil matrix by permeation, uniform dispersion near a river may not be easy because of the contribution of the seepage flow from the water body.

The sheet pile is one of the reinforcement techniques commonly used to prevent the lateral spreading of the liquefied soil. Application of sheet pile to prevent the lateral spreading of the foundation soil under existing houses or earthen dykes/embankments have been studied before (Tanaka, Kita, Iida, & Saimura, 1996; Tanaka, Murata, Kita, & Okamoto, 2000; Kogai, Towhata, Amimoto, & Putra, 2000; Mizutani & Towhata, 2001; Motohashi, Yasuhara, Komine, & Murakami, 2011; Rasouli, Towhata, & Rattez, 2017; Yasuda & Ishikawa, 2018). The sheet pile in all these cases can significantly reduce the lateral spreading of the subsoil irrespective of the type of superstructures. The sheet pile is usually installed near the toe of both sides of the embankment to prevent the lateral spreading of the foundation soil. The heads of the sheet pile installed at the opposite sides of the embankment are recommended to tie together to enhance its mitigation effects (K. Adalier, Pamuk, & Zimmie, 2004). Besides, the liquefaction of the loose foundation soil inside sheet piles confinement provides base isolation thus reduce the seismic demand of the embankments (Korhan Adalier et al., 1998; Korhan Adalier & Aydingun, 2003). Motamed &Towhata (2010) installed a fixed-end sheet pile in between the quay walls and the pile groups to prevent the failure of the pile group caused by lateral spreading. The installation of sheet pile efficiently reduced the bending moment of the pile groups as well as the lateral spreading of the ground. The observation of the previous studies shows that the sheet pile technology could be a potential remedial measure against liquefaction-induced lateral spreading under the existing structures.

This study focuses on an effective remedial measure to mitigate liquefaction-induced lateral spreading of the loose soil layer under an existing approaching embankment of a river spanning bridge. The ground improvement techniques may not be feasible here, as it is mentioned before. Therefore, the authors consider sheet piles as a potential remedial measure in this case. Besides, the fixed-end sheet pile is almost impossible to achieve in reality. Therefore, the performance of a sheet pile to prevent the lateral spreading of the loose ground is studied here where the sheet pile tip is embedded into the underlying dense ground. Moreover, this study focuses on the performance of sheet pile in various thicknesses of the liquefiable layer, which has not been well studied yet. It is worth mentioning that the effect of bridge abutment is omitted for these series of experimental setups.

This chapter describes the dynamic centrifuge experiments conducted on different foundation and reinforcement conditions. Two experiments are benchmark experiments where the embankment is constructed over a thick and thin liquefiable layer without any reinforcement. The sheet pile reinforcement is used in another three experiments for both the thick and the thin liquefiable layers. The geometry of the embankment remains the same in all the experiments. The dynamic response of the ground, characterized by the surface settlement of the embankment, and lateral movement of the embankment and liquefiable foundation, are compared between the reinforced and unreinforced cases under the action of sequential ground motions.

3.2 Test conditions and procedures

3.2.1 Test conditions

Five centrifuge experiments are carried out at 50 g using the Tokyo tech Mark III centrifuge facility (Takemura, Kondoh, Esaki, Kouda, & Kusakabe, 1999) to examine the applicability of sheet pile as a seismic retrofit against the liquefaction-induced lateral spreading. A sheet pile is used in this study as an indirect reinforcement to mitigate the lateral spreading of the foundation soil. The typical experimental setup consists of a loose liquefiable sand layer (Dr=50%) over a dense sand layer (Dr=90%), supporting an approach embankment. Generally, the embankments are compacted up to some desired level during the construction in reality. However, a loose embankment is used in this experiment to avoid densifying the loose foundation layer. Test conditions are summarised in Table 3-1. Two centrifuge experiments are carried out without any reinforcement to examine the effect of the liquefiable layer thickness on the deformation pattern of the ground. The thickness of the liquefiable layers is 8 m in C-1, and 4 m in C-2 in the prototype scale. The detailed experimental setup for C-1 and C-2 is shown in Fig. 3.1 and the applied scaling law is explained later. Since a river spanning bridge is assumed to be located around section X1, all the sensors are placed in section X1. A sheet pile is used as a mitigation measure in the other three experiments where the thickness of the loose foundation layer is 8 m in C-3 and 4 m in C-4 and C-4S in the prototype scale. The sheet pile tip is installed deep into the dense ground while the other end is extended into the slope of the embankment passing through the loose liquefiable sand layer, as shown in Figs. 3.2 and 3.3. To observe the effect of the width of the sheet pile, C-4S is conducted with limited width (5 m in prototype scale) sheet pile. Whereas, a full-width sheet pile is used in C-3 and C-4. It is to be mentioned here that the half-width of the sheet pile is modelled in C-4S to observe the ground deformation at the middle of the protected area visually from the side window.

Table 3-1: Test conditions.

Test ID	Thickness of liquefiable layer (m)	Existence of sheet pile	Width of sheet pile (m)	Relative density (%)		
				Embankment	Loose foundation	Dense foundation
C-1	8.0	No	-	54	53	92
C-2	4.0	No	-	51	54	90
C-3	8.0	Yes	Full-width	54	50	90
C-4	4.0	Yes	Full-width	54	52	88
C-4S	4.0	Yes	5.0	53	52	92

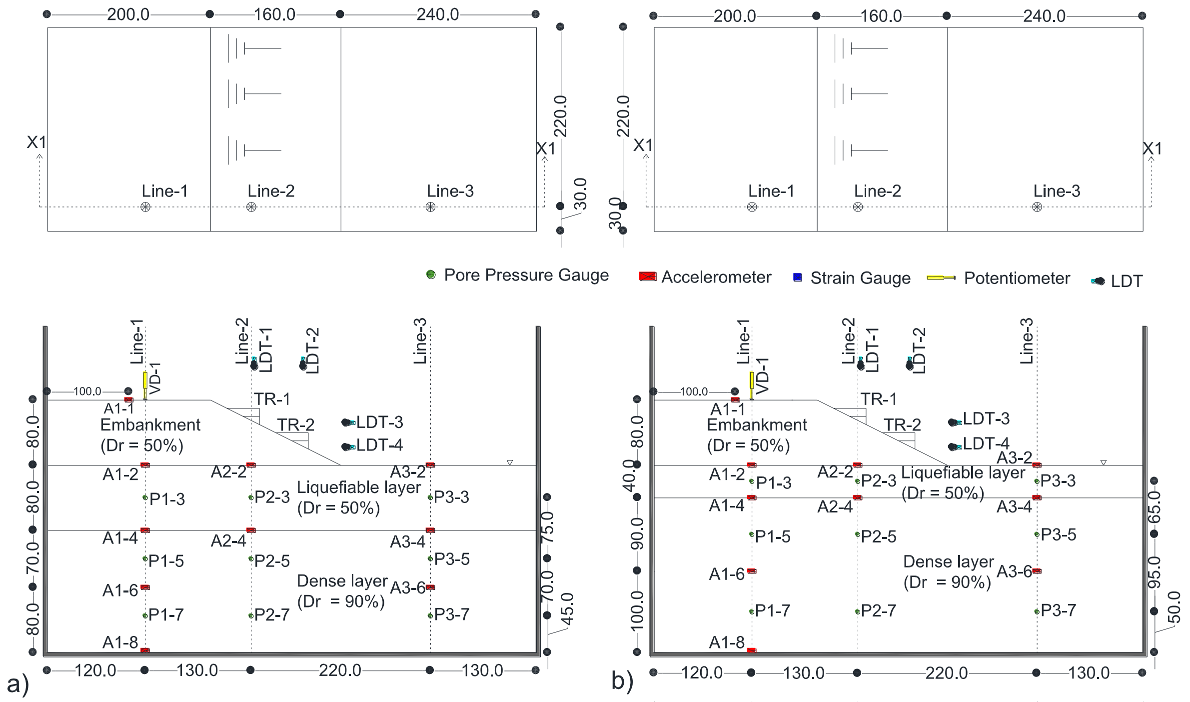

Fig. 3.1: Plan and cross-sectional view of a) C-1 and b) C-2 (all the dimensions are in mm in model scale).

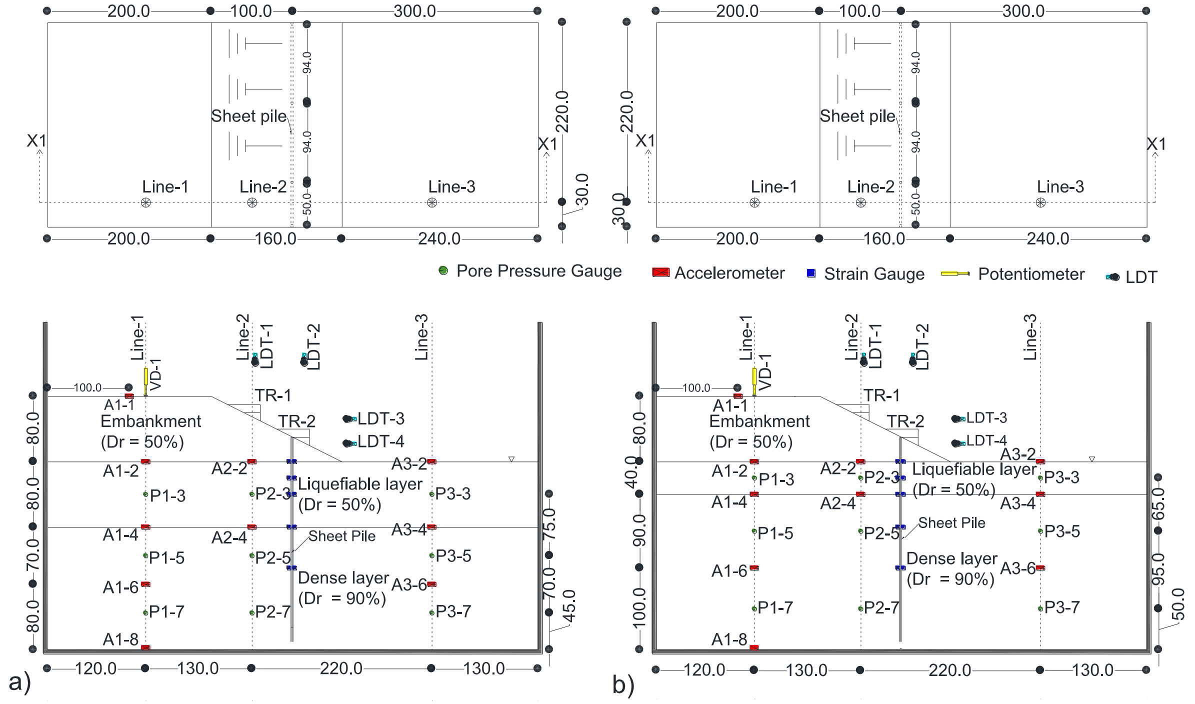

Fig. 3.2: Plan and cross-sectional view of a) C-3 and b) C-4 (all the dimensions are in mm in model scale).

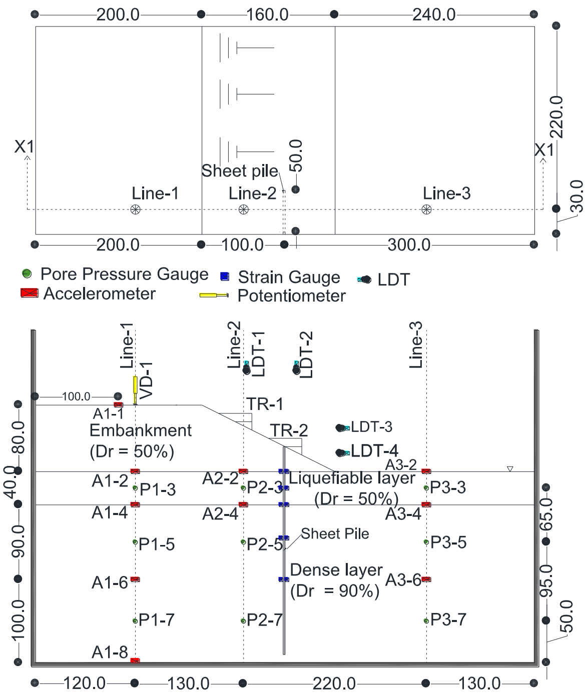

Fig. 3.3: Plan and cross-sectional view of C-4S (all the dimensions are in mm in model scale).

3.2.2 Preparation of the model ground

A rigid container, having the inner dimensions of 600 mm × 250 mm × 400 mm in length, width, and height, respectively, is used to prepare the model ground. The model ground is prepared with Toyoura sand. The physical properties of Toyoura sand are listed in Table 3-2. The air pluviation method is used to prepare the model ground with the desired relative density. The sheet piles are usually driven into the ground in reality. Whereas, the sheet piles during the model preparation are placed inside the container first. The sands are deposited afterward for ease of construction and avoiding excessive densification of the surrounding soils during the preparation at 1 g. A 2.5 mm thick steel plate is used here as a sheet pile. Both ends of the sheet pile are kept free to make the dynamic response more comparable to the real sheet pile. The specifications of the sheet pile in model scale and prototype are tabulated in Table 3-3. Three separate steel plates are used in these experiments to accommodate different widths. The width of the target area that needs to be protected is 50 mm (in model scale) from the container wall. A 50 mm width steel plate is installed at that location in C-4S where the soil beside the steel plate is allowed to move freely. Whereas, in the cases of full-width sheet pile (C-4), two additional plates are added beside the 50 mm width steel plate to mitigate the lateral spreading in the full-width. Two different configurations of sheet pile are used in C-4 and C-4S to investigate whether the uneven lateral spreading of the surrounding ground affects the response of the target area. The steel plates in C-3 and C-4 are jointed together with rubber strips, and the joints are sealed with water repellent material to prevent the flow of fluid between the adjacent sections separated by sheet pile. Different stages of model ground preparation are depicted in Fig. 3.4.

Once the construction of the model ground is finished, the model ground is placed inside an airtight chamber with 760 mm Hg vacuum pressure to saturate with the de-aerated Metolose (60 SH-50) solution (2.2% by weight) to make the viscosity of the pore fluid 50 times of water. Metolose, the commercial name of Hydroxypropyl Methylcellulose from Shin-Etsu Chemical Company, is mixed with water at a specified proportion to increase the viscosity (Adamidis & Madabhushi, 2015) of the solution by keeping the density and surface tension nearly identical to water. Metolose solution is dripped slowly from the top of the model ground and allowed to permeate through the soil media towards the bottom of the container. Thus, the model ground is gradually saturated with the viscous Metolose solution. The model ground is taken out of the vacuum chamber after the saturation of the foundation layers is completed. An embankment is then constructed over the saturated ground. A river approaching embankment is replicated in this experiment. Therefore, the embankment having one side slope (1:2) towards to river channel is prepared, as shown in Figs. 3.1 - 3.3.

Accelerometers, pore pressure gauges, potentiometer, and Laser Displacement Transducers (LDT) are installed to monitor the response of the ground. The accelerometers and the pore pressure gauges are installed during the preparation of the model ground. Several white color markers made of a small nail are placed at different levels inside the model ground, as shown in Fig. 3.4 to track the ground deformation at different layers after the application of sequential ground motions. The sensors are arranged in three lines inside the model, as shown in Figs. 3.1-3.3. The sensors in Line-1 and Line-3 are located under the embankment and inside the river channel, respectively. Whereas, the sensors in Line-2 are located under the slope of the embankment. The potentiometers are placed to monitor the settlement of the embankment surface. The LDTs are installed to track the horizontal movement at the slope.

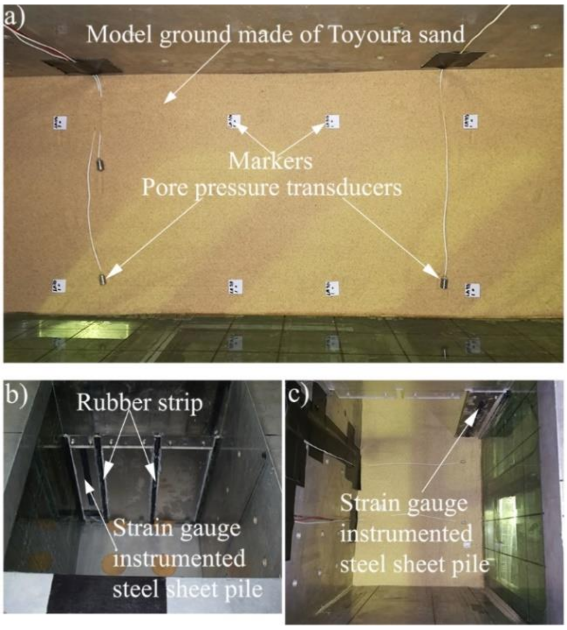

Fig. 3.4: Preparation of model ground; a) placement of sensors inside the ground, b) installation of sheet pile for continuous sheet pile, and c) installation of sheet pile for limited width sheet pile.

Table 3-2: Physical properties of Toyoura sand.

Specific gravity	2.65
Maximum void ratio	0.973
Minimum void ratio	0.609
Mean diameter D_{50} (mm)	0.19
Uniformity coefficient C_u	1.32
Coefficient of permeability (m/s)	2.0×10^{-4} (Dr=50%) and 1×10^{-4} (Dr=90%)

Table 3-3: Specifications of sheet pile in model scale and prototype.

	Model	Prototype
Material type	Steel	Steel
Stiffness EI ($N\text{-}m^2/m$)	2.6×10^2	5.2×10^8
Target sheet pile	-	Hat-type and H-shape composite

3.2.3 Applied ground motions

Two successive ground motions applied to the model ground are shown in Fig. 3.5. The model ground first experiences the Tohoku ground motion. The recorded motion at the base of the model container is similar to the actual one in the Tohoku Earthquake recorded at the ground surface near the New Bansuikyo Bridge, Tochigi (2-I-I-3, NS component), but the magnitude is comparatively smaller. The Tohoku Earthquake recorded at the ground surface near the New Bansuikyo Bridge, Tochigi (2-I-I-3, NS component) is the Level-2 earthquake used for bridge design. The first ground excitation applied to the model ground will be regarded as the Tohoku Earthquake throughout this chapter. The second ground motion consists of sinusoidal waves having a frequency of 1.42 Hz with a maximum amplitude a_{max} = (0.48 - 0.51) g. The sinusoidal waves are applied when the excess pore water pressure developed during the first ground excitation is dissipated completely. One of the purposes of applying the sinusoidal waves is to visualize the ground deformation more clearly. For this purpose, a high frequency and high amplitude sinusoidal waves are applied to the model ground.

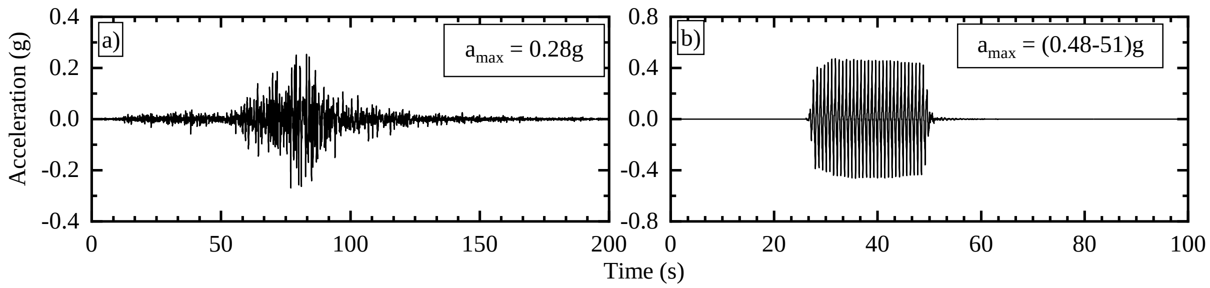

Fig. 3.5: Applied ground motions; a) Tohoku Earthquake and b) sinusoidal waves.

In order to check the repeatability of the applied ground motions, the Arias intensity (Arias, 1970) of the applied ground motions in all the cases is compared for both Tohoku Earthquake and sinusoidal waves. Arias intensity represents the amount of energy applied to the model ground.

The Arias intensity of Tohoku Earthquake and sinusoidal waves for all five cases are compared in Fig. 3.6. The figure shows that the Arias intensity of the applied ground motion in all the cases is almost similar, which indicates the repeatability of the input ground excitation.

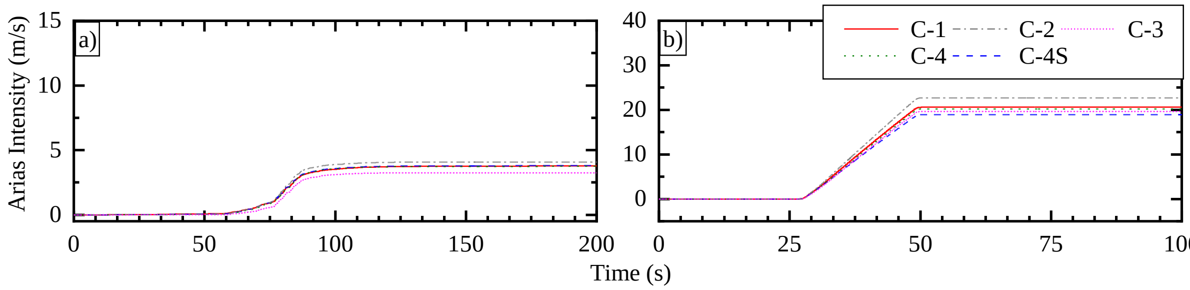

Fig. 3.6: Comparison of Arias intensity of input ground motions; a) Tohoku Earthquake and b) sinusoidal waves.

3.2.4 Scaling laws used in the experiments

The experiments are conducted under the 50 g environment. In order to accommodate a large prototype within the limited dimensions of the centrifuge, a generalized scaling law (Iai, Tobita, & Nakahara, 2005) is applied here. An 1:2 scaled shake table experiment is considered to perform under the 50 g environment. Therefore, a scaling law for the 1 g shake table experiment along with a scaling law for the 50 g centrifuge is applied together while designing the experimental model. The scaling factors used in the experiments for different important parameters are tabulated in Table 3-4. As for the viscosity of the pore fluid, if we follow the generalized scaling law, it should be 70.71 times of water. However, due to difficulties in saturating the model ground with larger viscosity fluid, the viscosity of the pore fluid is set 50. Thus, the permeability of the soils is rather large, and the relatively faster dissipation of the excess pore water pressure is expected.

Table 3-4: Scaling factors used in the experiments assuming $\lambda_\varepsilon = 1.0$ (Iai et al., 2005).

Length	$1/(50 \times 2) = 1/100$
Acceleration	$(50 \times 1) = 50$
Displacement	$1/(50\times2) = 1/100$
Time (dynamic)	$1/(50 \times 2^{0.5}) = 1/70.71$
Frequency	$50 \times 20^{0.5} = 70.71$
Bending stiffness, EI (structure)	$1/(50^4 \times 2^5) = 5 \times 10^{-9}$
Stress	1/2

3.3 Test results and discussions

The dynamic response of saturated ground predominantly depends on the generation of excess pore water pressure and the propagation of the seismic wave. In the following, the ground response to the seismic excitations is described and discussed. All the results are presented in the prototype scale unless mentioned otherwise.

3.3.1 Excess pore water pressure evolution

The soil is considered to be liquefied when the excess pore water pressure (Δu) reaches the initial vertical effective stress (σ_o'). In other words, the liquefaction takes place when the excess pore pressure ratio $r_u = \Delta u / \sigma_o'$ approaches to unity. Pore pressure gauges are placed at different depth under the embankment (P1-7, P1-5 and P1-3), under the soil slope (P2-7, P2-5 and P2-3), and inside the river channel (P3-7, P3-5, and P3-3) to observe the evolution of excess pore water pressure at different locations. The seismic response of the soil inside the river channel significantly influences the ground movement under the embankment. Therefore, the excess pore water pressure time histories inside the river channel (P3-3, P3-5 and P3-7) for the benchmark cases C-1 and C-2 are shown in Fig. 3.7, and Fig. 3.8, respectively.

The pore pressure gauges P3-3 is located in the middle of the liquefiable layer. The r_u value is observed to reach 1.0 at 71.6 s and 61.6 s in C-1 and C-2, respectively during the Tohoku Earthquake, which is 28.0 s and 27.1 s, respectively during sinusoidal waves. It refers that the locations near the surface are liquefied earlier than the deeper locations in the free field. The liquefaction in the dense layer is also observed in the experiments. The pore pressure gauges P3-5 and P3-7 are placed inside the dense layer. P3-5 is located 11.5 m and 8.5 m below the river channel surface in C-1 and C-2, respectively. The r_u value reaches 1.0 at 85.0 s in C-1 while the dissipation of the excess pore water pressure starts immediately after that. Whereas, the liquefaction starts at 80.0 s in C-2 that continues until 128.0 s. The sinusoidal waves cause the liquefied state of the dense layer at P3-5 to continue even after the shaking, which is true for all the cases. The deeper dense layer (P3-7) is not liquefied during the Tohoku Earthquake. The maximum r_u values measured at P3-7 are 0.6 and 0.7 in C-1 and C-2, respectively. However, the sinusoidal waves cause liquefaction in the deeper dense layer as well. The seismic response of the layered ground in the river channel depicts that the dense sand (Dr=90%) can also liquefy under the action of strong ground motion. Similar behavior is also reported by Zeng and Liu (Zeng & Liu, 2012). Besides, the dense soil just below the loose liquefiable layer is found more susceptible to liquefaction than the deeper dense layer.

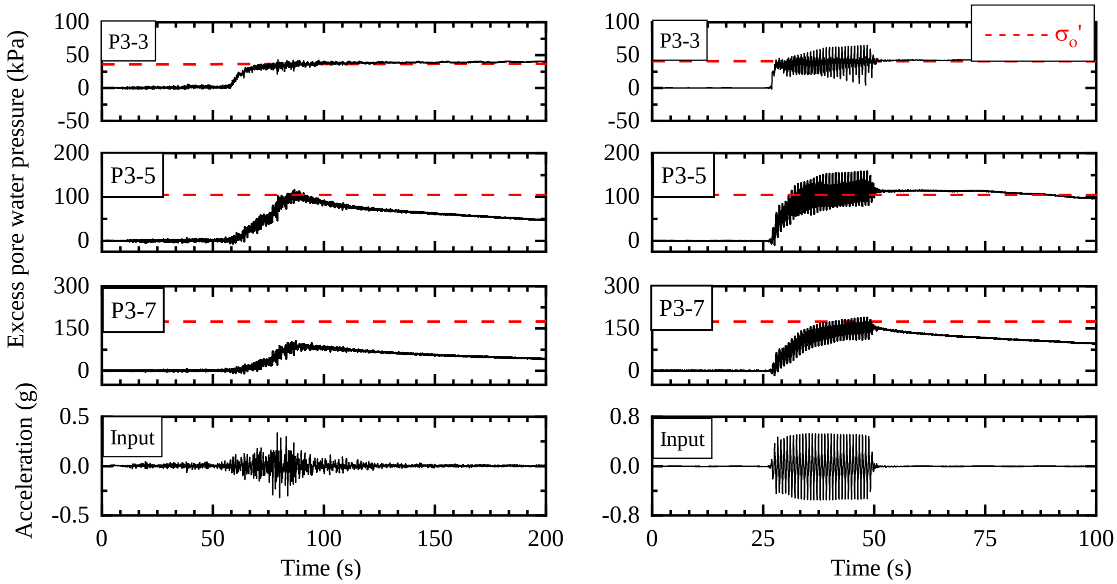

Fig. 3.7: Excess pore water pressure time histories inside the river channel in C-1 during Tohoku Earthquake (left column) and sinusoidal waves (right column).

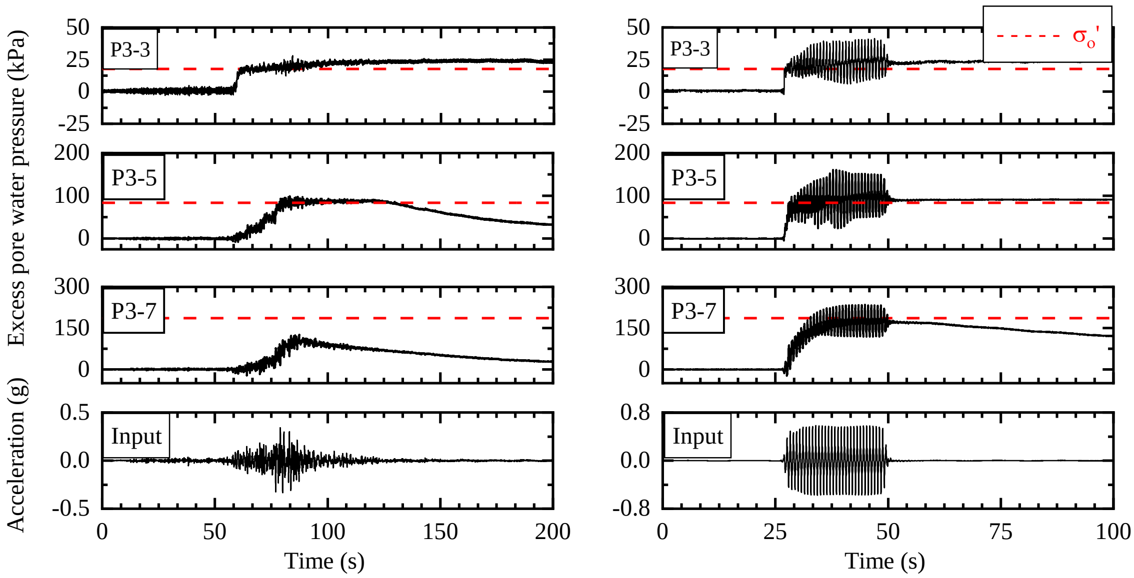

Fig. 3.8: Excess pore water pressure time histories inside the river channel in C-2 during Tohoku Earthquake (left column) and sinusoidal waves (right column).

Figure 3.9 presents the excess pore water pressure time histories in the middle of the liquefiable layer under the embankment (P1-3) for C-1 and C-2. The figure shows that the maximum r_u value is about 0.5 in C-2 whereas the maximum r_u in C-1 reaches 0.9 with larger fluctuation during the Tohoku Earthquake. Similarly, during the sinusoidal waves, the r_u value in C-2 is lower than 1.0, whereas, the middle of the liquefiable layer in C-1 almost get liquefied. Compared to the river channel, the state is relatively far from the liquefaction, probably because of the confinement provided by the embankment. The shear strain time histories, calculated in the middle of the liquefiable layer under the embankment and inside the river channel during the Tohoku Earthquake, are shown in Fig. 3.10 for C-1. The shear strain of a soil layer is calculated from the acceleration time histories recorded at the bottom and the top of the layer at that corresponding location as described in Elgamal et al. (1996). The shear strain in the liquefiable layer under the embankment is significantly smaller in magnitude than the shear strain in the middle of the liquefiable layer inside the river channel. A smaller shear strain in the liquefiable layer under the embankment, probably because of the confinement provided by the embankment, prevents the soil from reaching the liquefied state.

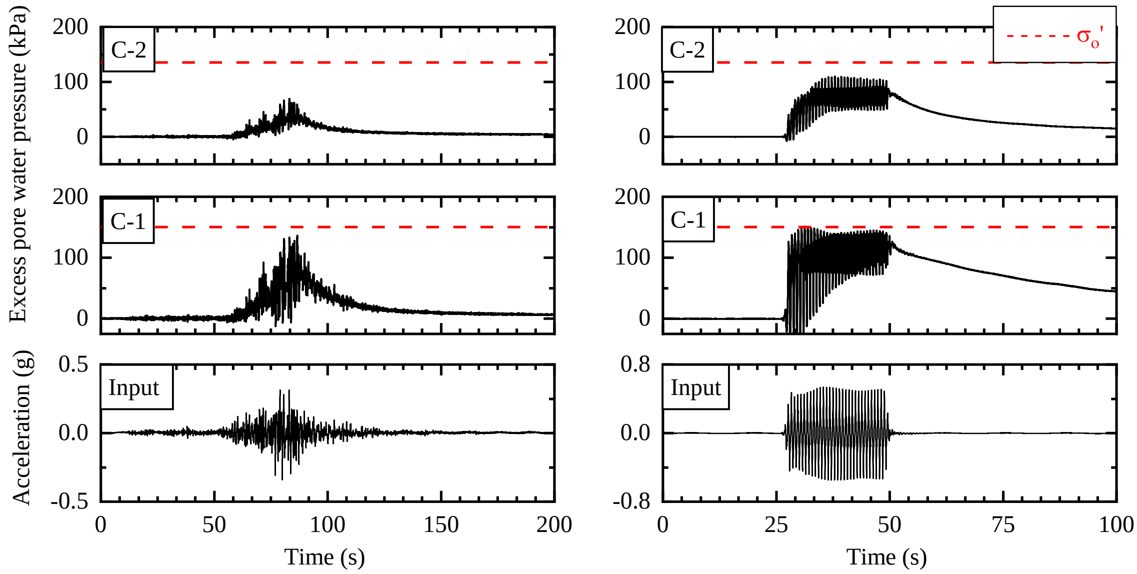

Fig. 3.9: Excess pore water pressure time histories in the middle of the liquefiable layer under the embankment (P1-3) in C-1 and C-2 during the Tohoku Earthquake (left column) and sinusoidal waves (right column).

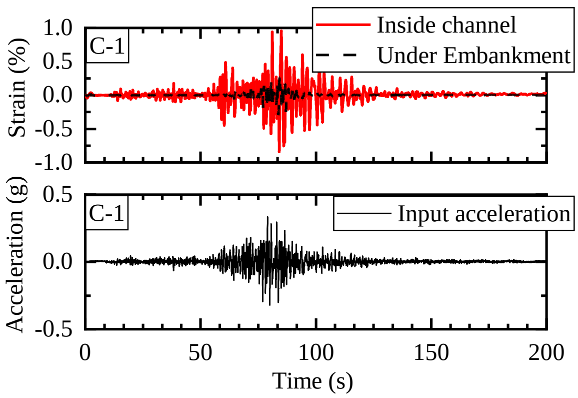

Fig. 3.10: Comparison of shear strain in the middle of the liquefiable layer inside the river channel and under the embankment in C-1.

Figure 3.11 shows the excess pore water pressure time histories in the middle of the liquefiable layer under the embankment slope for C-2, C-4 and C-4S. The excess pore water pressure for both the unreinforced (C-2) and the reinforced cases (C-4 and 4S) are shown here. The figure shows the loose soil under the embankment slope in C-2 almost reaches the liquefied state during the Tohoku Earthquake, whereas, the soil gets liquefied during the sinusoidal waves. The excess pore water pressure in the unreinforced (C-2) and reinforced (C-4 and C-4S) cases is almost similar which is true for the response observed inside the river channel and under the embankment as well. The pore pressure gauges under the embankment slope are installed 5 m away from the sheet piles. It implies that the response of the zone far from the sheet piles is probably insignificantly influenced by the sheet piles. Unfortunately, as the excess pore water pressure at P2-3 in C-3 cannot be recorded because of the malfunctioning of the pore pressure gauge during the experiment, the comparison between the unreinforced and the reinforced cases with thick liquefiable layer cannot be made here.

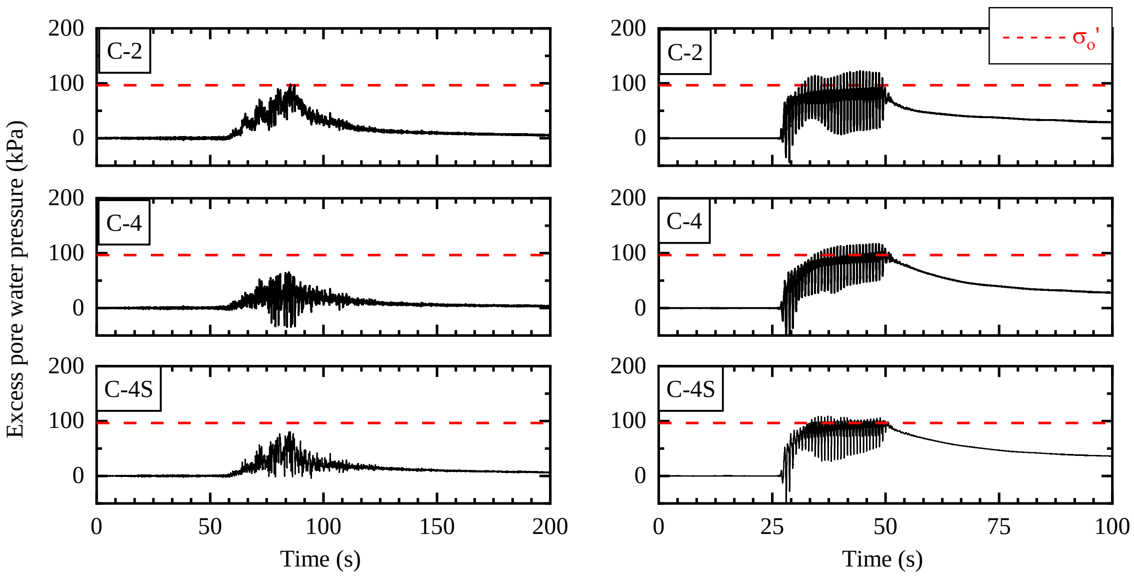

Fig. 3.11: Excess pore water pressure time histories in the middle of the liquefiable layer under the embankment slope (P2-3) in C-2, C-4 and C-4S during Tohoku Earthquake (left column) and sinusoidal waves (right column).

3.3.2 Ground deformation without reinforcement

The centrifuge experiments can successfully produce the liquefaction-induced lateral spreading of the liquefiable soil both in the cases of the thick and thin liquefiable layer. A significant channel-ward movement of the liquefiable foundation soil, as well as the approach embankment, is observed. An attempt is made to show the ground deformation pattern using PIV (Particle Image

Velocimetry) analysis (White & Take, 2002). The embankment slope and the underlying loose foundation is focused in this analysis since the major lateral spreading is observed in this region. The region of PIV analysis in the model ground for C -1 and C-2 is shown in Fig. 3.12. A smaller area is covered in C-2 because of the insufficient light outside of this region. Figures 3.13 and 3.14 show the ground deformation for C-1 and C-2, respectively. All the figures shown here are plotted in the model scale. The movement of the soil at several locations cannot be properly detected in PIV analysis due to the optical obstruction caused by scotch tape attached to the glass window. The displacement vectors at those locations have been removed and left it blank in the figures.

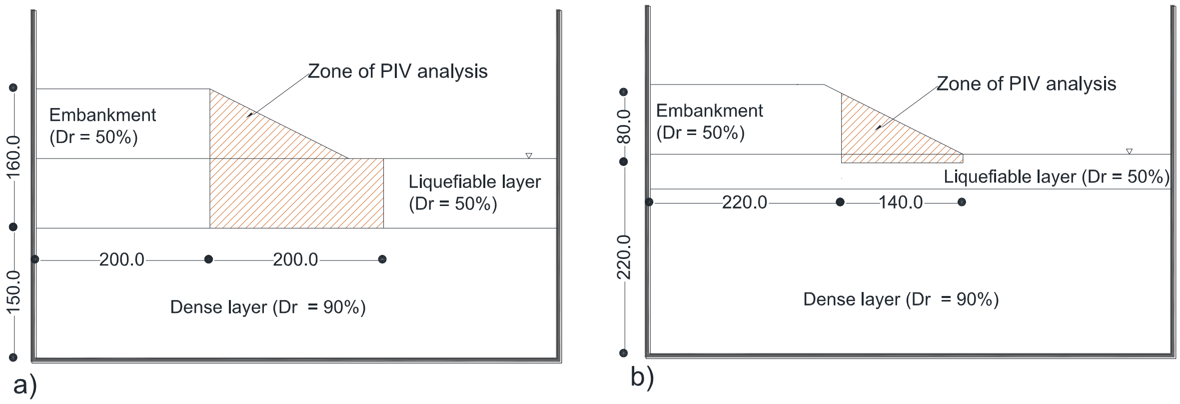

Fig. 3.12: Experimental model along with the zone of PIV analysis for; a) C-1 and b) C-2.

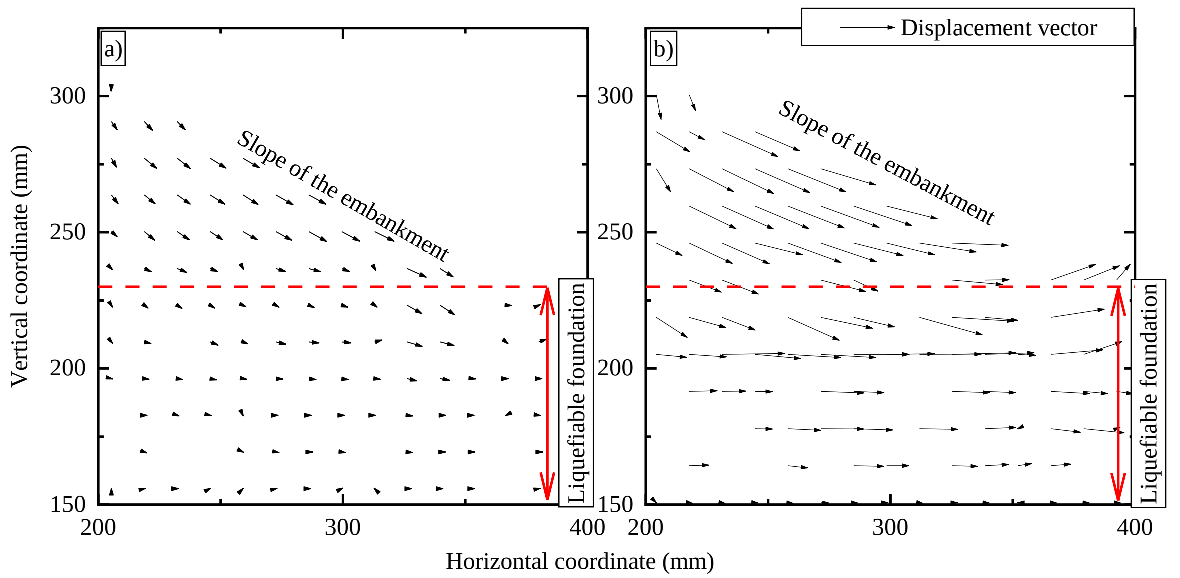

Fig. 3.13: Movement of the embankment slope and the loose foundation soil layer for C-1 in model scale; a) Tohoku Earthquake and b) sinusoidal waves.

The displacement vectors in PIV results show that dry loose soil in the embankment slope moves horizontally as well as goes under a significant settlement. On the other hand, the channel-ward movement is dominant in the loose foundation soil layer. A heaving near the toe of the embankment is also observed especially in the case of thick loose foundation soil layer (C-1) under the strong ground motion of sinusoidal waves. The graphs show that the sinusoidal waves, in comparison with the Tohoku Earthquake, cause a larger ground deformation of the loose embankment as well as a larger lateral spreading of the liquefiable foundation

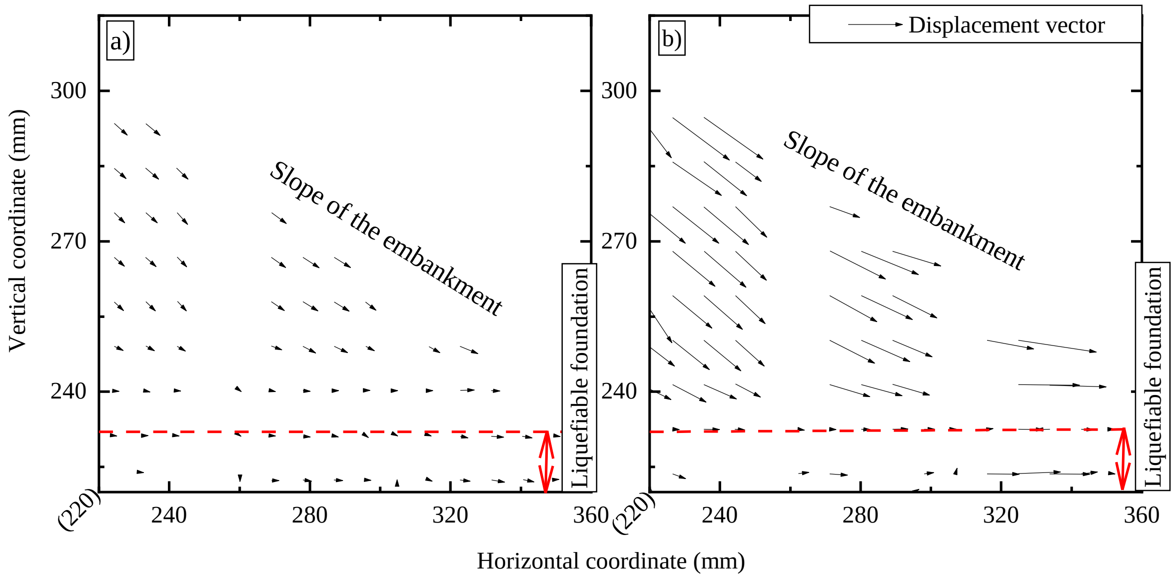

Fig. 3.14: Movement of the embankment slope and the loose foundation soil layer for C-2 in model scale; a) Tohoku Earthquake and b) sinusoidal waves.

3.3.3 Performance of sheet pile to mitigate lateral spreading of liquefiable soil

The sheet pile is used to mitigate the liquefaction-induced lateral spreading of the ground. It is expected that the sheet pile installed deep into the dense ground will perform as a cantilever retaining structure that can prevent or reduce the channel-ward movement of the liquefied soil and the associated deformation of the embankment. The horizontal and vertical displacements at two locations on the embankment slope (TR-1 and TR-2) are measured and compared, as shown in Fig. 3.15.

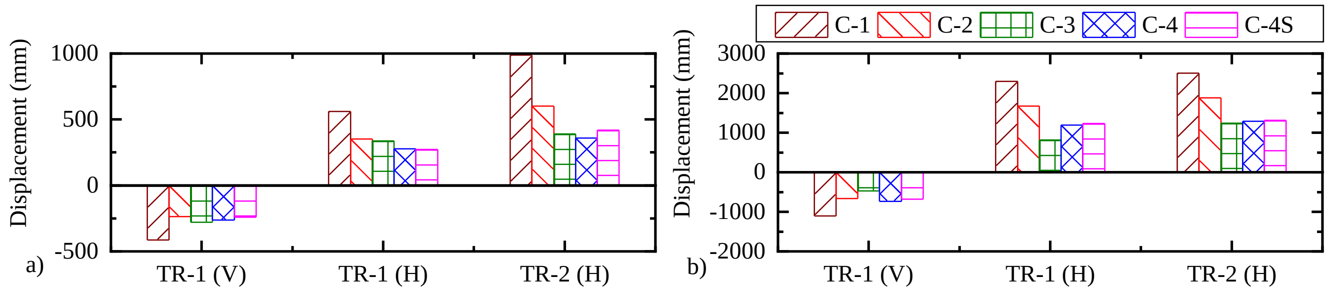

Fig. 3.15: Comparison of horizontal and vertical displacement of targets TR-1 and TR-2 among the reinforced and unreinforced cases; a) Tohoku Earthquake and b) sinusoidal waves.

The term "V" and "H" inside the brackets in Fig. 3.15 represents the vertical and horizontal displacement of the targets, respectively. The results show that the sheet pile can reduce the lateral displacement nearly up to 50% in the case with the thick liquefiable layer (C-3) and 30% in the case of a thin liquefiable layer (C-4 and C-4S) in the middle of the slope (TR-2). Limited width of the ground is protected in C-4S. The soil beside the sheet pile is left unprotected. The unprotected ground aligned in the same position with the sheet pile in the transverse direction (in C-4S) is observed to have larger channel-ward movement than the sheet pile. However, the ultimate horizontal displacement at the head of the sheet pile in C-4 and C-4S is almost similar during the Tohoku Earthquake as well as in sinusoidal waves. It implies that the lateral spreading of the unprotected ground beside the sheet pile doesn't affect its performance much. Therefore, the performance of the limited width sheet pile (C-4S) and the full-width sheet pile (C-4) is almost similar in terms of preventing the lateral displacement of the ground. The result shows that the sheet pile effectively reduces the lateral spreading under sequential ground motions. One of the purposes of the application of sequential ground motion is to observe the applicability of sheet pile if the target structure experiences two strong ground motions. The primary focus is the total reduction of the lateral spreading by the sheet pile. Therefore, the difference in the ground condition between the reinforced and unreinforced model before the application of the sinusoidal waves is not considered during the comparison of the experimental results.

A comparison of the ground deformation (at TR-1) between the unreinforced and reinforced cases during the Tohoku Earthquake is shown in Fig. 3.16. The figure shows that the embankment slope starts to deform with the generation of the excess pore water pressure in the middle of the liquefiable layer under the embankment nearly at 60.0 s. The ground deformation stops immediately after the dissipation of the excess pore water pressure starts at 90.0 s. Since no significant post liquefaction settlement or post-earthquake ground movement is observed, it can be said that the ground deformation is driven by the combination of the cyclic and static shear stress. Installation of the sheet pile can considerably reduce the horizontal movement of the embankment slope for all the cases. However, the vertical settlement of the embankment slope (TR-1 (V)), especially in the cases of the thin liquefiable layer (C-4 and C-4S) cannot be significantly reduced. The vertical settlement of the target is almost similar in both reinforced and unreinforced cases. It implies that the settlement is predominantly caused by the compaction of the loose soil due to seismic excitation.

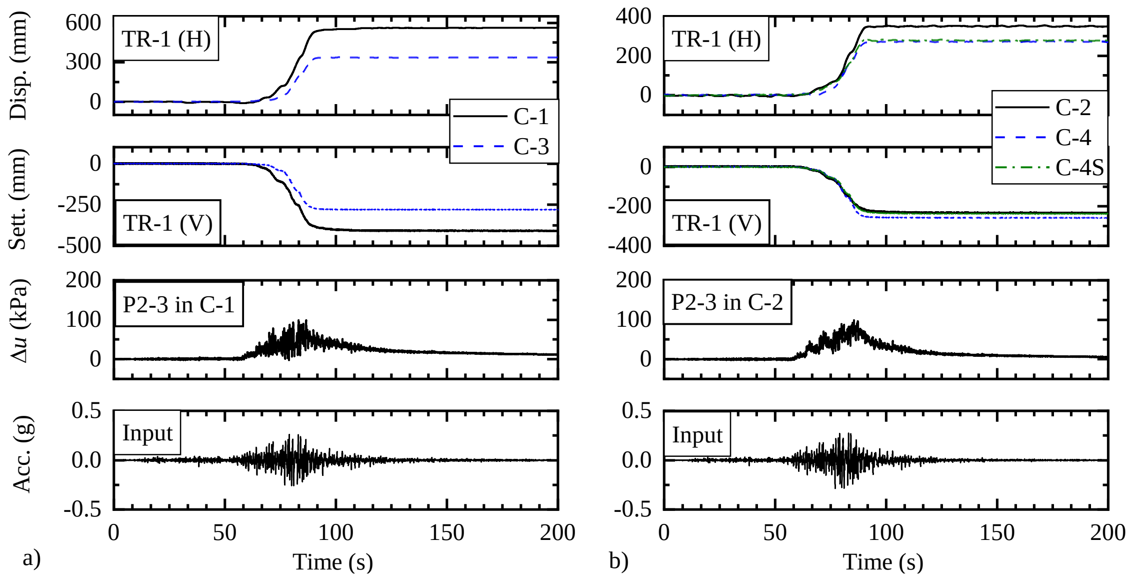

Fig. 3.16: Comparison of the ground deformation time histories at the slope of the embankment (TR-1) between the unreinforced and reinforced cases during Tohoku Earthquake; a) thick liquefiable layer (C-1 andC-3) and b) thin liquefiable layer (C-2, C-4 and C-4S).

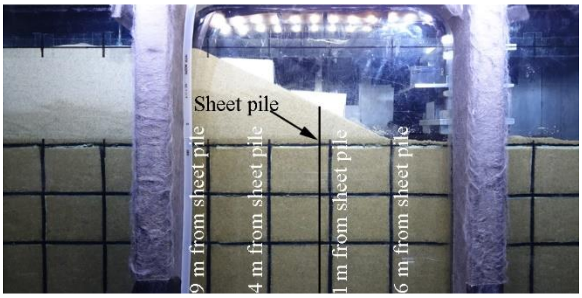

Fig. 3.17: Grid made of colored noodles to observe the deformation of the ground.

An attempt is made to quantify the lateral movement of the liquefied soil behind and in front of the sheet pile. A grid pattern made of vertical and horizontal colored noodles, as shown in Fig. 3.17, are placed at the back of the glass window of the model container to monitor the lateral spreading of the soil. The lateral displacement of the vertical noodles is manually measured after the application of the sequential earthquakes. The displacements of four different lines in Fig. 3.17 are measured and compared, as shown in Figs. 3.18 and 3.19 for the cases of thick and thin liquefiable layers, respectively. The figures show that the maximum lateral spreading of liquefied soil takes place in the thick liquefiable foundation (C-1), which is significantly reduced by the installation of sheet pile (see Fig. 3.18). Similarly, the lateral spreading of soil reinforced with sheet pile for the thin liquefiable layer cases (C-4 and C-4S) is observed to be smaller in comparison with the unreinforced case (C-2), as shown in Fig. 3.19. However, the reduction of the lateral displacement of soil, achieved due to the installation of the sheet pile, decreases with the distance behind the sheet pile (see Figs. 3.18 and 3.19). In general, the installation of the sheet pile makes the horizontal displacement profile of the ground rather straight. Because of this, the displacement in the liquefiable layer is suppressed, while that in the dense layer just below the liquefiable layer becomes somewhat large.

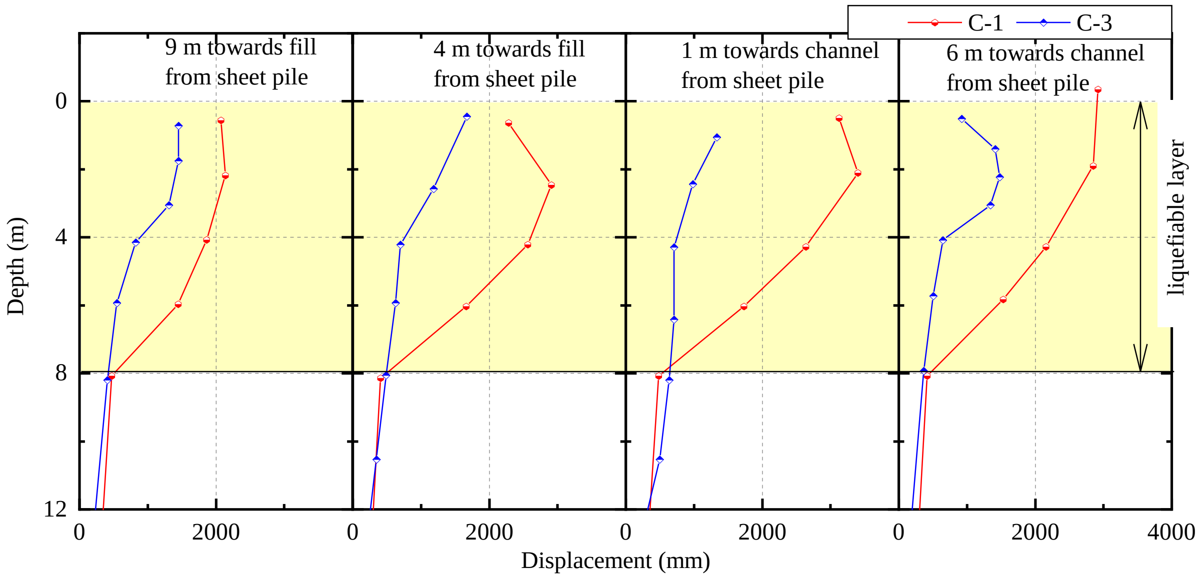

Fig. 3.18: Lateral displacement profiles of sand layers for the cases of thick liquefiable foundation (C-1 and C-3) (measured manually).

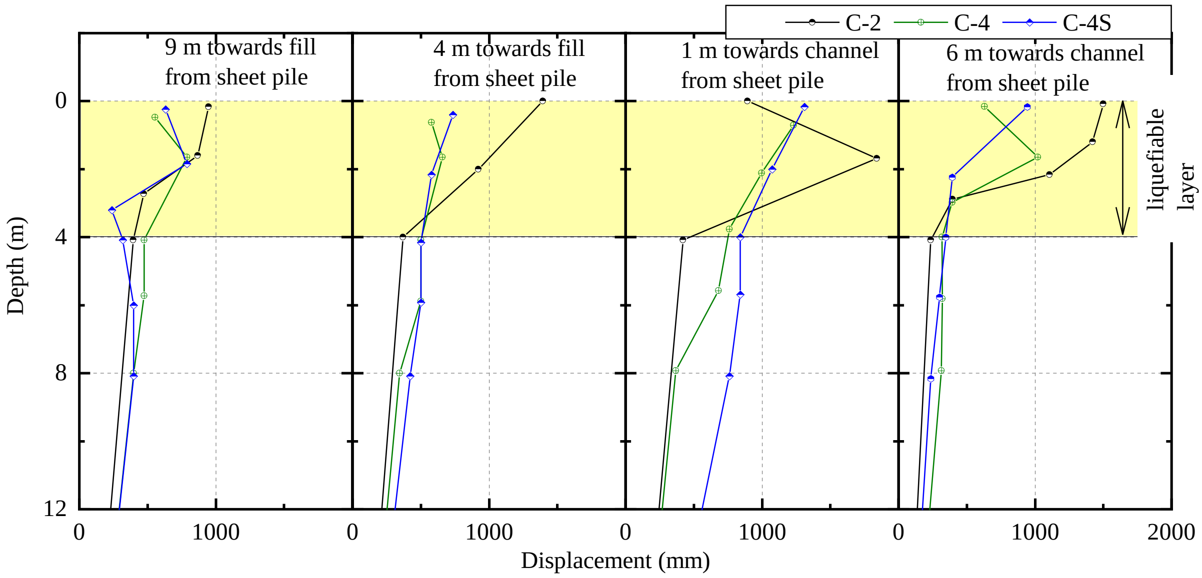

Fig. 3.19: Lateral displacement profiles of sand layers for the cases of thin liquefiable foundation (C-2, C-4 and C-4S) (measured manually).

3.3.4 Bending moment of sheet pile

The sheet pile is expected to experience a large bending moment caused by the forces from destabilized soil due to liquefaction. The sheet pile having a 50 mm width (in model scale) is instrumented with strain gauges at different depths to measure the bending moment. Wheatstone half-bridge configuration is used to wire two strain gauges attached to the opposite side of the sheet pile to get the bending strain only. The installation of strain gauges along the surface of the sheet pile is shown in Fig. 3.20 (a). The sign convention of the bending moment used here is shown in Fig. 3.20 (b).

The sheet pile experiences maximum bending moment around 86.0 s during the Tohoku Earthquake and 48.0 s during sinusoidal waves in all the three cases. A comparison of the bending moment profiles of the sheet pile in C-3, C-4, and C-4S, when the sheet pile experiences maximum bending moment, both under Tohoku Earthquake and sinusoidal waves is shown in Fig. 3.21. The forwards diagonal cross-hatched region in the figure represents the liquefiable layer for C-4 and C-4S, and the combination of forwards and backward diagonal cross-hatched regions in the figure represents the liquefiable layer for C-3. The figure shows that the maximum bending moment takes place 4 m deep into the dense layer rather than the interface of the dense and the loose layer in C-4 and C-4S. The magnitude of the maximum bending moment in the thin liquefiable layer is almost similar in both cases with the full-width sheet pile (C-4) and limited width sheet pile (C-4S). Whereas, the maximum bending moment of sheet pile in the case of the thick liquefiable layer (C-3) is quite larger than the other cases because of the contribution of the thick liquefiable layer. However, the shapes of the bending moment distribution profile in all three cases are almost similar.

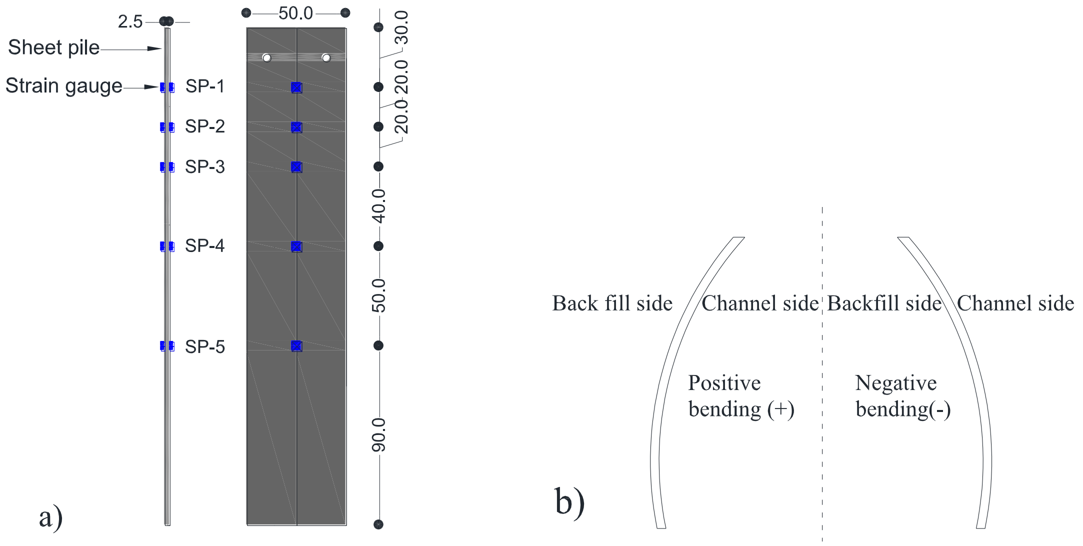

Fig. 3.20: a) Instrumentation of sheet pile with strain gauges (in model scale) and b) sign convention for bending moment.

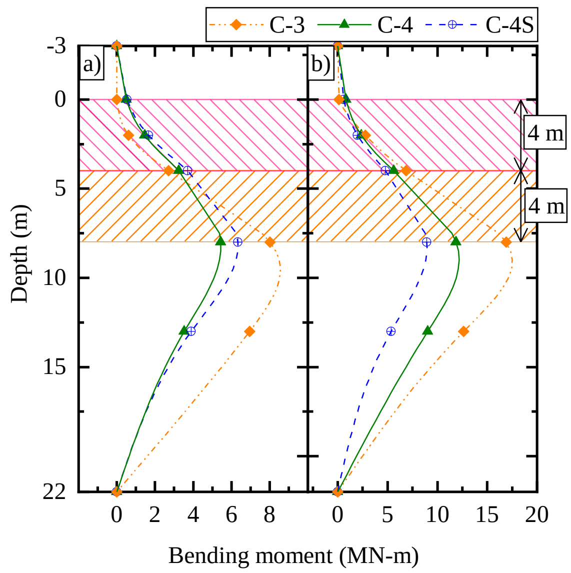

Fig. 3.21: Comparison of bending moment profiles of sheet pile in C-3, C-4, and C-4S while the sheet pile experiences maximum bending moment under; a) Tohoku Earthquake and b) sinusoidal waves.

3.3.5 Earth pressure acting on the sheet pile

The sheet pile is expected to experience a significant earth pressure exerted by the build-up of excess pore water pressure and the spreading of the liquefied soil with the crust layer. The resultant earth pressure that represents the difference of the channel-ward pressure and the resisting pressure acting on the sheet pile is back-calculated from the bending moment distribution using the following equations.

$$p(z,t)=\frac{\partial^2 M(z,t)}{\partial z^2} \tag{5.1}$$

To estimate the resultant earth pressure, double differentiation of fitted polynomial curve through the discrete bending moment data points is one of the popular methods. However, double differentiation of a fitted polynomial curve may produce potential errors, especially near the ends of the structural elements that may mislead the value of the earth pressure. Therefore, the weighted residual method proposed by Brandenberg et al. (2010) is used here. The weighted residual method yields approximate solutions of a differential equation only valid at the boundaries which are assumed to produce less noise in comparison with the exact solution of continuous equations. Both ends of the sheet pile are kept free in the experiment, which yields zero shear force at that location. Therefore, a boundary condition is imposed on the solution that refers to the first derivative of the bending moment $\left(\frac{\partial M}{\partial z}\right)$ at the ends of the sheet pile will remain zero.

Lateral spreading is sometimes considered as a post-liquefaction phenomenon that may take place even after the earthquake stops. Therefore, the trend component of the bending moment is sometimes used to calculate the earth pressure caused by lateral spreading (Haeri et al., 2012). However, in this study, no post-earthquake ground movement is observed. Moreover, the contribution of the cyclic component to the maximum bending moment of the sheet pile especially in the event of the sinusoidal waves is found to vary from 20% (C-3) to 40% (C-4 and C-4S) of the trend component depending on the thickness of the liquefiable layer, as shown in Fig. 3.22. The cyclic component is significantly large, which can change the earth pressure distribution as well. Therefore, the real-time bending moment data, combining both the cyclic and trend components, is used for further analysis.

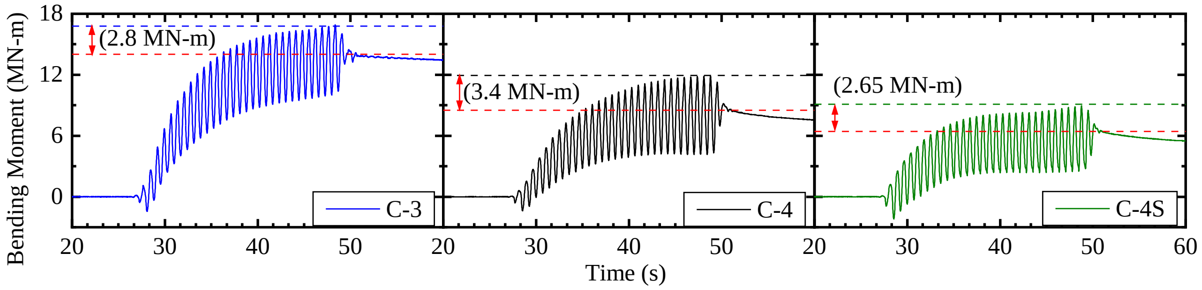

Fig. 3.22: Bending moment time histories of the sheet pile where the sheet pile experiences maximum bending moment (SP-4) in C-3, C-4, and C-4S.

The resultant earth pressure back-calculated from the measured bending moment data represents the difference of the channel-ward pressure and the resisting pressure acting on the sheet pile. Resultant earth pressure profiles of the sheet pile during the maximum bending event in C-3, C-4, and C-4S that takes place nearly at 86.0 s during the Tohoku Earthquake are shown in Fig. 3.23. The negative value represents the resultant earth pressure acting towards the backfill, and the positive value indicates the resultant earth pressure towards the river channel. The resultant channel-ward earth pressure, acting on the upper part of the sheet pile, is affected by the embankment and the liquefiable layer. The maximum resultant channel-ward earth pressure imposed by the liquefiable layer is observed to increase proportionally with its thickness.

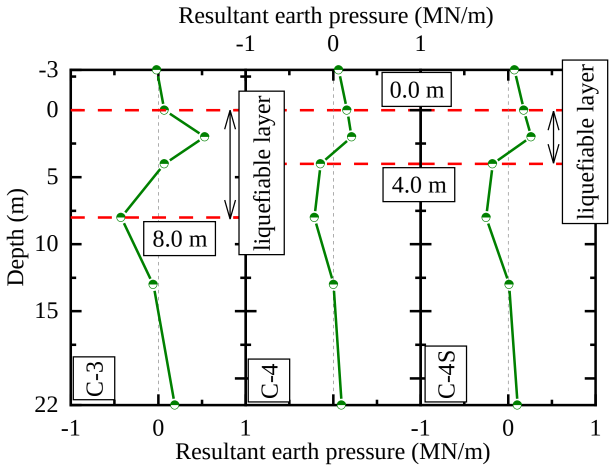

Fig. 3.23: Resultant earth pressure profiles in C-3, C-4 and C-4S when the sheet pile experiences maximum bending moment during the Tohoku Earthquake.

Liquefaction inside the river channel causes a considerable softening of the soil thus reduces the resistance provided by the channel-side soils. A plot of the resultant earth pressure time histories at SP-3 and SP-4 along with the excess pore water pressure time histories of the surrounding soil inside the river channel are shown in Figs. 3.24 and 3.25 for C-3 and C-4, respectively. SP-3 (at a depth of 4 m from the liquefiable layer top) is located at the middle of the liquefiable layer in C-3, and at the interface of the loose and the dense layer in C-4. Whereas, SP-4 (at a depth of 8 m from the liquefiable layer top) is located at the interface of the loose and the dense layer in C-3 and inside the dense ground in C-4. According to the pore pressure gauge readings, in C-3 the liquefaction takes place from the surface to the depth between P3-3 and P3-5 (around 8 m deep from the surface), while that was down to the depth between P3-5 and P3-7 (around 8.5 m deep from the surface) in C-4. The figures show that the resultant earth pressure towards the backfill, which is influenced by the liquefaction extent of the channel-side soils at SP-3, gradually increases (the value in the figure decreases) until 75.0 s in C-3 and 80.0 s in C-4 before the channel-side soils at that vicinity get liquefied. However, once the soil gets liquefied, the resisting earth pressure is observed to decrease (the value in the figure increases) because of the softening of the soil inside the river channel. On the other hand, the resisting earth pressure at SP-4 is observed to increase (the value in the figure decreases) gradually and reach a residual value since the supporting dense soils don't liquefy.

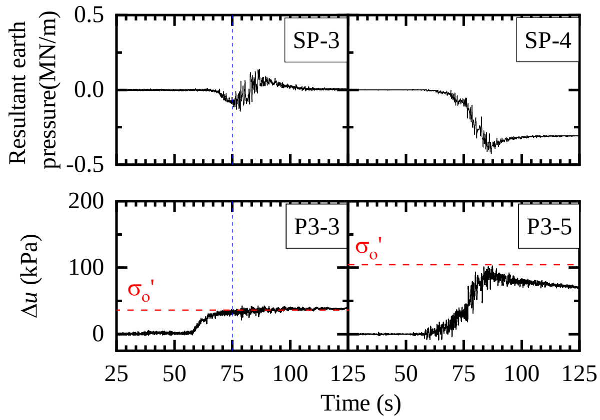

Fig. 3.24: Time histories of resultant earth pressure at SP-3 and SP-4 and the excess pore water pressure (Δu) inside the river channel for C-3.

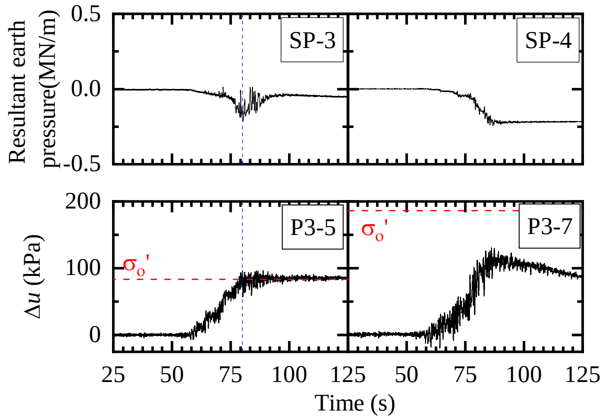

Fig. 3.25: Time histories of resultant earth pressure at SP-3 and SP-4 and the evolution of excess pore water pressure (Δu) inside the river channel for C-4.

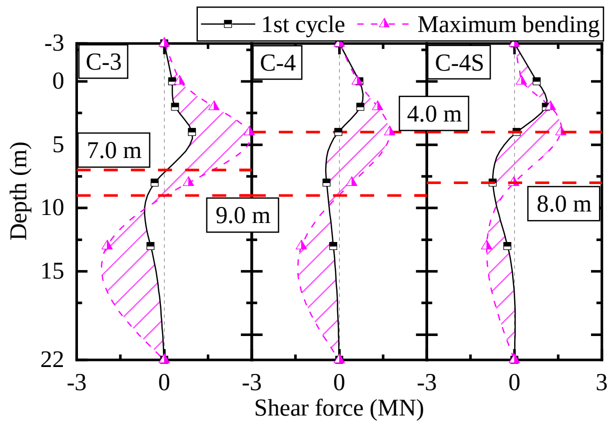

Fig. 3.26: Shear force distributions at the cyclic peaks of the 1st cycle and the maximum bending event during sinusoidal waves.

The shear force distributions of the sheet pile at the cyclic peaks of 1st cycle and the maximum bending event during the sinusoidal waves in all three cases (C-3, C-4 and C-4S) are shown in Fig. 3.26. The peak in the first cycle takes place around 28.0 s when the loose layer in all three cases get liquefied, whereas, the upper dense layer is yet to be liquefied. The shear force distribution for the first cycle shows that it changes its sign at a depth of 4 m in C-4 and 4S, and 7 m in C-3 that represents the location of maximum bending moment at that event. However, the shear force distribution when the sheet pile experiences the maximum bending changes its sign at a depth of 9 m in C-3 and C-4 and 8 m in C-4S. The liquefaction of the upper dense layer is responsible for these considerable downward shifts of the location of the maximum bending moment from the first cycle to the cycle of the maximum bending event, particularly in C-4 and C-4S. The liquefaction of the upper dense layer significantly reduces its resistance to prevent the channel-ward forces from the backfill. Thus, the location of the maximum bending moment moves to a greater depth. It implies that the liquefaction of the shallow dense layer significantly influences the response of the sheet pile.

3.4 Summary

A series of dynamic centrifuge tests were performed to investigate the performance of sheet pile installed into the dense soil to mitigate the liquefaction-induced lateral spreading of the loose foundation soils under the embankment. The performance of sheet pile was investigated for both thin (4 m) and thick (8 m) liquefiable foundations under the 8 m height embankment. Moreover, the effect of the width of sheet pile on its performance as a possible seismic retrofit for the embankment of a river spanning bridge was also investigated. Several conclusions can be drawn from the experimental results.

The model ground was observed to go under significant deformation because of the lateral spreading of the foundation soil as well as the compaction of the loose embankment in the unreinforced condition. The installation of sheet pile can effectively mitigate the liquefaction-induced lateral spreading during the moderate to strong ground motions and equally effective in various thicknesses of liquefiable foundation ranging from 4 m to 8 m. The sheet pile was observed to reduce the channel-ward ground movement up to 30 to 50% at its closer vicinity. The extension of the width of sheet pile beyond the target area doesn't have any additional advantage. The performance of limited width (5 m) sheet pile in terms of mitigating lateral spreading was found similar to that of the full-width sheet piles. The liquefaction of the dense layer just below the loose layer significantly affects the overall response of the sheet pile. It causes the location of the maximum bending moment of the sheet pile to move to a greater depth inside the dense layer. Therefore, the liquefaction susceptibility of the dense layer immediately below the loose layer should be considered in the determination of the sheet pile specifications.

[This page intentionally left blank]

Chapter 4

Effect of thickness of liquefiable layer and embedment depth on the performance of sheet pile as a seismic retrofit

4.1 Introduction

The migration or the lateral spreading of the liquefied foundation triggers the seismic settlement or deformation of the embankment (Bhatnagar, Kumari, & Sawant, 2016). The installation of the sheet pile is a commonly used technique to mitigate the lateral spreading of the liquefied soil. Several factors could potentially influence the performance of sheet pile, for example, the thickness of the liquefiable layer, embedment depth into the bearing stratum, and the stiffness of the soil and pile materials. Two-dimensional finite element analysis is used in this study to observe the effects of these factors on the seismic performance of the sheet pile. Two-dimensional finite element analysis is nowadays a widely used numerical tool to determine the dynamic response of the ground related to liquefaction and liquefaction-induced lateral spreading. Aydingun and Adalier (2003b) used two-dimensional finite element analysis to observe the seismic response of the liquefiable foundation of an earth embankment. The effect of different remedial measures, i.e., densification of the sand layers, gravel berm surcharge, and sheet pile enclosure to mitigate liquefaction-induced lateral spreading is also studied using finite element analysis. Chang et al. (2014) conducted a two-dimensional finite element analysis to observe the dynamic response of the pile-supported structures subjected to lateral spreading. Armstrong et al. (2013) performed a two-dimensional finite element analysis to study the pile-pinning effect on the performance of piled bridge abutment affected by earthquake-induced liquefaction. Li and Motamed (2017) also predicted the behavior of the pile group behind a quay wall subjected to liquefaction and liquefaction induced lateral spreading. All the previous works show that the two-dimensional finite element analysis can predict the seismic response of the liquefiable ground as well as the soil-structure interaction with considerable accuracy. Besides, the finite element numerical model, validated with experimental results, can be used for further parametric studies that can potentially eliminate the experimental cost.

Dynamic centrifuge experiment has been widely used to validate the finite element numerical model dealt with the liquefaction or liquefaction-induced lateral spreading of the loose foundation under an embankment (Aydingun & Adalier, 2003b; Korhan Adalier & Aydingun, 2003; Armstrong et al., 2013; Boulanger, Khosravi, Khosravi, & Wilson, 2018). This chapter also presents the numerical simulation of a dynamic centrifuge experiment of an embankment on a liquefiable foundation reinforced with a sheet pile near the toe of the embankment. The tip of the sheet pile is usually installed deep into the dense layer to mitigate the lateral spreading of the overlaying loose layer. The performance of the sheet pile as a seismic retrofit against liquefaction-induced lateral spreading largely depends on the thickness of the liquefiable layer and the embedment depth of the sheet pile into the dense layer. Therefore, the thickness of the liquefiable layer where sheet pile can be effectively used to mitigate lateral spreading needs to be specified along with its optimum embedment depth which is not much studied before. This chapter describes the performance of sheet pile in various thickness of liquefiable layer using validated finite element model. This chapter also describes effect of changing the embedment depth of the sheet pile. Moreover, the effectiveness of the additional measures for example anchorage near the head of the sheet pile to enhance its efficiency is also investigated.

4.2 Description of the Physical model

The experimental case C-3 described in Chapter 3 is numerically simulated using two-dimensional finite element analysis. The experimental setup consists of a loose liquefiable sand layer (Dr=50%), over a dense sand layer (Dr=90%), performs as a foundation of an approach embankment of a river spanning bridge. Generally, the embankments are compacted up to some desired level during the construction in reality. However, a loose embankment (Dr=50%) is used in this experiment to avoid the densification of the loose sand layer. The thickness of the liquefiable layer is 8 m in the prototype scale. The sheet pile is installed near the toe of the embankment. The detailed description is given in Chapter 3 (C-3). The experimental setup is shown in Fig. 4.1.

The foundation of the model embankment is saturated with the de-aerated Metolose solution (2.2% by weight) to make the viscosity of the pore fluid 50 times of water. Metolose, the commercial name of Hydroxypropyl Methylcellulose from Shin-Etsu Chemical Company, is mixed with water at a specified proportion to increase the viscosity (Adamidis & Madabhushi, 2015) of the solution by keeping the density and surface tension nearly identical to water. According to the generalized scaling law, the viscosity should be 70.71 times of water. However, due to difficulties in saturating the model ground with larger viscosity fluid, the viscosity of the pore fluid is set 50 time as that of water. Thus, the permeability of the soils is relatively large.

The sheet piles made of steel plates are placed inside the container first during the model preparation. The sands are deposited afterwards for ease of construction and avoiding excessive densification of the surrounding soils during the preparation at 1 g. The specifications of the sheet pile in the prototype are tabulated in Table 4-1. The model ground in the centrifuge experiment experiences two sequential ground motions. The first input ground motion, similar to the actual one in the Tohoku Earthquake recorded at the ground surface near the New Bansuikyo Bridge, Tochigi (2-I-I-3, NS component) but the magnitude is comparatively smaller, is used in the numerical analysis, as shown in Fig. 4.2. The dynamic response of the model ground characterized by the acceleration, evolution of excess pore water pressure, and ground deformation is duly recorded with extensive instrumentation, as shown in Fig. 4.1. The recorded experimental results of different parameters are compared with numerical results to validate the numerical model.

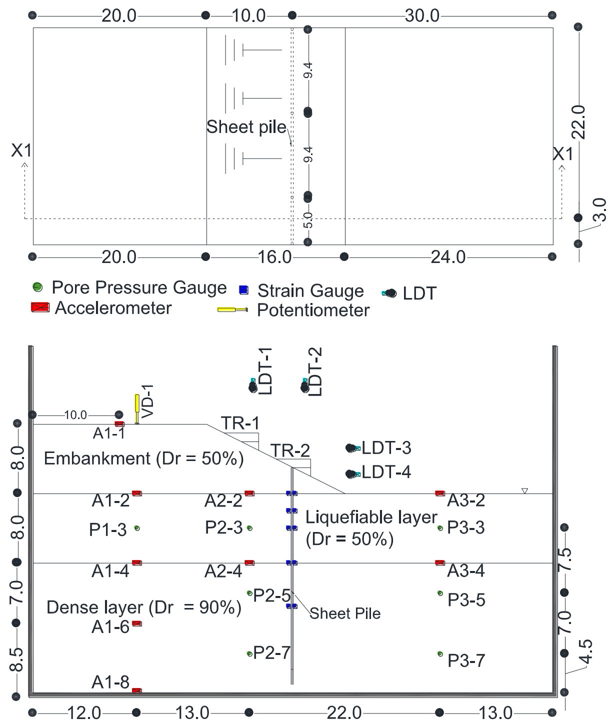

Fig. 4.1: Plan and the cross-sectional view of the experimental setup in the prototype.

Table 4-1: Specifications of the sheet pile in the prototype.

	Prototype
Material type	Steel
Stiffness EI (N-m^2/m)	5.2×10^8
Target sheet pile	Hat-type and H-shape composite

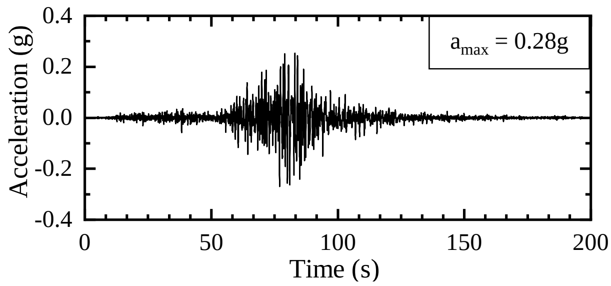

Fig. 4.2: Input ground motion.

4.3 Validation of the numerical model

4.3.1 Numerical model and boundary conditions

Two-dimensional finite element simulation of the centrifuge experiment is conducted under plain-strain condition considering a domain with a unit width in the transverse direction. The discretized mesh of the numerical model is shown in Fig. 4.3. A uniform mesh having the dimensions of 1 m × 1 m in X and Y direction, respectively, is used throughout the foundation ground. Besides, the embankment is modeled with a comparatively finer mesh having the dimensions of 1 m × 0.5 m in X and Y direction, respectively, to accommodate the slope of the embankment having the side slope 1:2. Boundary conditions in the numerical model are imposed in such a way that it can simulate the experimental boundary conditions. All the movements of the nodes are restricted at the bottom boundary. The nodes along the vertical boundary are kept free to move vertically during the initial stress analysis, which is restricted in the dynamic analysis. Whereas, the horizontal movement is restricted in both cases. All other nodes are set free against translational and vertical movement. Besides, the fluid flow velocity in the horizontal direction at the boundaries of the analytical domain are set to zero.

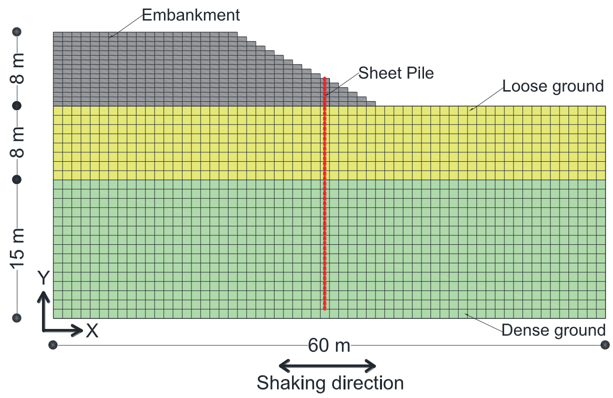

Fig. 4.3: Discretized mesh for the two-dimensional finite element model.

The soil ground is modeled as a four-nodes quadrilateral solid element. An elasto-plastic soil constitutive model proposed by Asaoka et al. (2002) is used to simulate the dynamic response of the modeled ground. The constitutive model is formulated with fourteen parameters out of which κ and λ are the tangent of the swelling and the normal compression line and can be determined from the consolidation test. e_o, ν, and G_s are, respectively the initial void ratio, Poisson's ratio, and the specific gravity of soil, which can be determined from element tests. All other parameters are determined by trial and error so that the numerical liquefaction resistance curve closely fits the experimental one. The soil parameters used in the finite element analysis are listed in Table 4-2. The typical response of the Toyoura sand in the undrained cyclic triaxial test using the Asaoka model is shown in Fig. 4.4 (a) and (b). Figure 4 (c) shows the liquefaction resistance curve of loose and dense Toyoura sand. The number of cycles required to attain 1% double amplitude strain is plotted against the corresponding cyclic stress ratio. The graph shows that the soil model exhibits relatively stiff behavior in a higher cyclic stress ratio. However, the simulated value is very closer to the experimental value in the lower cyclic stress ratio. The sheet pile is modeled as an elastic beam element. The bending stiffness (EI) of the sheet pile is 5.2×10^8 N-m^2/m. The bending stiffness of a one-meter width sheet pile is used in the numerical analysis to model the sheet pile in the plane strain condition. A master-slave node technique is applied to connect the sheet pile with the soil domain at its specified location. The master and slave node technique offers an identical deformation between the nodes of the structural element and the corresponding linked node of the soil element.

Table 4-2: Parameters for loose and dense soils.

Parameters	Loose sand (Dr=50%)	Dense sand (Dr=90%)
κ	0.0064	0.0064
λ	0.05	0.05
e_o	0.791	0.645
ν	0.33	0.33
G_s	2.65	2.65
φ	40°	44°
φ_d	38°	38°
b_r	3.0	5.0
m	0.75	1.5
a	2.7	1.0
R	0.25	0.09
R_o^*	0.5	0.5
K_o	1.0	1.0
k (m/s)	1.0×10^{-3}	4.9×10^{-4}

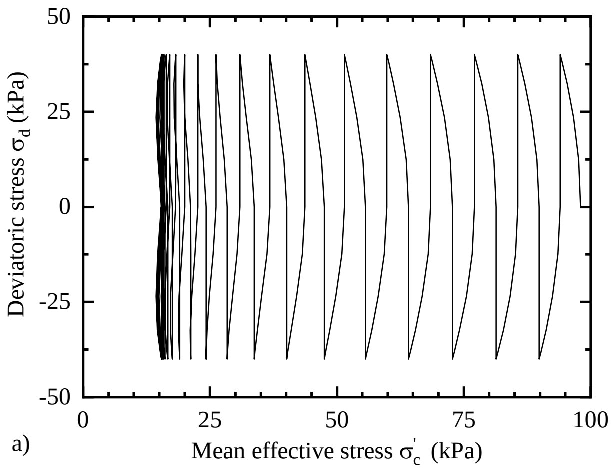

a)

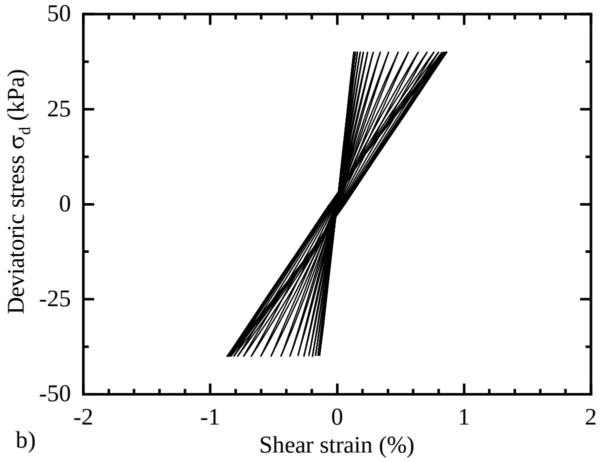

b)

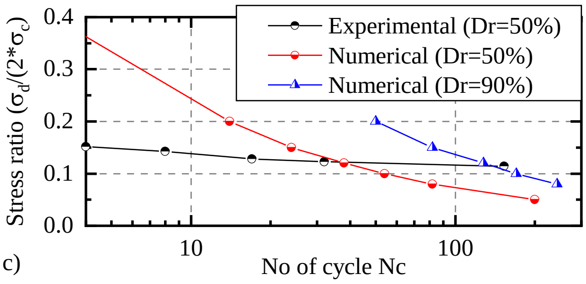

c)

Fig. 4.4: The typical response of Toyoura sand in undrained cyclic triaxial test using Asaoka model; a) stress path (Dr=50%), b) stress-strain curve (Dr=50%), and c) liquefaction resistance curve for loose (Dr=50%) and dense (Dr=90%) sand.

4.3.2 Comparison of the experimental and numerical results

The simulation of the centrifuge experiment justifies the capability of the numerical model to capture the dynamic response of the ground, particularly the liquefaction-induced lateral spreading and the associated damages. The dynamic response of the ground is characterized by the evolution of the excess pore water pressure, propagation of the seismic wave, and associated ground deformation. The lateral spreading of the loose ground is usually triggered by the generation of the excess pore water pressure. The comparison of the measured and simulated excess pore water pressure time histories in the loose and dense ground inside the channel (P3-3, P3-5, and P3-7), dense layer under the embankment slope (P2-5 and P2-7), and in the loose layer under the embankment (P1-3) is shown in Fig. 4.5. The graphs show that the simulated results can capture both the trend and the magnitude of the excess pore water pressure with a considerably good agreement. The measured excess pore water pressure at the middle of the liquefiable layer inside the channel (P3-3) reaches the liquefied state at the early stage of shaking that continues even after the end of shaking. Whereas, the simulated result presents a comparatively rapid dissipation starts nearly at 100 s. The ground deformation observed in the experiment, as well as in the numerical simulation, stops well before that time. Therefore, it is expected that the early dissipation of the excess pore water pressure at P3-3 in the numerical simulation does not significantly affect the overall ground response.

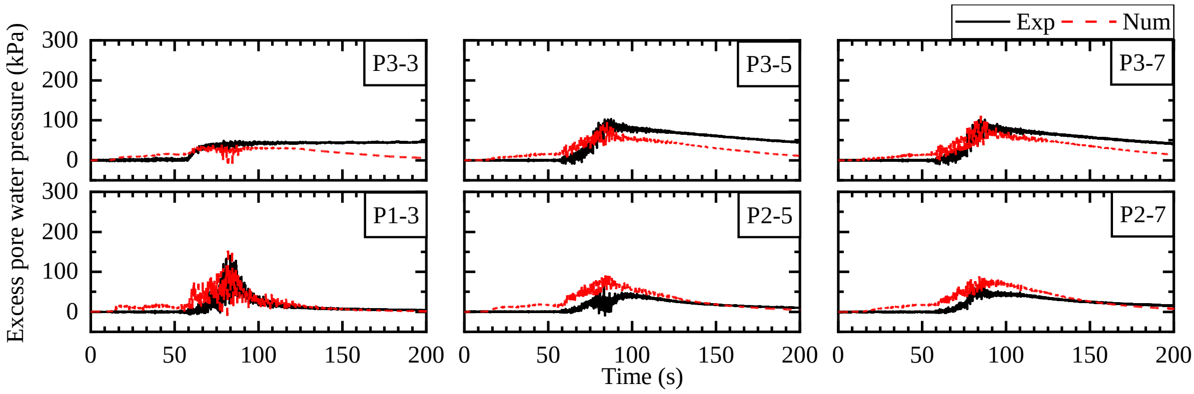

Fig. 4.5: Comparison of measured and simulated excess pore water pressure time histories at six locations P3-3, P3-5, P3-7, P1-3, P2-5, and P2-7 inside the model ground.

A comparison of the measured and simulated acceleration time histories inside the dense ground and on the embankment surface (A1-6, A1-4, and A1-1) is shown in Fig. 4.6 (a). The graphs show that the propagation of the seismic waves can be reproduced with a reasonable agreement by the numerical simulation, particularly in the dense soil. However, an amplification of the acceleration is observed in the dry loose sand at A1-1. Besides, the numerical results also produce a reasonable agreement in the frequency content of the responses in the dense soil, as shown by the spectral acceleration in Fig. 4.6 (b). Whereas, a considerable amplification is observed at the surface of the embankment, which might cause comparatively larger ground deformation in the embankment.

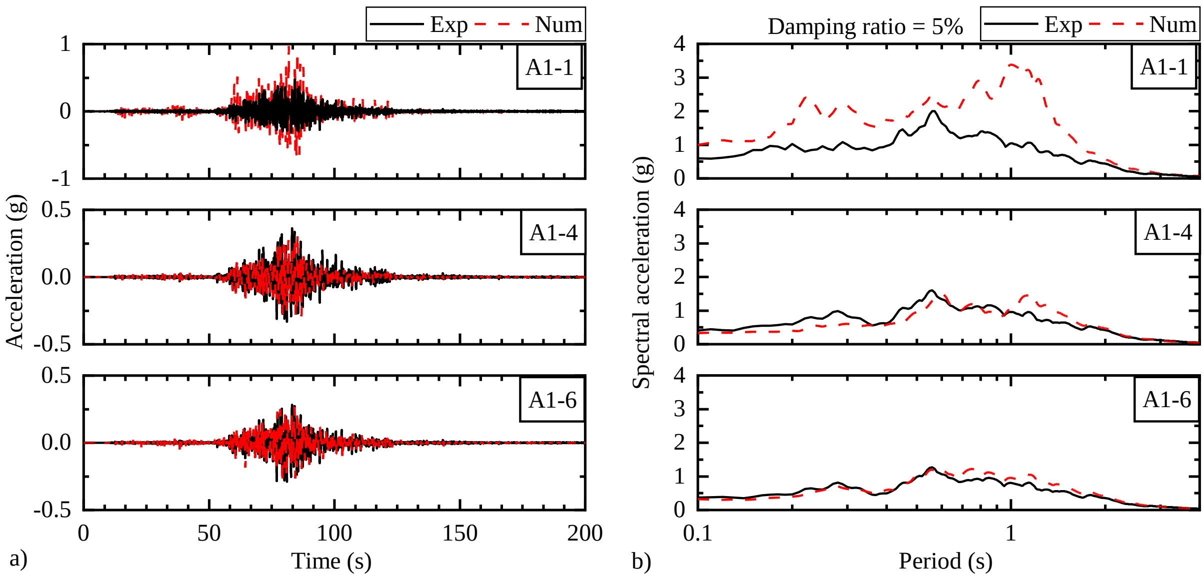

Fig. 4.6: Comparison of measured and simulated a) acceleration time histories and b) spectral acceleration (damping ratio = 5%) at three locations A1-1, A1-4, and A1-6 in the embankment side.

The measure and simulated surface settlement at VD-1 and the horizontal ground displacement of two targets TR-1 and TR-2 placed on the slope of the embankment are compared in Fig. 4.7. The graph shows that the simulated surface settlement is significantly larger than the measured value. The settlement of the embankment is predominantly caused by the lateral outflow of the liquefied ground, shear deformation of the embankment, and the contraction of the soil below the embankment (Okamura & Tamura, 2004; Maharjan & Takahashi, 2014). However, the volumetric compaction of the loose embankment might significantly influence the surface settlement. The simulated result exhibits a large settlement at the early stage of shaking well before the lateral spreading of the loose ground is initiated at 65 s. This settlement is predominantly caused by the compaction of loose ground, which is not significantly observed in the experimental study. It shows that the current soil model overestimates the volumetric compaction of the loose dry ground. Since the primary focus of this study is to predict and mitigate the lateral spreading of the liquefied ground, this limitation of the soil model is believed not to affect the overall response of the ground. On the other hand, the graphs show a reasonable agreement between the measured and simulated values of the horizontal displacement at TR-1 and TR-2 with a minor exaggeration in magnitude in numerical simulation.

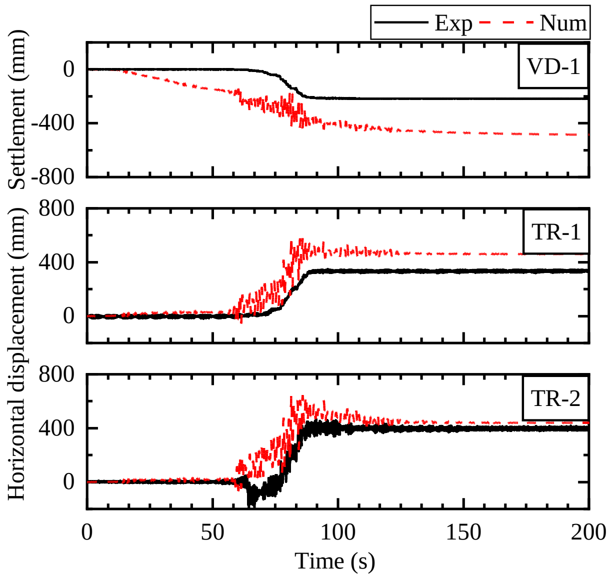

Fig. 4.7: Comparison of measured and simulated ground displacements at VD-1, TR-1, and TR-2.

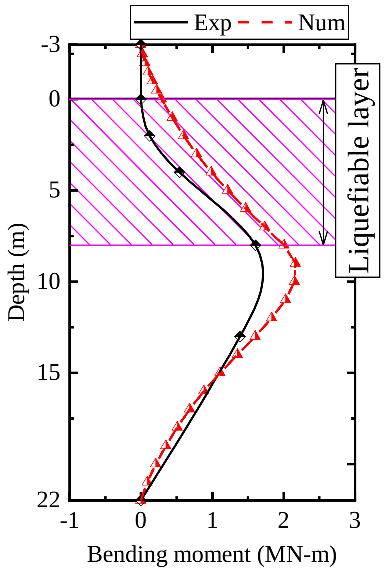

Fig. 4.8: Comparison of the measured and simulated bending moment profile when the sheet pile experiences maximum bending moment.

Figure 4.8 shows the comparison of the measured and the simulated bending moment profile of the sheet pile when it experiences the maximum bending moment. The maximum bending moment of the sheet pile is observed to take place nearly at 86.2 s in centrifuge experiment as well as in numerical simulation. The graphs show that the simulated bending moment profile can follow a similar trend of the experimental bending moment profile. Moreover, the location of the maximum bending moment can also be mapped in the numerical simulation with a reasonable agreement. The forward diagonal hatched region in Fig. 4.8 represents the loose liquefiable layer. It is observed that the maximum bending moment takes place near the interface of the loose and dense layer. It is worth mentioning that the magnitude of the simulated bending moment is comparatively larger than the experimental bending moment. It is observed that the numerical simulation sometimes overestimates the dynamic response of the ground, particularly the ground deformation, which may yield a larger bending moment in the sheet pile.

4.4 Results and discussions

The comparison of the experimental and numerical results in the previous section shows that the current finite element model can reproduce the overall dynamic response of the ground with a reasonably good agreement. It justifies the use of this finite element model for further parametric studies to observe the effect of different parameters of the ground. Several factors that can significantly affect the performance of sheet pile as a seismic retrofit for example; a) the thickness of the liquefiable layer, b) embedment depth of the sheet pile into the dense ground, and c) the anchorage of the sheet pile near its head. The effect of these factors is discussed in this section.

4.4.1 Effect of thickness of liquefiable layer

The thickness of the liquefiable layer under the embankment significantly affects the performance of the sheet pile as a seismic retrofit. A series of two-dimensional finite analyses are carried out to observe the effect of thickness of the liquefiable layer. The geometrical configuration of the embankment and the foundation soil layer is kept similar as it is described in the previous section except for the thickness of the liquefiable layer. The thickness of the liquefiable layer immediately under the embankment varies from 3 m to 10 m, whereas, the total thickness of the foundation layer is kept similar in all the cases that are 23 m. All the cases are analyzed in reinforced as well as unreinforced conditions. The similar type of sheet pile described in the previous section is also used in this study as a reinforcement. The analysis conditions in different cases are tabulated in Table 4-3. The primary objective of the sheet pile installation is to mitigate the channel-ward movement of the ground. Therefore, the final horizontal ground displacement near the shoulder (TR-1) (see Fig. 4.1) and near the toe of the embankment (TR-2) (see Fig. 4.1) are plotted against the thickness of the liquefiable layer in Fig. 4.9. Besides, the horizontal displacement of those two targets is also compared between the unreinforced and reinforced cases to observe the performance of the sheet pile as a seismic retrofit. The graphs show that the channel-ward displacement of both TR-1 and TR-2 gradually increases with the thickness of the liquefiable layer. Besides, the installation of the sheet pile potentially reduces the channel-ward displacement, as shown in Fig. 4.9.

The ground deformation of the embankment resting on a liquefiable foundation largely depends on the lateral spreading of the foundation soil and the propagation of the seismic wave to the base of the embankment. The increase in lateral spreading increases the horizontal ground deformation. Similarly, the increase in seismic demand at the base of the embankment might trigger larger displacement. However, the thickness of the liquefiable layer shows an opposite response in these two aspects. It is observed that the lateral spreading of the foundation layer increases with the thickness of the liquefiable layer. In contrast, the seismic demand at the base of the embankment decreases with the thickness of the liquefiable foundation. The seismic demand is mainly governed by three factors such as peak ground acceleration, the characteristics of earthquake spectrum and duration. Intensity parameters of ground motions are usually used as a scaling parameter in performance-based design. Arias Intensity (Arias, 1970) is one of the ground motion intensity related to the energy content of the ground motion (Yakut & Ylmaz, 2008) that can capture the potential destructiveness of an earthquake. It is useful to predict several commonly used demand measures of structural performance, liquefaction, seismic slope stability (Travasarou, Bray, & Abrahamson, 2003). The Arias Intensities of the acceleration time histories recorded at the base of embankment in different analyzed cases are estimated and plotted against the thickness of the liquefiable layer, as shown in Fig. 4.10. The graph shows that Arias Intensity decreases with the thickness of the liquefiable layer. The horizontal displacement at TR-1 in the unreinforced condition in Fig. 4.9 shows a gradual increase with the thickness of the liquefiable foundation. It implies that the ground deformation caused due to lateral spreading dominates in the unreinforced cases even there is a decrease in seismic demand.

Table 4-3: Analysis conditions to observe the effect of thickness of the liquefiable layer.

Case ID	Total thickness of foundation layer (m)	Thickness of liquefiable layer (m)	Height of embankment (m)	Existence of sheet pile
N-1	23	3	8	No
N-2	23	4	8	No
N-3	23	5	8	No
N-4	23	6	8	No
N-5	23	8	8	No
N-6	23	10	8	No
N_SP-1	23	3	8	Yes
N_SP-2	23	4	8	Yes
N_SP-3	23	5	8	Yes
N_SP-4	23	6	8	Yes
N_SP-5	23	8	8	Yes
N_SP-6	23	10	8	Yes

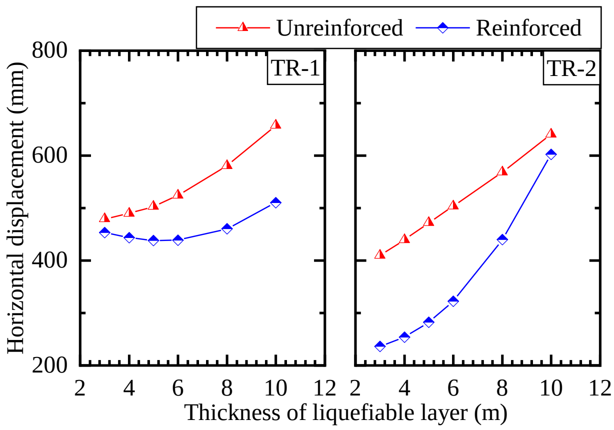

Fig. 4.9: Comparison of horizontal displacements at TR-1 and TR-2 between reinforced and unreinforced cases in various thicknesses of liquefiable layer.

The sheet pile installation increases the Arias Intensity under the embankment than the unreinforced cases (see Fig. 4.10), probably because of the confinement provided by the sheet pile. Besides, it provides reinforcement against lateral spreading, thus reduces the channel-ward ground movement. Therefore, the efficiency of the sheet pile to mitigate the horizontal displacement depends on the combined response of the sheet pile to mitigate lateral spreading and the seismic energy propagated to the embankment. The horizontal displacement of TR-1 in the reinforced cases in Fig. 4.9 is observed to remain the same up to the case of 6 m thick liquefiable layer (N_SP-4), where there is a sharp increase in horizontal displacement afterwards. It implies that the efficiency of the sheet pile to reduce lateral spreading works well up to the 6 m thick liquefiable layer. Besides, the reduction of the seismic energy with the increased thickness of the liquefiable layer reduces the ground deformation as well. On the other hand, the sharp increase of TR-1 (see Fig. 4.9) in the cases of the thick liquefiable layer (more than 6 m) represents the reduction of the efficiency of sheet pile to mitigate lateral spreading.

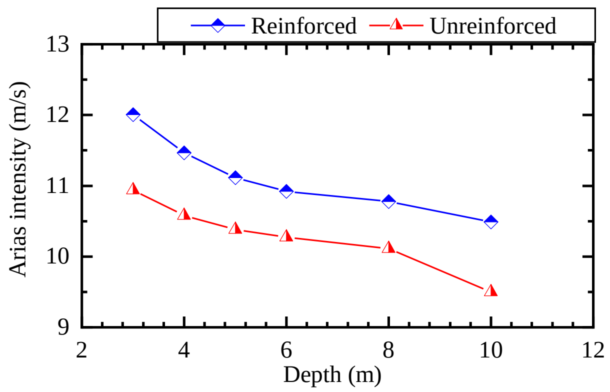

Fig. 4.10: Arias intensity of the ground accelerations recorded immediately under the embankment.

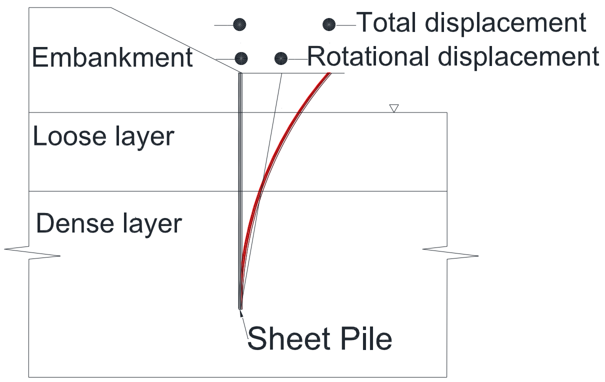

Fig. 4.11: Concept of rotational displacement.

The horizontal displacement of TR-2 in the reinforced cases is also observed to increase with the thickness of the liquefiable layer, as shown in Fig. 4.9. The rate of increment is comparatively higher when the thickness of the liquefiable layer is more than 6 m. The combination of the displacement due to bending and displacement due to the rotation represents the total displacement at TR-2 (in Fig. 4.9). The sheet pile goes under some tilting due to the softening of the shallow dense layer caused by the generation of excess pore water pressure. This tilting causes some amount of displacement at the sheet pile head, which is considered as rotational displacement in this study. Therefore, the rotational displacement at the head of the sheet pile is the component of the total displacement caused by the lateral movement of the sheet pile at the interface of the loose and dense layer triggered by softening of the dense layer as it is illustrated in Fig. 4.11. A comparison of the total horizontal displacement and the displacement due to the rotation at TR-2 is shown in Fig. 4.12. The rotational displacement at TR-2 (see Fig. 4.12) is also observed to increase with the thickness of the liquefiable layer. It exhibits a comparatively sharp change in the case of a thick liquefiable layer of 10 m. Relatively large rotational displacement and excessive bending due to the load from the liquefiable layer reduces the efficacy of the sheet pile to mitigate lateral spreading inside the thick liquefiable layer. Therefore, the sheet pile is recommended to use as a seismic retrofit for the embankment resting on a liquefiable layer having the thickness up to 6 m considering its performance to mitigate lateral spreading. The rotational displacement of the sheet pile is typically controlled by the stiffness of the bearing stratum, depth of embedment of the sheet pile into the bearing stratum, and obviously the stiffness of the sheet pile itself that is discussed in detail in the next section.

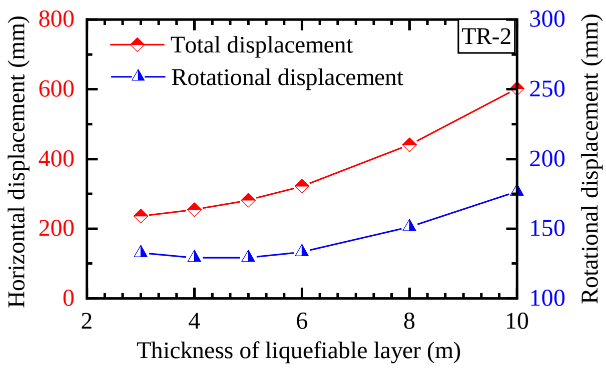

Fig. 4.12: Comparison of the total displacements and the rotational displacements at TR-2 in the reinforced cases having various thicknesses of liquefiable layer.

4.4.2 Embedment depth of sheet pile

The depth of embedment of the sheet pile into the bearing stratum significantly affects its performance as a seismic retrofit. Several two-dimensional finite element analyses have been carried out to observe the effect of embedment depth of sheet pile, where the thickness of the liquefiable layer is kept 6 m, and the depth of embedment varies from 5 m to 16 m. The geometry of the model ground is kept similar to the experimental model, as described in the previous section. The model ground is reinforced with sheet pile in all the analyzed cases. The bending stiffness of the sheet pile is changed as well to observe its effects on the performance of the sheet pile. The analysis conditions are tabulated in Table 4-4.

The performance of the sheet pile is also evaluated here according to its efficiency to prevent horizontal ground deformation. The horizontal displacement of the ground at TR-1 and TR-2 (see Fig. 4.1) at the end of shaking is plotted against the depth of embedment of the sheet pile in Fig. 4.13. It is worth mentioning that the bending stiffness of the sheet pile used in these analyses is similar to the experimental one. The graphs for both TR-1 and TR-2 shows that the horizontal displacement is considerably larger in the case of smaller embedment depth. A significant reduction in horizontal displacement, especially at TR-2, can be attained by increasing the embedment depth. On the other hand, the rate of increase in horizontal displacement is steeper when the embedment depth is smaller than 9 m. It is already mentioned in the previous section that the rotational displacement significantly affects the total displacement of the sheet pile, thus affects the overall performance to mitigate lateral spreading. The smaller embedment depth triggers larger rotational displacement that prompts a sharp increase in the horizontal displacement in the cases of smaller embedment depth. Therefore, the sheet pile should be embedded up to the optimum depth that minimizes the rotational displacement.

The rotational displacement of the sheet pile is significantly influenced by the stiffness of the soil, bending stiffness of the pile, and the embedment depth. The equation provided by PWRI (PWRI, 2016) is commonly used in japan to calculate the embedment depth of the sheet pile. According to the guideline, the embedment depth should be larger than 2/β, where the characteristic value of a pile $\beta = \sqrt[4]{k_h W/4EI}$, k_h is the coefficient of subgrade reaction of the bearing stratum, "EI" is the bending stiffness of the pile. This equation provides the minimum embedment depth for a sheet pile. However, it does not provide any information about the horizontal displacement at the top. The total displacement is governed by the rotation displacement as well as the displacement due to bending. For example, the installation of a flexible sheet pile inside a stiff soil may result in large total displacement due to bending even though the required embedment depth is comparatively smaller. It is important to select the sheet pile according to the allowable displacement under loading in the performance-based design. Besides, the product of the embedment depth and the characteristic value D*β is considered as 2 in this guideline, which needs to justify for the saturated dense ground. Therefore, an attempt is made to correlate the horizontal displacement of the sheet pile, the characteristics value β of the sheet pile installed in a saturated dense ground (Dr=90%), and the D*β value, as shown in Fig. 4.14.

Table 4-4: Analysis conditions to observe the effect of embedment depth of sheet pile.

Case ID	Total thickness of foundation layer (m)	Thickness of liquefiable layer (m)	Height of embankment (m)	Embedment depth of sheet pile (m)	Bending stiffness of sheet pile (EI**)
N_SP-7	23	6	8	5	EI
N_SP-8	23	6	8	7	EI
N_SP-9	23	6	8	9	EI
N_SP-10	23	6	8	11	EI
N_SP-12	23	6	8	13	EI
N_SP-12	23	6	8	16	EI
N_SP-13	23	6	8	5	2*EI
N_SP-14	23	6	8	7	2*EI
N_SP-15	23	6	8	9	2*EI
N_SP-16	23	6	8	11	2*EI
N_SP-17	23	6	8	13	2*EI
N_SP-18	23	6	8	16	2*EI
N_SP-19	23	6	8	5	4*EI
N_SP-20	23	6	8	7	4*EI
N_SP-21	23	6	8	9	4*EI
N_SP-22	23	6	8	11	4*EI
N_SP-23	23	6	8	13	4*EI
N_SP-24	23	6	8	16	4*EI

**Bending stiffness EI = 5.2×10^8 N-m^2/m

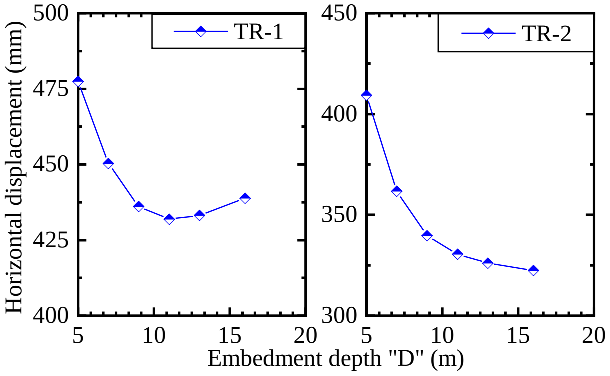

Fig. 4.13: The effect of embedment depth on the performance of sheet pile to mitigate lateral spreading where the bending stiffness of sheet pile EI = 5.2 × 10^8 N-m^2/m.

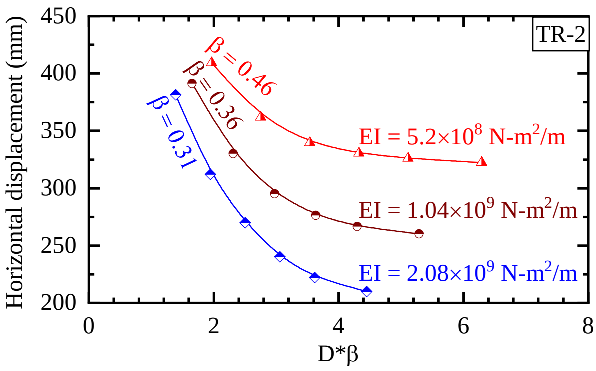

Fig. 4.14: The horizontal displacements at the head of the sheet pile having various stiffnesses and embedment depths installed in a saturated dense ground (Dr=90%).

The final horizontal displacement at the head of the sheet pile having three different β values 0.31, 0.36, and 0.46 is plotted against D*β in Fig. 4.14. The saturated dense layer (Dr=90%) is used as a bearing stratum in all the analyses. The standard penetration test value (N) is commonly used in the engineering practice to determine the subgrade reaction of the ground. The average standard penetration resistance is estimated by Dr $=\sqrt{N/46}$ (Idriss & Boulanger, 2003) that gives the N value of 37 for dense sand (Dr=90%). The subgrade reaction coefficient is estimated according to the equation given by PWRI (PWRI, 2016). The subgrade reaction coefficient $K_H = K_{H_o}[B_H/0.3]^{(-3/4)}$, where $K_{H_o} = {}^{1}/_{3}\,\alpha E_o$, α = 2 for earthquake, E_o = 2800*N (kN/m^2), and B_H is the width of sheet pile which is 10 m for continuous sheet pile. The estimated subgrade reaction coefficient for dense soil (Dr=90%) is 50 × 10^3 kN/m^3 which is also close to the range of subgrade reaction for dense sand proposed by Bowles (1996). Three different bending stiffness of the sheet pile is used to get the β value 0.46, 0.36, and 0.31.

The graph shows that there is a steep increase in the horizontal displacement at the head of the sheet pile when the D*β value is smaller than 4. It implies that the horizontal displacement in this zone is dominated by rotational displacement. Besides, the horizontal displacement does not change much when the D*β is larger than 4, which implies the zone is dominated by the displacement due to bending. Therefore, the observation from numerical results recommends that the maximum efficiency in terms of reducing lateral spreading can be achieved with an embedment depth of the sheet pile 4/β into the saturated dense sand having average N value of 37. Moreover, the bending stiffness of the sheet pile significantly influences the horizontal displacement when the displacement is dominated due to bending. Figure 4.13 shows that the sheet pile with larger bending stiffness sufficiently embedded into the dense layer significantly reduces the horizontal displacement. Therefore, the chart provided in Fig. 4.14 might be very helpful in selecting the sheet pile and its sufficient embedment depth in the performance-based design approach. This chart is prepared on the consideration of a 6 m thick liquefiable layer. The horizontal displacement decreases or increases almost linearly with the change of the liquefiable layer thickness reinforced by a particular sheet pile sufficiently embedded into the bearing stratum. Therefore, the proposed chart can be applied to the thin liquefiable layer as well. A flow chart for selecting the appropriate sheet pile and the corresponding embedment depth is shown in Fig. 4.15. The permissible displacement "Δ" in the flow chart is the maximum allowable horizontal displacement of the sheet pile head. Whereas, the minimum sheet pile head displacement "ψ" is the minimum horizontal displacement of sheet pile head that can be achieved for a sheet pile having a specific bending stiffness by increasing its embedment depth. In the design approach, the permissible horizontal displacement "Δ" of the sheet pile head needs to select first. Then the appropriate bending stiffness and the "D*β" value of the sheet pile for the corresponding horizontal displacement can be selected from the Fig. 4.14. For example, the permissible horizontal displacement Δ of the sheet pile head is chosen as 334 mm. The value of Δ is larger than the minimum sheet pile head displacement ψ of all the three types of sheet pile shown in Fig. 4.14. Therefore, any one of these three types of sheet pile can be selected. The "D*β" value can be selected as 4.0, 2.3, and 1.8 for the sheet pile having the β value 0.46, 0.36, and 0.31, respectively, depending on the designer's choice. Thus, the depth of that particular sheet pile can be estimated. However, the maximum efficiency for a particular sheet pile can be obtained for a "D*β" value 4.0.

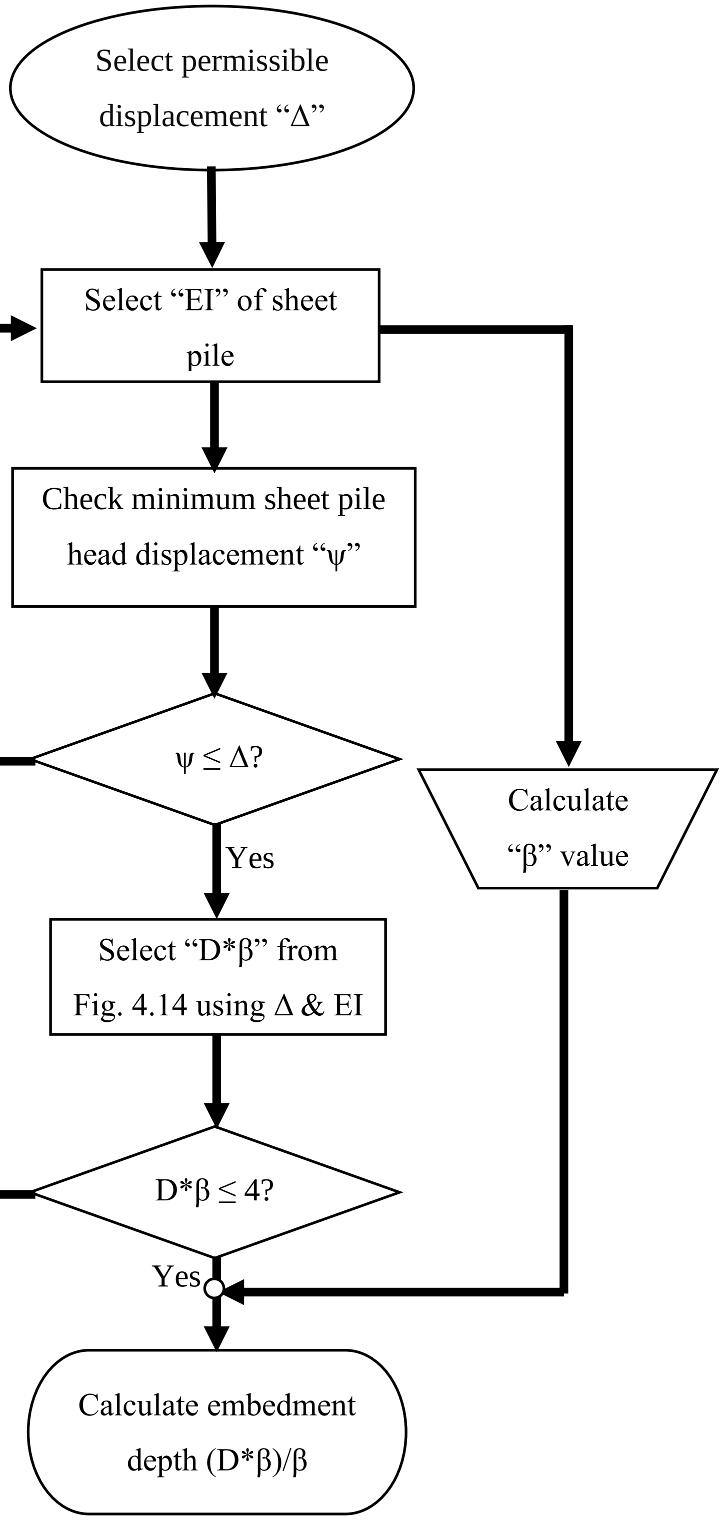

Fig. 4.15: Flowchart for sheet pile design.

4.4.3 Performance of sheet pile with anchorage

The effect of bending stiffness of the sheet pile and its embedment depth is described in the previous section. A comparatively stiff sheet pile having the bending stiffness 5.2×10^8 N-m^2/m embedded into the bearing stratum up to 9 m can considerably mitigate the lateral spreading of a 6 m thick liquefiable foundation layer up to 32% near the sheet pile, as shown in Fig. 4.17. It is also described that an increase in bending stiffness can improve its performance to reduce the lateral spreading of the liquefied ground. However, the increase in bending stiffness of the sheet pile requires to increase the embedment depth for stability that may make the reinforcement technique uneconomic. Therefore, the performance of the anchored sheet pile is studied here. Anchorage of the sheet pile is a commonly used technique to increase the lateral stability of the sheet pile. Anchorage is usually provided with a tie rod and an anchor (Zekri, Ghalandarzadeh, Ghasemi, & Aminfar, 2015). Anchorage with tie rod is not feasible here since this study primarily focuses on the retrofitting of the existing structures. Therefore, a hollow steel pile is used here as an anchorage, as shown in Fig. 4.16. Initially, a 100 mm outer diameter steel hollow pile having the inner diameter 75 mm is used as an anchorage, which is changed to a 125 mm diameter hollow pile having the wall thickness of 25 mm to improve its performance. The analysis conditions are listed in Table 4-5. It is to be mentioned here that the anchorage is modeled as an elastic beam element that is rigidly attached to the sheet pile at its upper end. The bottom end of the anchorage is installed 2 m deep into the dense ground where the nodes of the anchorage modeled as a beam element are connected to the surrounding node of the soil element using a master and slave node technique.

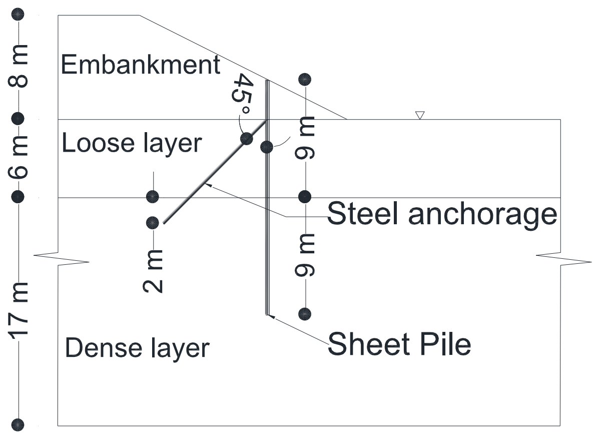

Fig. 4.16: Typical arrangement of anchored sheet pile.

Table 4-5: Analysis conditions to observe the performance of anchored sheet pile.

Case ID	Thickness of liquefiable layer (m)	Height of embankment (m)	Embedment depth of sheet pile (m)	Bending stiffness of sheet pile (N-m^2/m)	Axial stiffness of Anchorage (N)
N_UR	6	8	9	-	-
N_SP	6	8	9	5.2×10^8	-
N_SP_AN	6	8	9	5.2×10^8	7.22×10^8
N_SP_AN_1	6	8	9	5.2×10^8	9.28×10^8

A comparison of the final horizontal displacement at TR-1 and TR-2 (see Fig. 4.1) among the cases of unreinforced ground, ground reinforced with sheet pile, and the ground reinforced with anchored sheet pile is shown in Fig. 4.17. The graph shows that the sheet pile reinforcement can reduce the channel-word ground movement up to 17% and 32% at TR-1 and TR-2, respectively. Whereas, the anchored sheet pile can reduce the horizontal displacement at the same locations up to 46% and 73%, respectively. The results clearly show the anchored sheet pile with the anchorage sufficiently capable of carrying the axial load comes from the laterally spreading soil exhibits better performance than the sheet pile without anchorage.

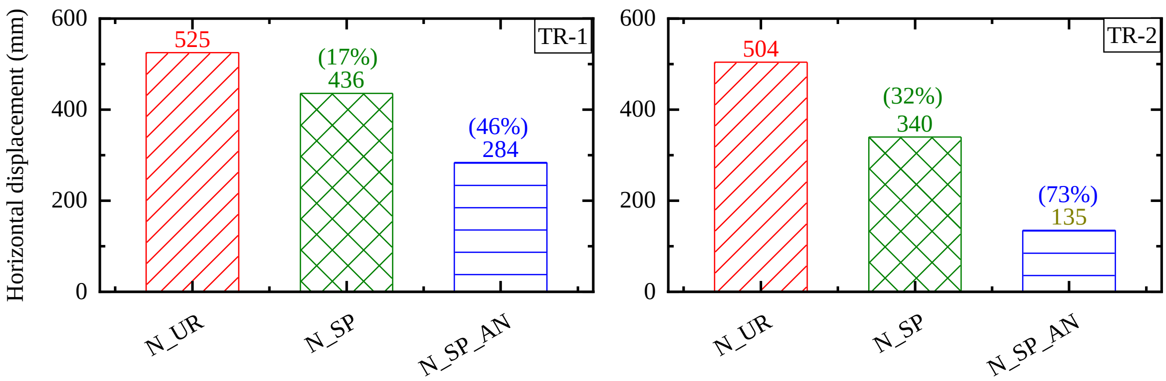

Fig. 4.17: Horizontal displacements at TR-1 and TR-2 at the end of shaking with different reinforcement measures.

The performance of the anchored sheet pile significantly depends on the capacity of the anchorage to carry the axial load from the laterally spreading soil. A 100 mm diameter hollow pile having the 25 mm thick wall is used in the analysis in N_SP_AN, as shown in Fig. 4.17. The axial stiffness of the anchorage pile is 7.22×10^8 N. The axial stiffness is increased by nearly up to 30% in N_SP_AN_1 to observe the effect of axial stiffness. The horizontal displacement at TR-1 and TR-

2 in both cases are almost similar, as shown in Fig. 4.18 (a). The time histories of the axial load carried by the anchorage pile are shown in Fig. 4.18 (b). The graph shows that the load carried by the anchorage in N_SP_AN and N_SP_AN_1 most of the times is smaller than its carrying capacity before yielding. It implies that the anchorage pile with sufficient axial stiffness to carry the load from the laterally spreading soil exhibits similar performance in mitigating lateral spreading. The numerical results show that the anchorage pile experiences the maximum axial load nearly around 1000 kN/m while a 6 m thick liquefiable layer reinforced with an anchored sheet pile having the optimum embedment depth of 9 m. This calculated value of the axial load will provide an idea to select the desired cross-section and the corresponding spacing between the anchorage piles for a continuous sheet pile wall.

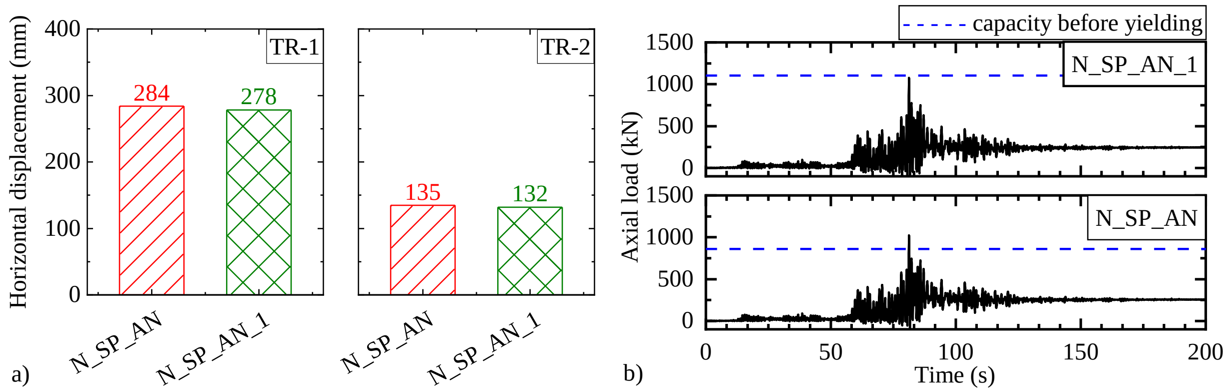

Fig. 4.18: a) Performance of two types of anchorage and b) the axial load time histories carried by the anchorage pile.

4.5 Summary

Several two-dimensional finite element analyses have been carried out in this study to observe the effect of thickness of the liquefiable layer on the performance of the sheet pile to mitigate liquefaction-induced lateral spreading of the foundation soils under an embankment. The numerical model is first validated with the experimental results. Then the thickness of the liquefiable layer has been changed to observe the ground response under different geographical conditions with and without sheet pile reinforcement. The optimum embedment depth for a sheet pile to avoid excessive rotation is studied here. Moreover, the application of an anchorage pile to improve the performance of the sheet pile as a seismic retrofit is also investigated in this study.

The comparison of the experimental and simulated results shows that the two-dimensional finite element analysis can reproduce the overall dynamic response of the ground. The simulated results exhibit considerably good agreement with the experimental results. Parametric studies using finite element analysis show that the sheet pile reinforcement can be efficiently used to mitigate lateral spreading of the loose foundation having the thickness up to 6 m. Significant rotational displacement of the sheet pile is observed in the case of a thick liquefiable foundation (nearly 10 m). Long embedment depth is required to mitigate rotational displacement in the thick liquefiable foundations. It may make the use of sheet pile uneconomic in a thick liquefiable layer. Numerical results recommend that the maximum efficiency in terms of reducing lateral spreading can be achieved with an embedment depth of a sheet pile 4/β where the thickness of the liquefiable layer is 6 m and a bearing stratum having average N value of 37. Moreover, a properly designed anchorage pile along with the sheet pile, can significantly reduce the channel-ward movement of the ground, which is about 73% near the sheet pile.

[This page intentionally left blank]

Chapter 5

Performance of sheet pile as a seismic retrofit for piled abutment subjected to lateral spreading

5.1 Introduction

Numerous observations of pile failure have been documented in the previous major earthquakes (Hamada & O'Rourke, 1992; Tokimatsu, Mizuno, & Kakurai, 1996; Tokimatsu & Asaka, 1998). The waterfront structures, for example, the bridge foundations resting on a liquefiable layer, are particularly vulnerable due to the lateral spreading (Abdoun, Dobry, O'Rourke, & Goh, 2003; Knappett, Mohammadi, & Griffin, 2010). A large number of bridge foundations are observed to fail or to be severely damaged due to the liquefaction or the liquefaction-induced lateral spreading of the loose foundation in the past earthquakes (Hamada & O'Rourke, 1992; Youd, 1993; Bartlett, 2014; Waldin et al., 2012; Haskell, Madabhushi, Cubrinovski, & Winkley, 2013; Mohanty & Bhattacharya, 2019). Because of the lateral spreading of the liquefied soils, the waterfront structures go under significant water-ward displacement. The lateral spreading is highly damaging if the loose sand layer is overlain by a non-liquefiable crust (Berrill, Christensen, Keenan, Okada, & Pettinga, 2001; Finn & Fujita, 2002). The non-liquefiable crustal layer can push the structure more since it does not lose its strength due to the liquefaction of the underlying sand. The bridge abutment, which is the first support of a river-spanning bridge, carries the load from the superstructure as well as it retains the approach embankment which is usually non-liquefiable. Thus, the piled abutment is probably the most crucial structural element of a river crossing bridge that can be severely damaged due to the lateral spreading of the loose foundation that needs more attention.

Extensive researches have been conducted to observe the response of the pile foundation subjected to lateral spreading. Large-scale shake table tests are conducted to observe the response of a pile group in a liquefied soil on the level ground and as well as on the sloping ground (Yasuda et al., 2000; Kavand et al., 2014). Motamed et al. (2013) carried out a large scale shake table test (E-Defense) to determine the response of the pile group behind a quay wall subjected to lateral spreading. The pile tips in the experiments described in the above-mentioned articles were kept either fixed or pinned to the bottom of the container. However, the actual response of the pile group is neither perfectly fixed nor pinned, which might affect the response of the pile group. Brandenberg et al. (2005) conducted several centrifuge experiments to study the behaviour of pile foundation in laterally spreading ground and characterizing the soil-pile interaction in the liquefied ground. They conclude that the response of the pile in the liquefied ground is significantly influenced by its relative stiffness.

Although a large number of research works exist on the response of the pile foundation in the laterally spreading ground, however, the behaviour of the piled abutment is rarely studied. The centrifuge model tests and finite element analysis by Takahashi et al. (2007, 2010) are a few of the limited number of studies. Saha and Takahashi (2017) and Saha et al. (2018, 2019) also studied the behaviour of the piled abutment by the finite element analysis. These studies were motivated by the fact that the piled abutments designed according to the old Japanese design guideline for highway bridges (Japan Road Association, 1964) are not resilient enough to sustain in a very strong earthquake as the liquefaction effects are not considered in the design.

The liquefaction-induced damage to the pile foundation can be remediated either by improving the ground against liquefaction or mitigating the lateral spreading through reinforcement. The ground improvement techniques to mitigate liquefaction, for instance, ground densification, were found effective in the experiments as well as in the previous earthquakes (Liu & Dobry, 1997; Korhan Adalier et al., 1998; Okamura & Matsuo, 2002; Korhan Adalier & Aydingun, 2003; Watanabe, 1966; Ishihara et al., 1980; Yasuda et al., 2012). However, ground improvement techniques are difficult to implement for the existing structures. Pamuk et al. (2007) implemented a passive site stabilization technique by using colloidal silica to remediate the piled foundation against lateral spreading. Although this passive stabilization technique looks attractive for the existing structures, the seepage flow might hinder the efficiency of this technique near a water body. Considering all the limitations to implement the ground improvement techniques, the authors consider using the sheet pile reinforcement technique to mitigate the lateral spreading of a loose foundation, thus prevent the failure of the pile foundations. Motamed and Towhata (2010) implemented a sheet pile to improve the performance of a pile group behind the quay wall subjected to lateral spreading. The fixed end sheet pile was found effective to mitigate the effect of lateral spreading, for instance, the bending moment of the piles behind the sheet pile. Further study is needed to ensure the efficiency of the sheet pile to mitigate lateral spreading since it is affected by the softening of the bearing stratum caused by the generation of excess pore water pressure.

In this study, to examine the efficiency of the sheet pile as a seismic retrofit for an old piled abutment subjected to liquefaction-induced lateral spreading, two dynamic centrifuge experiments are carried out. The experiments are conducted under different reinforcement and structural configurations. One experiment is conducted without any sheet pile reinforcement to study the seismic response of the old piled abutment subjected to lateral spreading. Whereas, the bridge abutment is indirectly reinforced with sheet pile in the other experiment to determine the efficiency of the sheet pile as a seismic retrofit. It should be mentioned that the bridge girder is not modelled in the centrifuge experiment, and the strut effect of bridge girder is not considered for simplicity. Simultaneously, a series of two-dimensional finite element analyses are carried out. The effect of bridge girder on the seismic response of the piled abutment is studied using finite element analysis. The bending moment near the pile head is caused due to combined action of the kinematic force from the soil and inertial force from the abutment. This chapter also describes the contribution of the inertia force to the bending moment near the pile head. Finally, this chapter describes an anchorage technique to improve the performance of sheet pile as a seismic retrofit

5.2 Experimental program

5.2.1 Test conditions

Two dynamic centrifuge experiments are carried out at 50 g using the Tokyo tech Mark III centrifuge facility. The experiments are conducted to study the seismic response of the old bridge abutment resting in a liquefiable layer and simultaneously investigate the efficacy of the sheet pile as a seismic retrofit for the piled abutment. The test conditions are summarised in Table 5-1. The generalized scaling law (Iai et al., 2005) is also used to model the ground and the structural elements in these experiments. The generalized scaling law allows using the combined scaling law of a 1 g shake table experiment and a 50 g centrifuge experiment to accommodate a large prototype within a limited dimension in the centrifuge. The combined scaling factor for a 1:2 scaled shake table experiment and 50 g centrifuge experiment is used here. The scaling factor for different important parameters, for example, length, acceleration, bending stiffness, etc. are described in Chapter 3. The centrifuge experiments (C-5 and C-6) consist of a piled abutment. The piles of the abutment pass through an 8 m thick loose layer while the pile tips are embedded 14 m into the dense ground. The model ground is reinforced with sheet pile to mitigate lateral spreading of the loose foundation in C-6. The typical model ground consists of an 8 m thick approach embankment (having a side slope 1:2) of a river spanning bridge resting on a layered foundation. The top 8 m of the foundation ground is made of loose liquefiable sand (Dr=50%) that is resting on a 15 m thick dense layer (Dr=90%). The water table is set at the foundation ground surface. The detailed plan and cross-sectional views of the experimental cases are shown in Fig. 5.1. The approach embankment is also made of loose sand (Dr=50%) to avoid unexpected densification of the liquefiable foundation. The model ground consisting of the approach embankment as well as the foundation ground is made of Toyoura sand in the centrifuge experiment.

Table 5-1: Test conditions.

Test ID	Existence of piled abutment	Width of abutment (m)	Existence of sheet pile	Width of sheet pile (m)	Relative density (%)		
					Embankment	Loose foundation	Dense foundation
C-5	Yes	5	No	-	53	52	91
C-6	Yes	5	Yes	5 (in front of abutment)	54	51	94

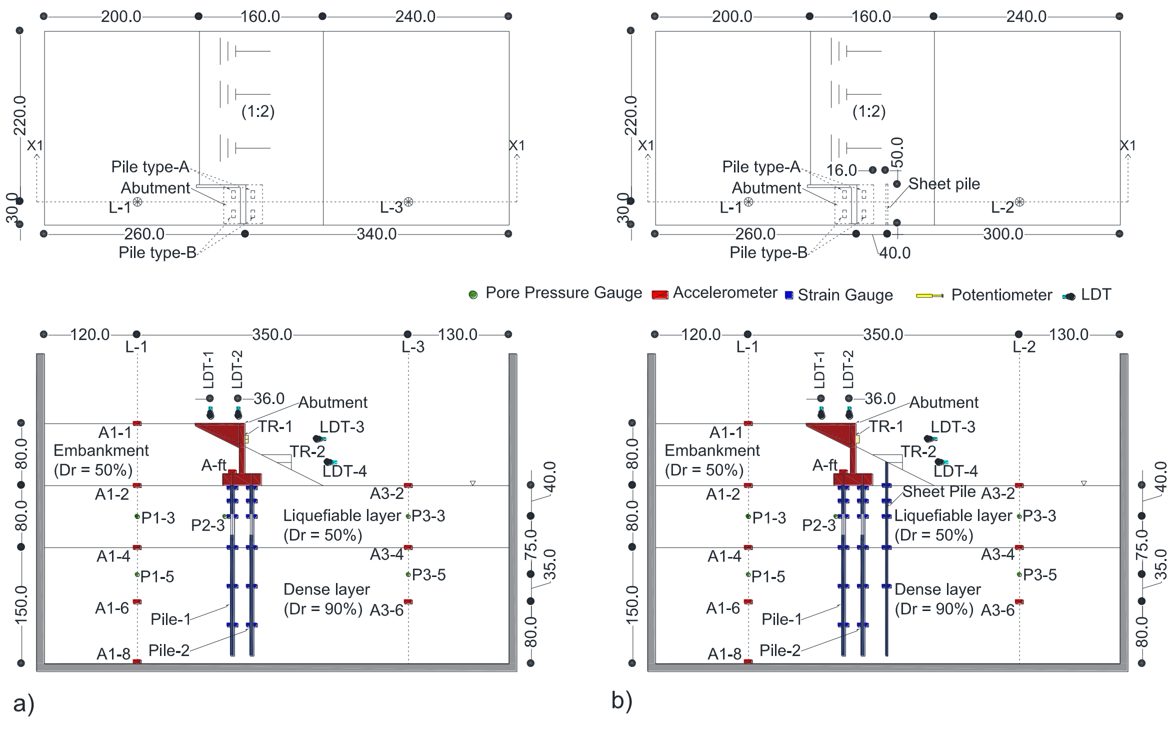

Fig. 5.1: Plan and the cross-sectional view of the experimental setups of a) C-5 and b) C-6 (all the dimensions are in mm in model scale).

The model abutment is placed at the channel end of the approach embankment, as shown in Fig. 5.1. The half-width of a 3×8 piled abutment is modelled to get the advantage of symmetry. Therefore, the abutment is placed at the side of the container in the centrifuge experiment. The abutment and the piles are designed according to the old Japanese design standard of highway bridges (Japan Road Association, 1964). The half abutment is supported by 12 piles according to the actual design. However, it is difficult to model 12 piles with instrumentation in the limited space of the centrifuge experiment. Therefore, a simplification is applied in the design of the model abutment. The frame formed with the piles rigidly connected to the abutment footing at their heads can be treated as a shear frame by considering the footing is infinitely rigid in comparison with the piles. Therefore, the three-column shear frame along the longitudinal axis can be modelled as an equivalent two-column shear frame by increasing the bending stiffness of each pile 1.5 times as that of the pile in the prototype (Chopra, 2012). Similarly, in the transverse direction, the piles in four rows are converted into two rows by increasing the bending stiffness two times as that of the original pile. Therefore, each pile in the simplified model corresponds to the three piles in the prototype. The concept of this simplification is illustrated in Fig. 5.2. The wing wall, vertical wall, and the footing of the abutment in the centrifuge experiment are made of aluminium. The specifications of the abutment are tabulated in Table 5-2. The details of the model abutment are shown in Fig. 5.3. In the experiment, four rectangular acrylic piles are used to support the abutment in the centrifuge experiment.

Table 5-2: Specifications of the abutment.

	Model	Prototype
Material type	Aluminium	Reinforced concrete
Length	50 mm	5 m
Width	50 mm	5 m
Height	80 mm	8 m
Weight (kN)	1.74×10^{-3}	1.74×10^{3}
Height of gravity center (from base)	26 mm	2.6 m

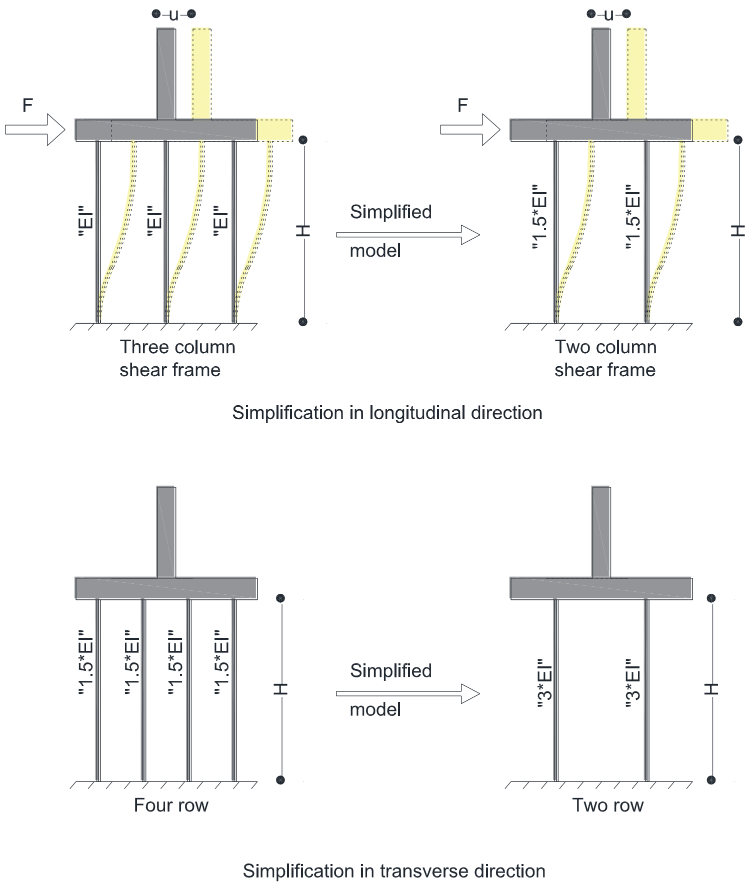

Fig. 5.2: Concept of simplification of the 3×4 piled abutment to the 2×2 piled abutment.

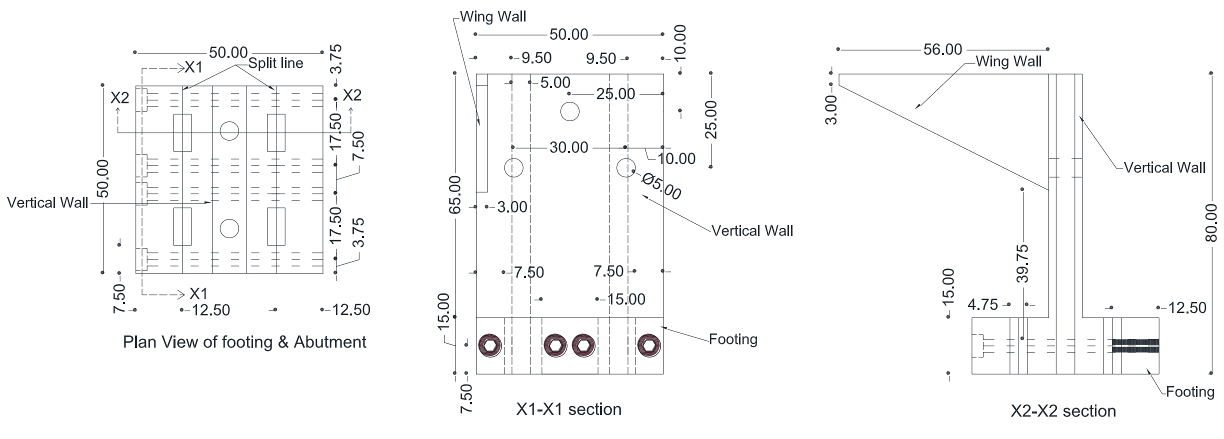

Fig. 5.3: Plan and cross-sections of the model abutment (all the dimensions are in mm in model scale).

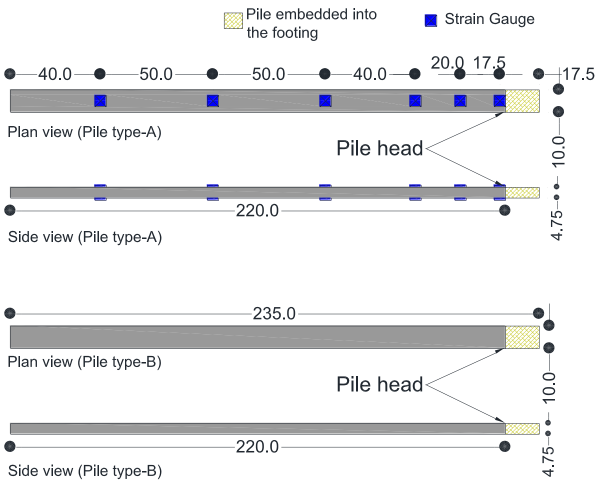

Fig. 5.4: Acrylic pile used in the centrifuge experiment and the instrumentation with strain gauges (the dimensions are in model scale).

The head of the piles is rigidly attached to the abutment footing. Whereas, the tip of the piles is kept free inside the ground. Two piles out of four are instrumented with strain gauges to measure the bending moment at different depths. The instrumented piles (Pile type-A) are attached to the abutment at the opposite side of the container wall, as shown in Fig. 5.1. The dimensions of the pile and the locations of the strain gauges on the pile are shown in Fig. 5.4. The specifications of the acrylic piles together with those aimed in the prototype are listed in Table 5-3.

Table 5-3: Specifications of the pile foundation.

	Model	Prototype
Material type	Acrylic	Reinforced concrete
Length	220 mm	22 m
Number of piles in half section	2 × 2	3 × 4
Sectional dimensions (mm)	4.75 × 10	360
Modulus of Elasticity (N/m2)	3.14×10^9	2.3×10^{10}
Bending stiffness of pile, EI (N-m^2)	0.28	1.9×10^7

It is already mentioned that the sheet pile reinforcement is used in this study. A 2.5 mm thick steel plate (in model scale) is used as sheet pile here. The sheet pile is embedded 14 m deep into the dense layer to mitigate the lateral spreading of the overlying loose sand. The top of the sheet pile is extended 3 m into the non-liquefiable embankment. The top and the tip of the sheet pile are kept free. It was found that the extension of the sheet pile width beyond the target area doesn't have any additional advantage, which is described in Chapter 3. Therefore, the region only in front of the abutment is reinforced with sheet pile in C-6. The 5 m width (in prototype) sheet pile is instrumented with strain gauges to measure the bending moment at different depths. The instrumentation and the specification of the sheet piles are described in Chapter 3.

The preparation of the model ground is described in Chapter 3. The piles of the abutment, as well as the sheet pile, are usually driven into the ground in practice. However, the sheet pile and the abutment piles are placed into the container before the soil is poured due to the ease of model preparation. Therefore, the effect of the ground densification due to the driven piles and sheet piles, in reality, cannot be simulated in the experiment. The ground response characterised by the surface settlement, horizontal ground movement, generation of excess pore water pressure and the seismic acceleration at different depth is properly recorded during the experiment. A sufficient number of sensors, for example, accelerometers, pore pressure gauges, potentiometers and Laser Displacement Transducers (LDT) are installed at different locations, as shown in Fig. 5.1. The sensors located inside the ground are installed during the model ground preparation.

5.2.2 Applied ground motions

Two successive ground motions are applied to the model ground, as shown in Fig. 5.5. The Japanese design specification for highway bridges (Japan Road Association, 2014) recommends the sustainability of the highway bridges should be checked for Level-2 earthquake. Therefore, the Tohoku ground motion is applied to the model ground. The recorded acceleration at the base of the container is similar to the real Tohoku Earthquake recorded at the ground surface near the New Bansuikyo Bridge, Tochigi (2-I-I-3, NS component) which corresponds to Type-1 Level-2 earthquake. Unfortunately, the magnitude is comparatively smaller. A comparison of the spectral accelerations of the applied ground motions and the design spectra of Level-2 earthquake (2-I-I-3) is shown in Fig. 5.6. The figure shows that the applied Tohoku ground motion is comparatively smaller than the design spectra. However, the first ground motion applied to the model ground will be described as the Tohoku Earthquake in this chapter.

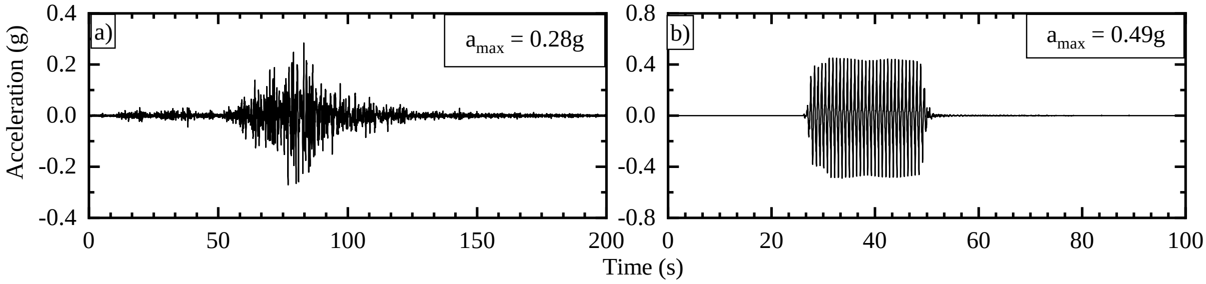

Fig. 5.5: Applied ground motions; a) Tohoku Earthquake and b) sinusoidal waves.

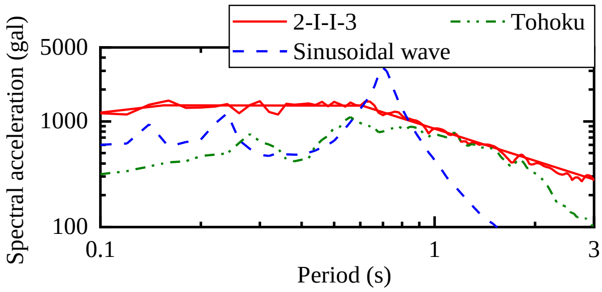

Fig. 5.6: Comparison of the design spectra of Level-2 earthquake and the spectral acceleration of the applied ground motions.

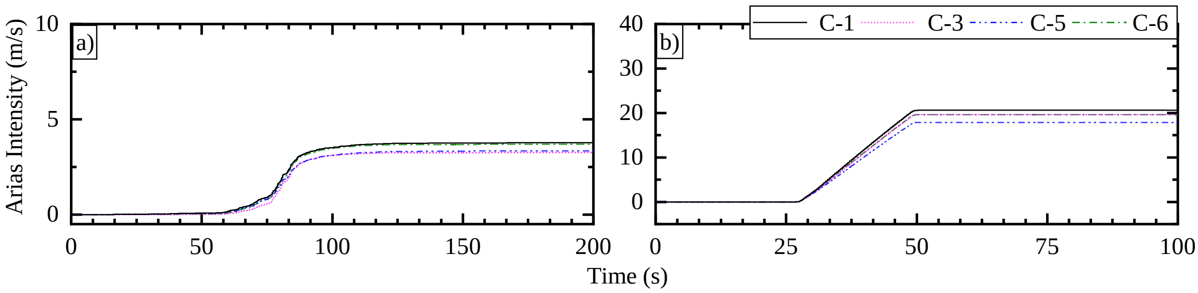

Fig. 5.7: Comparison of the Arias intensity of the applied ground motions in all the cases; a) Tohoku earthquake and b) sinusoidal waves.

Comparatively strong sinusoidal waves are applied in the second shaking as the first ground motion is smaller in magnitude than the design earthquake. The frequency and the amplitude of the sinusoidal waves are 1.42 Hz and 0.49 g, respectively. It is to be mentioned here that the second ground motion is applied once the excess pore water pressure by the first ground motion is completely dissipated. The Arias intensity (Arias, 1970) of the applied ground motions in C-5 and C-6 is compared along with C-1 and C-3, as shown in Fig. 9 to check the repeatability of the input motions in different experimental cases and the difference in the applied energy to the model.

The graphs show that the Arias intensity of the input ground motions in all the cases is quite comparable.

5.3 Experimental results and discussions

The recorded data are presented and described in the prototype scale. The important parameters include the propagation of the seismic wave, the evolution of excess pore water pressure, associated ground deformation, displacement of the abutment and the induced bending moment on the piles.

5.3.1 Evolution of excess pore water pressure

The generation of excess pore water pressure triggers the lateral spreading, which is augmented by the liquefaction of the soil inside the channel. Several pore pressure gauges are installed in the loose and the dense soil under the embankment slope (P2-3) and inside the river channel (P3-3 and P3-5) to monitor the evolution of excess pore water pressure.

The excess pore water pressure time histories in C-5 (abutment without sheet pile) and C-6 (abutment with sheet pile) under the slope (P2-3) and inside the channel (P3-3), and immediately below the liquefiable layer inside the river channel (P3-5) are shown in Fig. 5.8, and Fig. 5.9, respectively. The pore pressure gauge P2-3 is located right behind the abutment pile in C-5 and C-6. The graphs show namely the r_u values of the liquefiable layer inside the river channel (P3-3) reaches 1.0 at the early stage of shaking at about 71 s and 30 s during the Tohoku Earthquake and the sinusoidal waves, respectively. The soil at P3-5, located 3.5 m deep into the dense layer, almost reaches the liquefied state at about 85 s which is followed by a quick dissipation afterwards in the Tohoku Earthquake. Whereas, the soil at P3-5 gets liquefied for the sinusoidal waves. The soil at P2-3 doesn’t liquefy during the Tohoku Earthquake. However, the ground reaches the liquefied state nearly at 36 s for the sinusoidal waves.

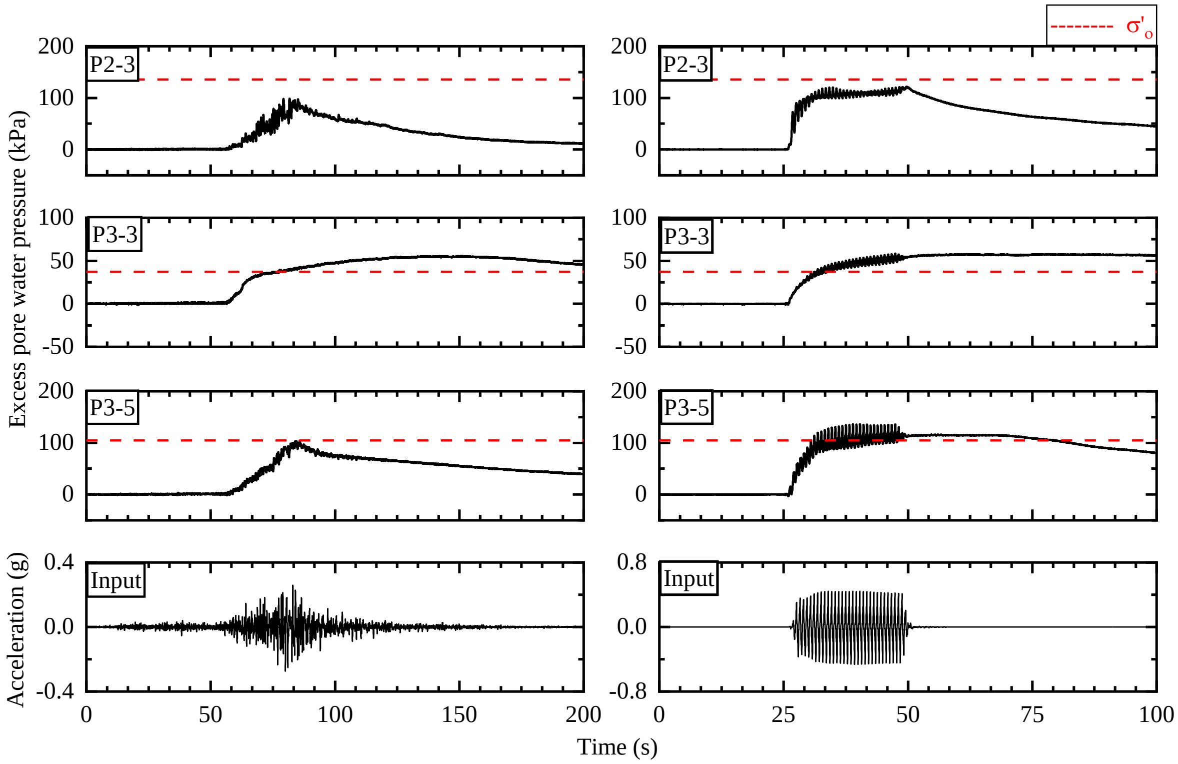

Fig. 5.8: Excess pore water pressure time histories at P2-3, P3-3, and P3-5 in C-5 during Tohoku Earthquake (left column) and sinusoidal waves (right column).

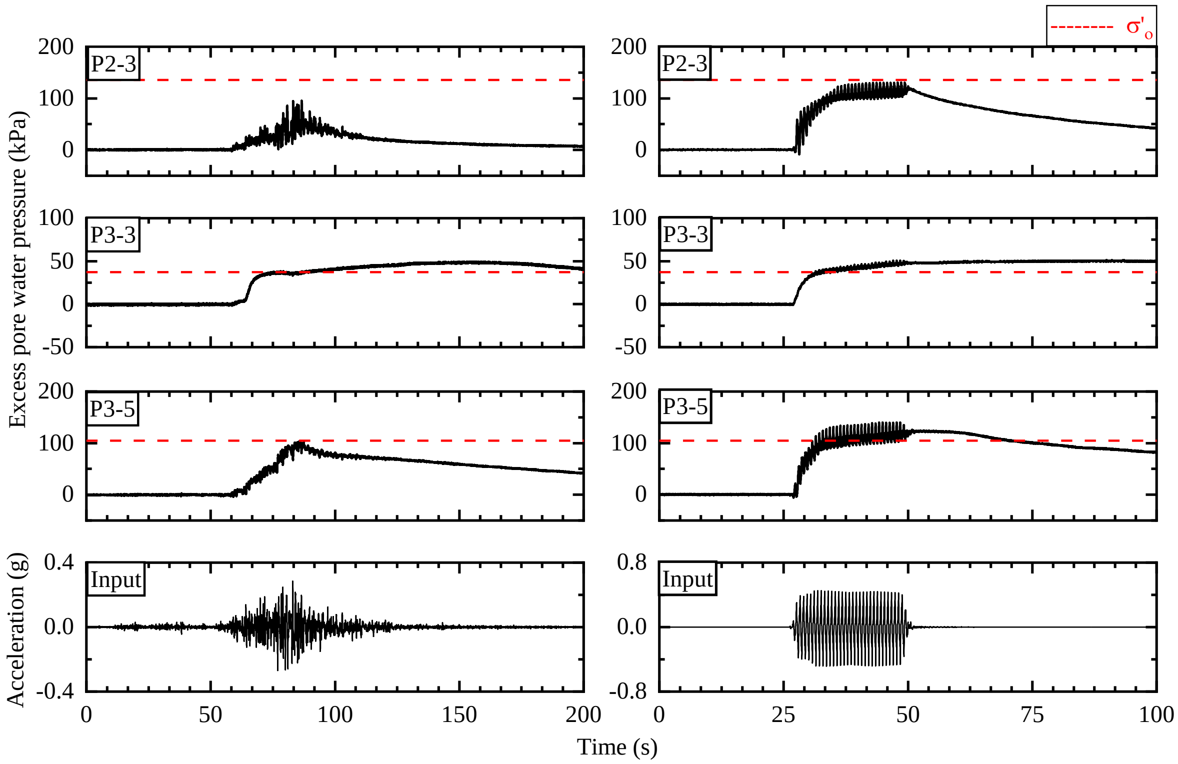

Fig. 5.9: Excess pore water pressure time histories at P2-3, P3-3, and P3-5 in C-6 during Tohoku Earthquake (left column) and sinusoidal waves (right column).

The evolution of the excess pore water pressure at the corresponding locations in the case on the embankment without abutment and sheet pile (C-1) (that is described in Chapter 3) is shown in Fig. 5.10. The comparison of the excess pore water pressure evolutions in the different cases reveals that the excess pore water pressure at P3-5 in C-1, C-5, and C-6 is almost the same in phase and magnitude. The r_u value at P3-3 also reaches 1.0 in all three cases. As for the pore pressure gauge at P2-3, although its position in C-1 is slightly different from that in C-5 and C-6, their trends of excess pore water pressure generation are comparable. The excess pore water pressure in C-3, which is not shown here is comparable to the other cases.

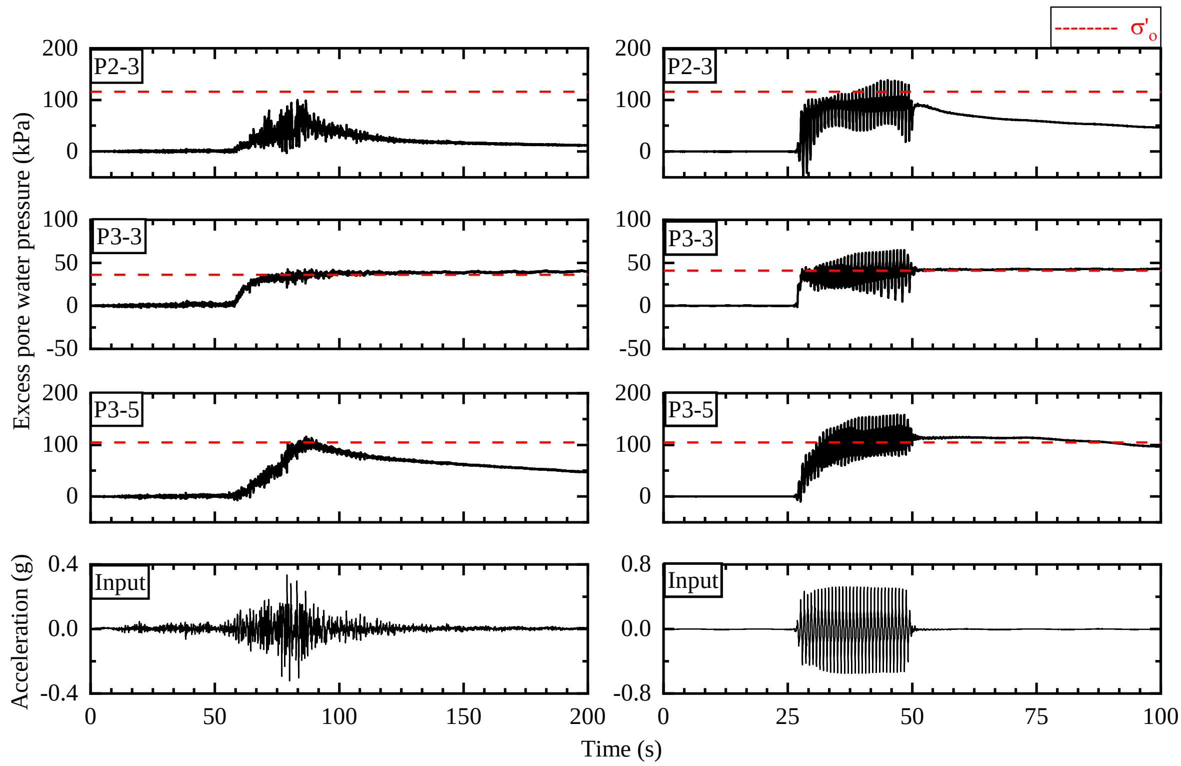

Fig. 5.10: Excess pore water pressure time histories at P2-3, P3-3, and P3-5 in C-1 during Tohoku Earthquake (left column) and sinusoidal waves (right column).

It is observed that the overall ground responses in terms of excess pore water pressure evolution in all the experimental cases are almost the same. It indicates that the structural elements have a minor influence on the evolutions of excess pore water pressure in the region located far from them. Besides, the experimental observation shows that dense soil can also liquefy depending on the magnitude and duration of the earthquake.

5.3.2 Efficiency of sheet pile to mitigate the channel-ward movement of the ground and the abutment

The expected function of the sheet pile is to mitigate the channel-ward movement of the ground. It is expected that the mitigation of the lateral spreading can reduce the channel-ward movement of the abutment thus minimize the damage associated with the lateral spreading. The channel ward ground movement of the cases with and without abutment is compared in this section. Two targets (TR-1 and TR-2) are placed on the embankment slope to monitor the channel-ward movement of the ground, as shown in Fig. 5.1. The target TR-1 is located near the shoulder in C-1 and C-3 (the cases without abutment) (see Figs. 3.1 and 3.2), whereas, TR-1 corresponds to the abutment (2.0 m below the crest) in C-5 and C-6. The target TR-2 is located in the middle of the embankment slope, where the sheet pile is installed in C-3 and C-6.

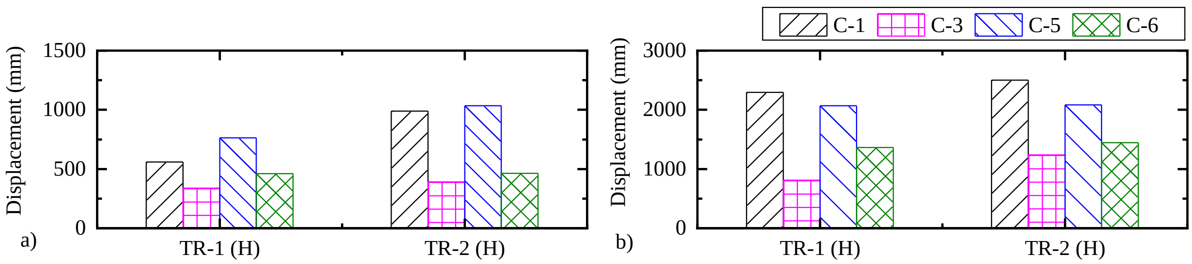

Fig. 5.11: Comparisons of the horizontal displacements at TR-1 and TR-2 in all the cases; a) Tohoku Earthquake and b) sinusoidal waves.

Comparisons of the horizontal displacement at TR-1 and TR-2 in all the cases are shown in Fig. 5.11 for the Tohoku Earthquake and the sinusoidal waves. The comparison of the horizontal displacement at TR-1 and TR-2 between reinforced and unreinforced cases with an abutment (C-5 and C-6) shows that the reinforcement can considerably reduce the channel-ward ground movement. Similarly, in C-1 and C-3, the horizontal displacement at TR-1 and TR-2 is also significantly reduced with the installation of sheet pile. The horizontal displacement time histories near the crest (2.0 m below the crest) of the abutment with and without the sheet pile (C-5 and C-6) are shown in Fig. 5.12. The graphs clearly illustrate that the channel-ward displacement of the abutment is reduced up to 41% for the Tohoku Earthquake, which is around 34% for the sinusoidal waves. This observation certifies the efficiency of the sheet pile as a seismic retrofit against the liquefaction-induced lateral spreading.

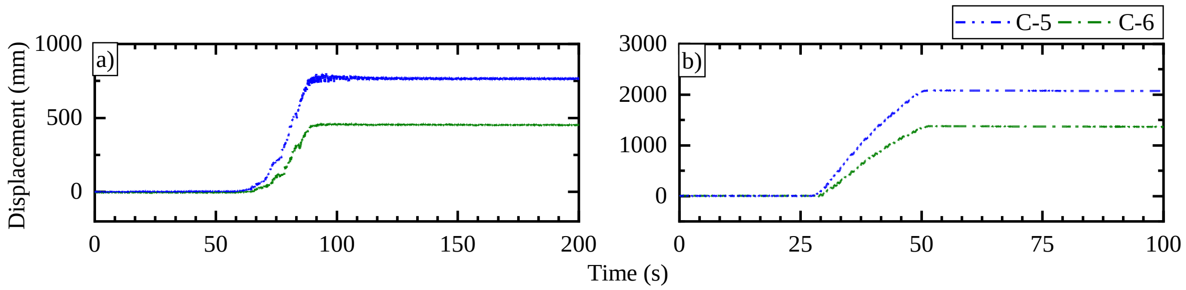

Fig. 5.12: Comparisons of the horizontal displacement time histories near the crest (2 m below the crest) of the abutment in C-5 and C-6; a) Tohoku Earthquake and b) sinusoidal waves.

The channel-ward movement of the embankment, as well as the abutment, is caused by the combined action of the propagated seismic energy to the embankment and the lateral spreading of the loose foundation. An attempt is made to quantify the channel-ward movement of the laterally spreading ground. Several vertical coloured noodles are placed at the various locations located at a certain distance from the sheet pile to track the ground movement after the shaking, as shown in Fig. 5.13. The coloured noodles are placed immediately behind the glass window to make the deformation visible from the outside of the container. The deformation of the coloured noodles after the successive shakings is manually measured and compared between the reinforced and unreinforced cases, as shown in Fig. 5.14. The coloured noodles are placed 9 m behind the sheet pile (towards the backfill), 1 m and 6 m in front of the sheet pile (towards the channel). Because of the build-up of excess pore water pressure in the dense layer as seen at P3-5 (see Fig. 5.9 for C-6,) a certain deformation of the ground takes place even in the dense layer, leading to the tilting of the sheet pile. However, the stiff sheet pile can constrain the liquefied soil in the loose layer and make the distribution of the horizontal displacement rather straight compared to the case without sheet pile (see the displacement profile at a distance of 1 m towards channel from sheet pile). As a result, the ground deformation in the reinforced cases (C-3 and C-6) is significantly smaller than the ground deformation in the unreinforced cases (C-1 and C-5). Therefore, the graphs clearly illustrate the efficiency of the sheet pile to mitigate lateral spreading.

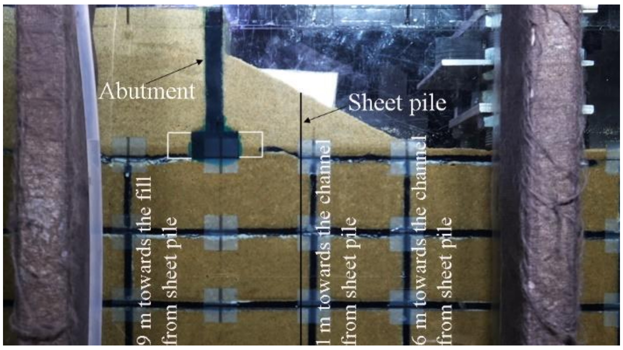

Fig. 5.13: Locations of the abutment, sheet pile and the vertical noodles in the experimental model.

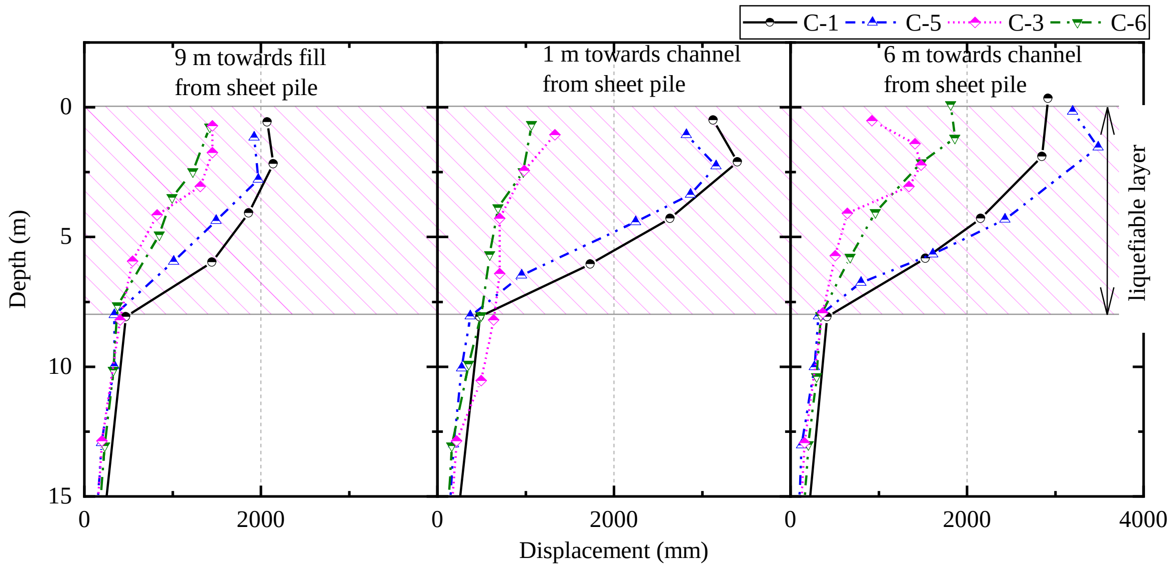

Fig. 5.14: Displacement profiles of the foundation ground at different distances from the sheet pile after the application of Tohoku Earthquake and sinusoidal waves.

The ground deformation profiles in Fig. 5.14 and the horizontal displacement of the targets TR-1 and TR-2 in Fig. 5.11 reveal that the channel-ward movement of the ground below the abutment (or below the embankment slope in the case without abutment) is not affected by the existence of the abutment but is controlled by the existence of the sheet pile. These indicate that the piled abutment is almost following the movement of the ground. A comparison of the displacement time histories at TR-2, which is at the top of the sheet pile in C-3 (without abutment) and C-6 (with abutment), are shown in Fig. 5.15. This graph also shows that the horizontal displacement of the sheet pile is almost the same irrespective to the existence of the abutment. These clearly illustrate that the old piled abutment is relatively flexible as compared to the sheet pile that has a minor pinning effect on the ground movement. Besides, the channel ward ground movement, which is predominantly controlled by the sheet pile in the reinforced cases, leading to the less rotation of the foundation in the reinforced cases as will be described in the following sections. On the contrary, in the case with comparatively stiff piles, marked pinning effect could be confirmed, and such piles could attract more load from laterally spreading soil (Armstrong et al., 2013).

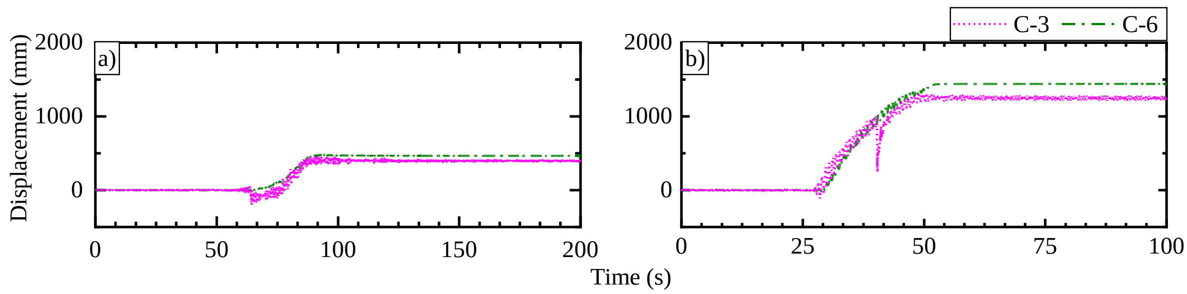

Fig. 5.15: Comparison of the displacement time histories at TR-2 in C-3 and C-6; a) Tohoku Earthquake and b) sinusoidal waves.

5.3.3 Bending moment response of sheet pile

The sheet pile as a seismic retrofit carries a large amount of kinematic load imposed by the laterally spreading soil and the embankment. The bending moment response of the sheet pile provides the information regarding its contribution to carrying the load imposed by lateral spreading. The sign convention used here for the bending moment of the sheet pile is shown in Fig. 5.16 (a). The bending moment that causes the curvature of the sheet pile concave towards the river channel is considered as positive bending moment. A comparison of the bending moment profiles of the sheet pile in C-3 (without abutment) and C-6 (with abutment) is shown in Fig. 5.17 when the sheet pile experiences the maximum bending moment. The maximum bending moment takes place around 86.0 s in Tohoku Earthquake and 48.0 s in sinusoidal waves. The graph demonstrates that the bending moment profiles of the case with and without abutment are comparable except the upper part (at a depth up to 4 m from the ground surface) of the sheet pile, particularly during the sinusoidal waves. The difference in the bending moment profile is probably because of the interaction between the abutment footing and the sheet pile. Apart from this minor difference, the bending moment profiles are very similar in terms of shape and magnitude. It indicates that the majority of the mobilized load from the laterally spreading soil is carried by the sheet pile rather than the abutment piles. In another word, the ground deformation around the old piled abutment is mostly controlled by the sheet pile reinforcement.

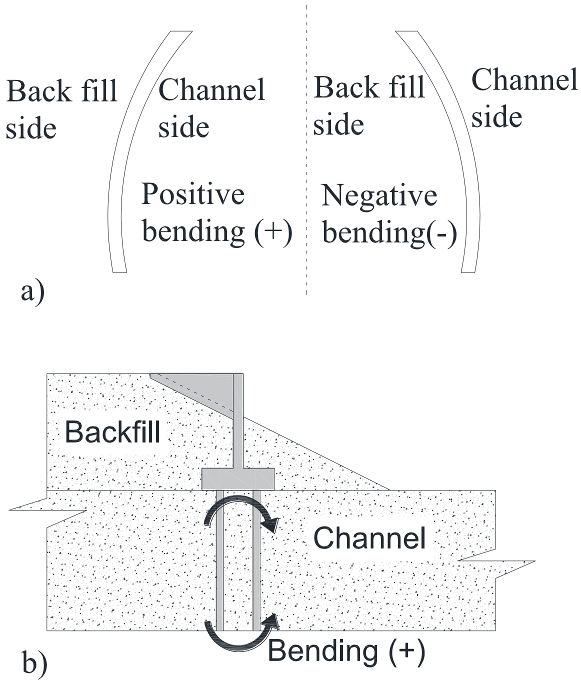

Fig. 5.16: Sign convention used in this study; a) sheet pile and b) bending moment.

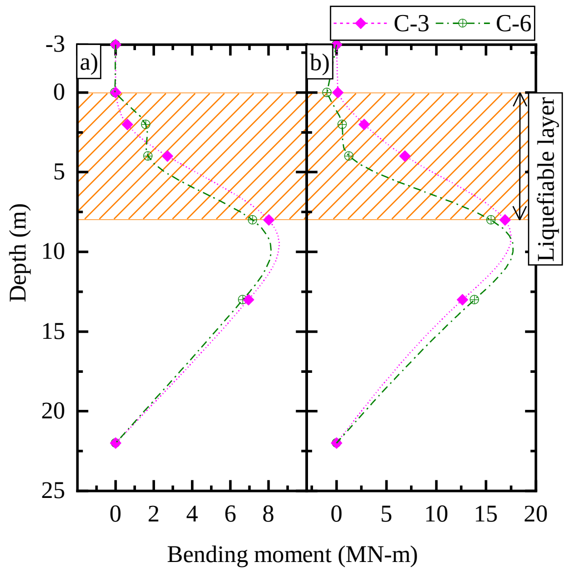

Fig. 5.17: Comparisons of the bending moment profiles of sheet pile in C-3 and C-6 when sheet pile experiences the maximum bending moment; a) Tohoku Earthquake and b) sinusoidal waves.

5.3.4 Mitigation of bending moment of abutment piles

The abutment pile in laterally spreading soil can be damaged due to bending caused by the kinematic force from the soil and the inertia force from the abutment. The efficiency of the sheet pile to mitigate the pile bending moment is investigated in this section. Two piles are instrumented with strain gauges, as shown in Fig. 5.4 to record the bending strain during the experiment. The sign convention used for the bending moment of the piles is shown in Fig. 5.16 (b). The sign convention for piles is the same as the sign convention used for the sheet pile. The channel-ward concave curvature of the pile is considered as positive bending.

The bending moment profiles of Pile-1 and Pile-2 (see Fig. 5.1) in C-5 (without sheet pile) and C-6 (with sheet pile) are shown in Fig. 5.18 when the piles experience the maximum bending moment. Pile-1_5 in Fig. 20 represents the bending moment profile of Pile-1 in C-5. Similarly, Pile-2_5, Pile-1_6 and Pile-2_6 represent Pile-2 in C-5, Pile-1 in C-6, and Pile-2 in C-6, respectively. The two piles do not necessarily experience the maximum bending at the same time. For example, Pile-1 and Pile-2 experience maximum bending moment both at 86.83 s during Tohoku Earthquake whereas, during the sinusoidal waves Pile-1 experiences the maximum bending moment at 49.59 s and Pile-2 experiences the maximum bending moment at 49.52 s. However, the piles most of the cases experience maximum bending moment almost at the end of the effective shaking. The bending moment distributions in Fig. 5.18 show that the piles exhibit different response due to the existence of sheet pile reinforcement. The piles in the reinforced case (C-6) experience maximum bending moment near its head whereas, the maximum bending moment is observed near the interface of the loose and the dense layer in the unreinforced case (C-5). This tendency is clearly seen for the Tohoku Earthquake.

The alteration of the pile response in the reinforced case is probably because of the change in the ground displacement profile around the piles and the limited rotation of the pile. The latter will be described in the next subsection. This largely influences kinematic load from the soils. The existence of the sheet pile alters the ground displacement profile around the abutment piles as explained in Subsection 5.3.2. The sheet pile erases the large change in the horizontal displacement around the interface between the loose and dense layers. This contributes to the significant reduction of the bending moment around the interface. The smaller channel-ward displacement of the abutment in the reinforced case decrease the bending moment near the pile heads. Besides, because of the frame formed with the footing and piles, the movement of the abutment is translational and hence the reduction of the bending moment around the interface also contributes to the reduction of the bending moment near the pile heads. As a result, the reduction of the bending moment is nearly around 40% near the pile head and the interface of the loose and the dense layer as well. It should be noted that the bending moment near the pile heads (at a depth of 2 m from the ground surface) cannot be measured during the sinusoidal waves in the unreinforced case (C-5) because of the malfunctioning of the strain gauges.

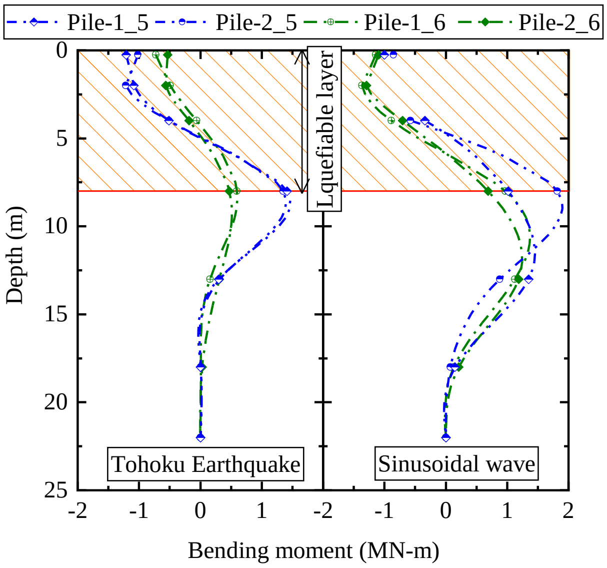

Fig. 5.18: Bending moment profiles for Pile-1 and Pile-2 in C-5 and C-6 when the piles experience the maximum bending moment.

The bending moment near the pile head is caused by the combined action of the kinematic load from the soils and the inertia force of the abutment. The effect of inertia force on the pile bending moment gradually decreases with depth. The time histories of the bending moment near the head of the Pile-1 and Pile-2 (at a depth of 0.25 m) along with the horizontal displacement at the middle of the embankment slope (TR-2) and acceleration of the abutment footing (A-ft) in C-6 (with sheet pile) are shown in Fig. 5.19 to observe the contribution of the inertia force of the abutment. The maximum bending moment appears just after the principal shock. The maximum bending moment takes place at 86.83 s in the Pile-1 and Pile-2 during the Tohoku Earthquake. Whereas, the peak acceleration of the abutment is recorded at 84.27 s. The bending moment is observed to increase with the increasing channel-ward movement of the embankment slope even after the principal shock. This indicates that the maximum bending moment does not necessarily coincide with the event of peak acceleration of the abutment and is predominantly guided by the lateral spreading of the ground. Therefore, simultaneous application of the inertia force using peak acceleration and the kinematic effect induced by the lateral spreading in the design calculation for piled abutment might yield a rather conservative result.

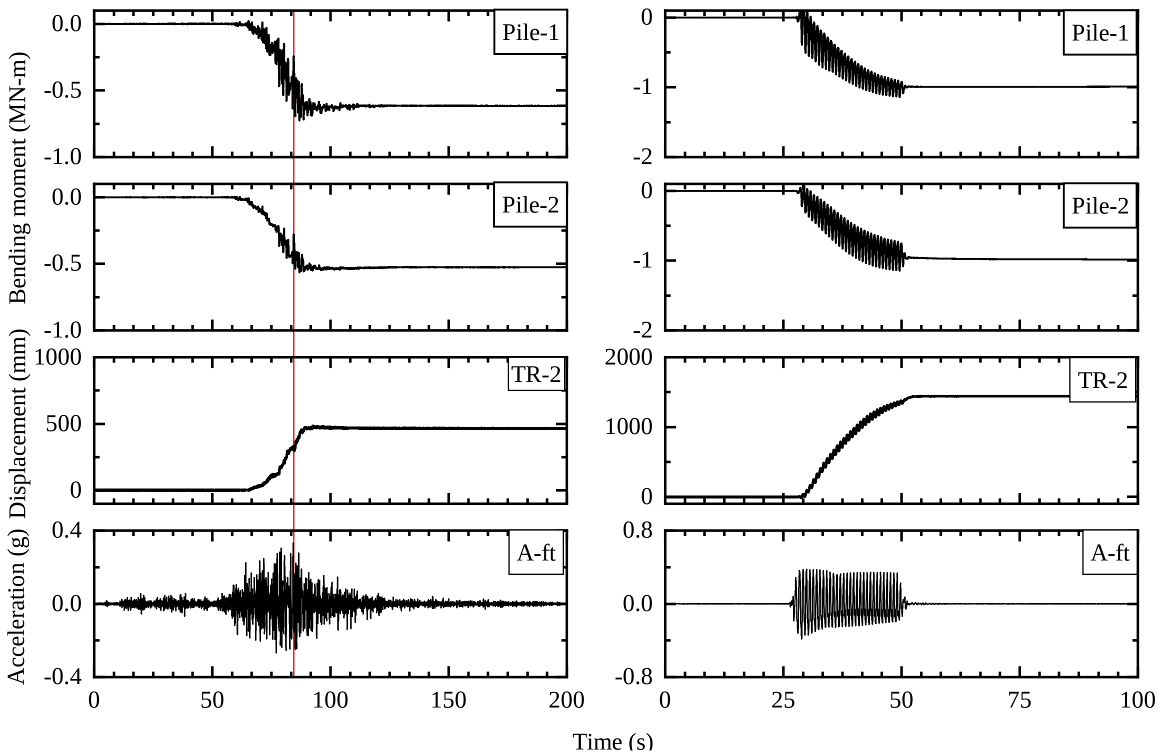

Fig. 5.19: Time histories of bending moment near the head of the Pile-1 and Pile-2 (at a depth of 0.25 m), horizontal displacement at the middle of the embankment slope (TR-2) and acceleration of the abutment footing (A-ft) in C-6.

5.3.5 Deformation mode of abutment piles

If we ignore the strut effect of the bridge girder as in this experiment, a piled abutment is expected to show the translational movement because of the frame formed with the footing and piles. In this type of deformation pattern, the bending stress in a pile arises due to the excessive translation of the comparatively rigid footing. The deformed shape of the pile provides an idea about the failure mechanism of the pile in this type of deformation pattern. The deformed shape of Pile-1 and Pile-2 along with the deformed shape of the abutment is plotted in Fig. 5.20 when the piles experience the maximum bending moment during the Tohoku Earthquake. The deformed shape is calculated from the bending moment recorded during the experiment. The simple area-moment method of beam deflection is used here to estimate the pile displacement. In the calculation, it is assumed that (1) the pile heads have equal translational displacement as they are connected to the rigid footing and (2) the horizontal movement of the pile tips is considered as zero. As for the second boundary condition, the pile tips are free to move in reality. However, as the magnitude of the displacement at the pile tip is negligibly small in comparison with the pile head displacement, this assumption is applied in the calculation.

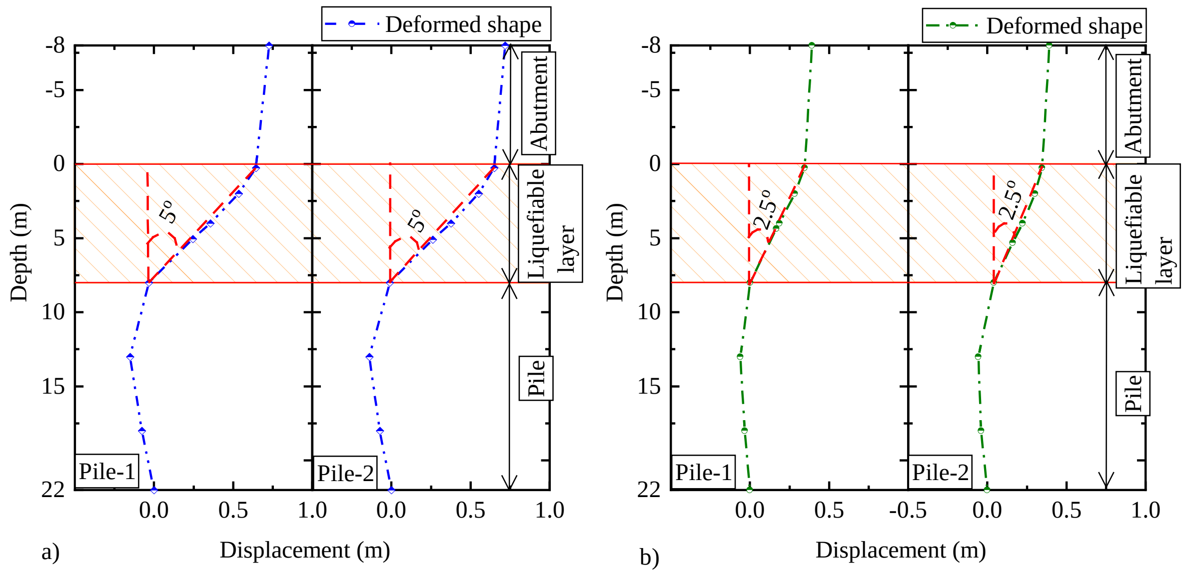

Fig. 5.20: Displacement profiles of Pile-1 and Pile-2 along with the abutment in a) C-5 (without sheet pile) and b) C-6 (with sheet pile) when the piles experience the maximum bending moment during Tohoku Earthquake.

The deformed shape of the piles and the abutment without reinforcement (C-5) shows that the piles go under significant rotation at the interface of the loose and dense layer without causing any major tilting of the abutment. The rotation of the pile described in this section differs from the rotational displacement described in Chapter 4. The rotational displacement of the sheet pile described in Chapter 4 is primarily caused due to the tilting of the sheet pile triggered by the softening of the shallow dense ground. Whereas, the rotation of the abutment piles described in this section is primarily because of the bending of the piles triggered by the lateral spreading in the liquefiable zone. The rotation of the pile is estimated around 5° in the unreinforced case. This excessive rotation of the pile without any significant tilting of the abutment increases the bending stress near the pile head and the interface of the loose and the dense layer. The installation of the sheet pile reduces the kinematic load acting on the piles and the translational movement of the abutment thus significantly reduce the rotation of the pile, as shown in Fig. 5.20 (b). The rotation of the pile is reduced to 2.5° in the reinforced case, which is resulted in the significant reduction of the bending stress at the pile head and the interface. The installation of the sheet pile without any direct connection to the abutment does not change the deformation pattern of the piles but could mitigate excessive displacement of the abutment and pile bending moment.

5.4 Simulation of centrifuge experiment

5.4.1 Numerical model and boundary conditions

Two-dimensional finite element analysis is also used in this chapter to simulate a dynamic centrifuge experiment dealing with the bridge abutment reinforced with sheet pile. Two-dimensional finite element analysis is conducted under plain-strain condition considering a domain with a unit width in the transverse direction. The discretized mesh for the numerical model is shown in Fig. 4.3. A uniform mesh having the dimensions of 1 m × 1 m in X and Y direction, respectively, is used throughout the foundation ground except near the structural elements. The mesh size has been changed a little in those particular areas to accommodate the structural elements. Besides, the embankment is modeled with a comparatively finer mesh having the dimensions of 1 m × 0.5 m in X and Y direction, respectively, to accommodate the slope of the embankment having the side slope 1:2. Boundary conditions in the numerical model are imposed in such a way that it can simulate the experimental boundary conditions. All the movements of the nodes are restricted at the bottom boundary. The nodes along the vertical boundary are kept free to move vertically during the initial stress analysis, which is restricted in the dynamic analysis. Whereas, the horizontal movement is restricted in both cases. All other nodes are set free against translational and vertical movement. Besides, the fluid flow velocity in the horizontal direction at the boundaries of the analytical domain are set to zero.

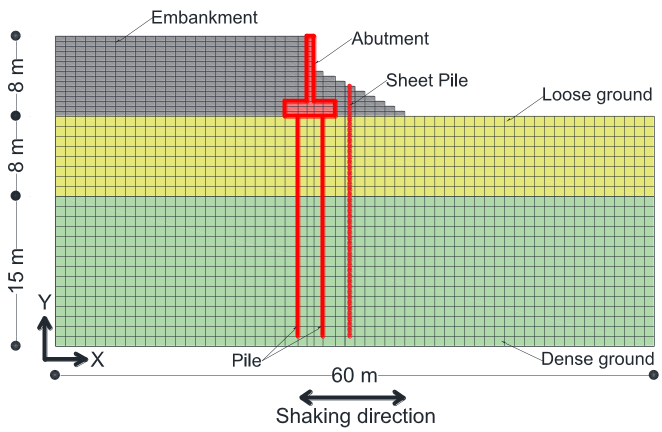

Fig. 5.21: Discretized mesh for the two-dimensional finite element model.

The soil ground is modeled as a four-nodes quadrilateral solid element. An elasto-plastic soil constitutive model proposed by Asaoka et al. (2002) is used to simulate the dynamic response of the modeled ground. The selection of soil parameters is described in section 4.3.1 in Chapter-4. The sheet pile is modeled as an elastic beam element. The bending stiffness (EI) of the sheet pile is 5.2×10^8 N-m^2/m. The bending stiffness of a one-meter width sheet pile is used in the numerical analysis to model the sheet pile in the plane strain condition. The footing and the vertical wall of the abutment are modeled as the quadrilateral elastic solid element. Whereas, the piles are modeled as an elastic beam element. The parameters for piled abutment are listed in Table 5-4. The crucial part of this modeling technique is to model the three-dimensional abutment in the plain strain condition. The unit width of the abutment is modeled here. Besides, the stiffness of the piles in a row is assumed to be uniformly distributed along the width of the abutment in the numerical analysis. For example, if the physical model has two piles in each row, the total stiffness of these two piles divided by the width of the abutment is assigned as the stiffness of the representative pile for that row in the numerical model. A master-slave node technique is applied to connect the structural elements to the soil domain at its specified location. The master and slave node technique offers an identical deformation between the nodes of the structural element and the corresponding linked node of the soil element.

Table 5-4: Material parameters for piled abutment.

Element	Parameters	Specification
Vertical wall	ρ (Mg/m^3)	2.63
	E (Pa)	6.9×10^{10}
	υ	0.33
Footing	ρ (Mg/m^3)	2.67
	E (Pa)	6.9×10^{10}
	υ	0.33
Pile	EI (N-m^2/m)	2.24×10^7
	EA(N/m)	1.19×10^9

5.4.2 Comparison of the experimental and numerical results

The capability of this numerical model to capture the dynamic properties of the ground is already described in Chapter-4. The dynamic response of the ground is characterized by the evolution of the excess pore water pressure, propagation of the seismic wave, and associated ground deformation. However, the dynamic response of the structural elements, for example, the displacement of the abutment and the sheet pile, and the bending moment of the piles, is particularly focused in this chapter. Two sequential ground motions are used in the centrifuge experiment. The sinusoidal waves applied in this experiment is the exaggeration of the seismic excitation to observe the response of the ground and the structures in the extreme situation. The numerical model cannot properly simulate the extreme ground response during the sinusoidal waves. Therefore, the sinusoidal waves are not used in the numerical simulation. The experimental and the numerical results are compared for the Tohoku Earthquake only.

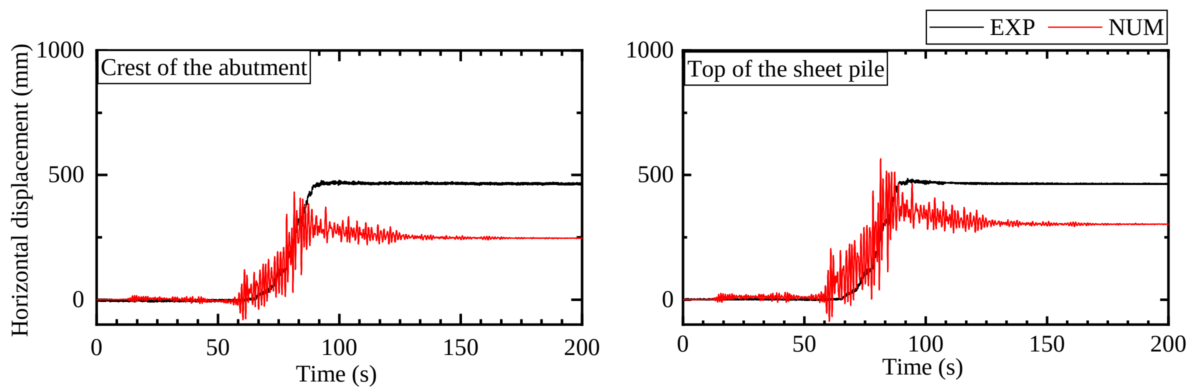

Fig. 5.22: Comparison of the experimental and numerical horizontal displacements at the crest of the abutment and the top of the sheet pile.

Figure 5.22 shows the comparison of the experimental and numerical horizontal displacement at the crest of the abutment and the head of the sheet pile. The horizontal displacement at the crest of the abutment is an important parameter to justify the performance of the retrofitting measure. The graph shows that the numerical simulation can map the experimental results with reasonable accuracy. The simulated results can map the horizontal displacements both in trend and magnitude up to 87 s and 88 s for the abutment and the sheet pile, respectively. Subsequently, a decreasing trend of the horizontal displacement at those locations is observed in numerical analysis. That yields a comparatively smaller horizontal displacement at the top of the sheet pile and the crest of the abutment in numerical analysis. This kind of structural rebound may take place in the case of very loose liquefied soil. However, the abutment and the sheet pile in this centrifuge experiment don't show this kind of phenomenon. The structural rebound in the numerical analysis may take place due to the fixity between the structural elements and the surrounding soils. The settlement of the soil elements behind the structures may pull it back towards its original position, thus reduce the total horizontal displacement.

A comparison of the bending moment profile of Pile-1 and Pile-2 when the pile head experiences the maximum bending moment is shown in Fig. 5.23. The graph shows that the simulated bending moment profile can exhibit good agreement with the experimental result. The numerical results also confirm that the maximum bending moment takes place near the head of the pile. Another peak is observed at the interface between the liquefiable and non-liquefiable layer. The pile head in numerical simulation experience a comparatively larger bending moment than the experimental results. The connection between the footing and pile head in numerical analysis is perfectly fixed that attract more bending moment. Whereas, the joint of the pile head and the footing in the centrifuge experiment is not perfectly fixed that might cause a comparatively smaller bending moment exactly at the head of the pile.

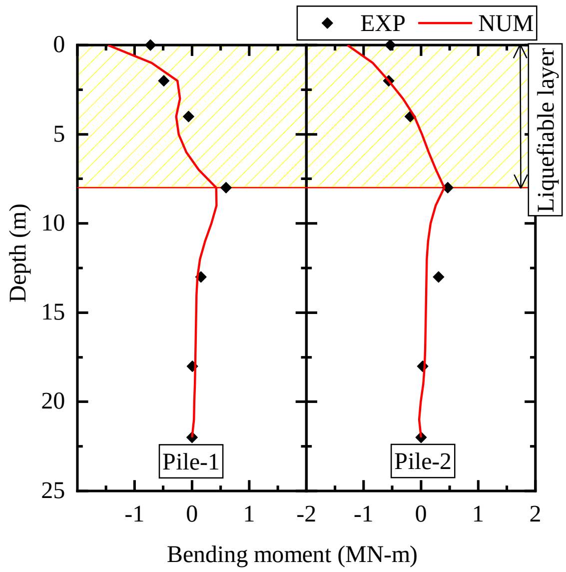

Fig. 5.23: Comparison of the experimental and numerical bending moments of Pile-1 and Pile-2 when the piles experience the maximum bending moment near its head.

5.5 Response of the bridge abutment without sheet pile reinforcement

The dynamic response of the bridge abutment with sheet pile reinforcement is experimentally determined that is numerically simulated using two-dimensional finite element analysis. The comparison of the experimental and numerical results in the previous section shows that the finite element model can reproduce the dynamic response of the ground as well as the structure with reasonable accuracy. Therefore, two-dimensional finite element analysis is used here to observe the seismic response of the bridge abutment without any reinforcement measure. The influence of the bridge girder on the dynamic response of the bridge abutment is also studied in this section. Usually, the bridge girder prevents the channel-ward movement of the abutment. Therefore, the horizontal movement near the crest of the abutment is restricted in the numerical analysis to simulate the effect of the bridge girder. The geometry of the ground and the bridge abutment is kept similar as it is described in the centrifuge experiment. The sheet pile is not used in these analyses. The analysis conditions are listed in Table 5-5. The case N_AB-1 represents the piled abutment passing through the 8 m thick liquefiable layer that is not reinforced with sheet pile. The effect of the bridge girder is not considered here. Whereas, in N_AB-2, the effect of bridge girder is taken into consideration. The case N_AB_SP is similar to the case N_AB_SP where the liquefiable layer is reinforced with sheet pile. It is worth mentioning that the Tohoku Earthquake is applied in the numerical analysis throughout this chapter.

Table 5-5: Analysis conditions to observe the effect of sheet pile and the bridge girder.

Case ID	Thickness of liquefiable layer (m)	Height of the abutment (m)	Existence of bridge girder	Existence of sheet pile
N_AB-1	8	8	No	No
N_AB-2	8	8	Yes	No
N_AB_SP	8	8	No	Yes

The horizontal displacements at the crest and the bottom of the abutment in N_AB-1 and N_AB-2 are plotted in Fig. 5.24 to show the effect of the bridge girder. The horizontal displacement of the abutment in N_AB-1 shows that the abutment goes under a significant channel-ward movement with a minor channel-ward inclination. Whereas, the abutment in N_AB-2 exhibits different response due to the effect of the bridge girder. The bottom of the abutment is observed to move towards the channel. Whereas, the movement near the crest of the abutment is restricted. This deformation pattern confirms the backward rotation of the abutment in the presence of a bridge girder. Besides, the horizontal displacement at the bottom of the abutment is also comparatively smaller than displacement recorded at the same location in N_AB-1.

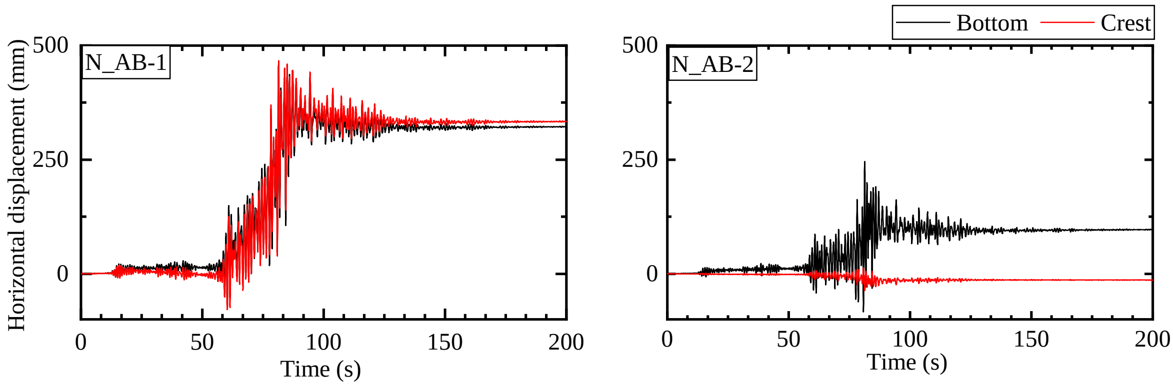

Fig. 5.24: The change in deformation pattern of the abutment with the effect of the bridge girder.

Figure 5.25 shows the bending moment profile of Pile-1 and Pile-2 at 81.4 s in N_AB-1 and 81.36 s in N_AB-2 when the piles experience the maximum bending moment profile near its head. The peak bending moment is observed to take place near the head of the piles as expected. It should be noted that the large bending moments are observed to take place near the pile heads and the interface of the loose and the dense layer in the experiments. The numerical analysis cannot precisely simulate the bending moment near the interface of the loose and the dense sand. The numerical analysis underestimates the bending moment at the interface, particularly in the unreinforced cases. The maximum bending moment in numerical analysis is always observed to take place near the pile heads both in the reinforced and the unreinforced cases probably because of the proper fixed connection between the pile heads and the footing. Careful observation shows that the shape of the bending moment profile of Pile-1 and Pile-2 is not very similar. It might happen because of the difference in the earth pressure distribution along with the pile. Figure 5.26 shows the shear force diagram of Pile-1 and Pile-2 in N_AB-1 at 81.4 s when the piles experience the maximum bending moment. The shear force diagram provides an idea regarding the earth pressure distribution of the pile. A clear difference in the earth pressure distribution is observed in the middle of the liquefiable layer, which is probably due to the effect of the lateral spreading. In finite element analysis, the soil nodes are connected to the pile nodes, which restricts the soil flow through the piles in the two-dimensional analysis. Therefore, the Pile-1 carries a large portion of the earth pressure imposed by the lateral spreading that changes the shape of the bending moment profile.

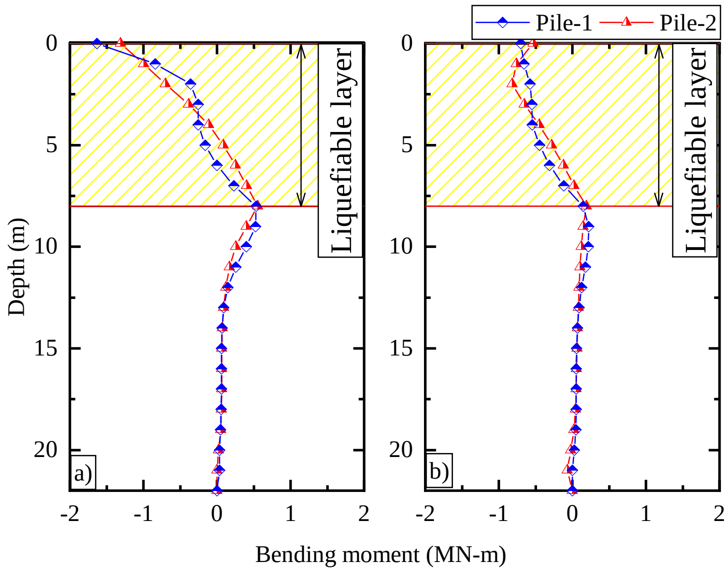

Fig. 5.25: Bending moment profiles of Pile-1 and Pile-2 when the pile experiences maximum bending moment near its head in a) N_AB-1 and b) N_AB-2.

A comparison of the magnitude of peak bending moment, as shown in Fig. 5.27, reveals the effect of the bridge girder on the seismic response of the piles. The graph shows that the existence of a bridge girder reduces the peak bending moment nearly up to 38% in Pile-2 and 57% in Pile-1. This reduction of the bending moment near the pile head is probably because of the considerable contribution of the bridge girder to carry the seismic load from the backfill, as shown in Fig. 5.28. Figure 5.27 also shows the peak bending moment near the head of the piles in the case of sheet pile reinforcement (N_AB_SP). The graph shows the peak bending moment of Pile-1 can be reduced up to 10% that is almost negligible in Pile-2. However, the experimental results show a higher efficiency of the sheet pile as a seismic retrofit to mitigate the bending moment near the pile heads. The development of the bending moment near the head of the pile is the complex interaction between the inertia force of the abutment and the kinematic force from the backfill soil and the laterally spreading soil. Therefore, the contribution of the inertia force of the abutment might play an important role here, which will be discussed in the next section.

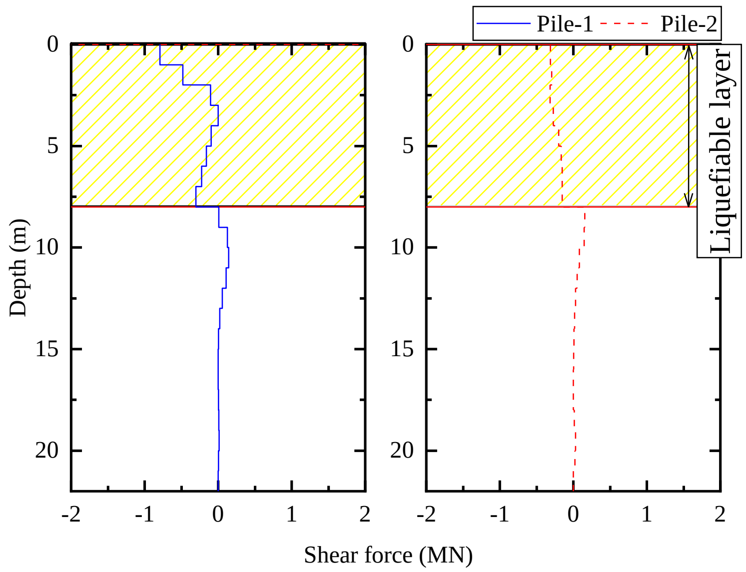

Fig. 5.26: Shear force distribution of Pile-1 and Pile-2 at 81.4 s when the pile heads experience maximum bending moment in N_AB-1.

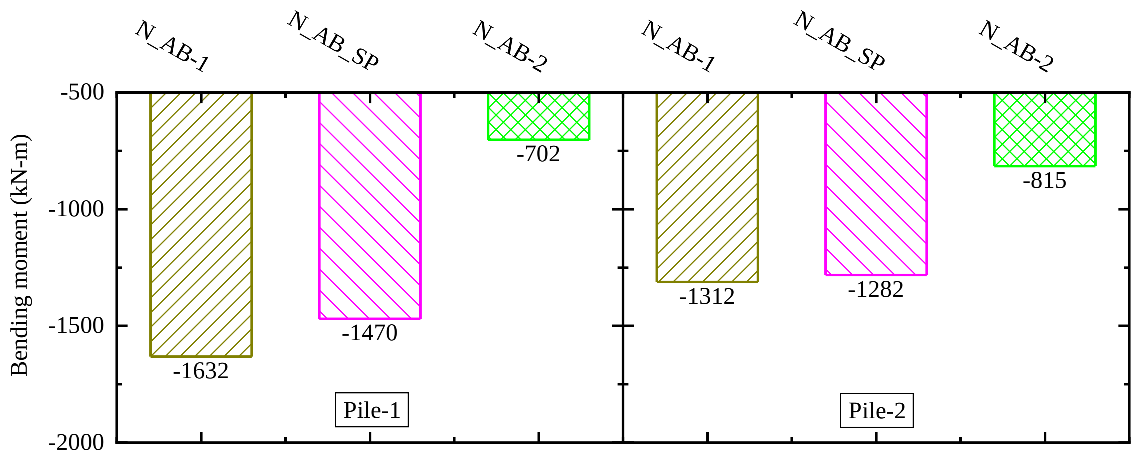

Fig. 5.27: Comparison of the peak bending moments of Pile-1 and Pile-2 near its head in three cases.

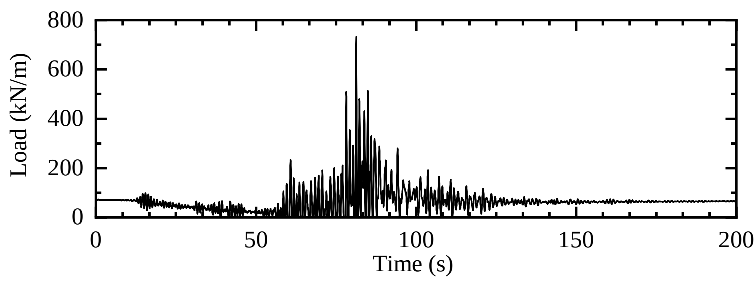

Fig. 5.28: Time histories of the load carried by the bridge girder in N-AB-2.

5.6 Effect of inertia force of the abutment

Two 2D finite element analyses are carried out to study the effect of the inertia force of the abutment. A comparatively uniform abutment is used here to avoid the effect of non-uniformity of the abutment. The discretized mesh used in these finite element analyses is shown in Fig. 5.29. The sheet pile is not used in these analyses. The analysis conditions are listed in Table 5-6. The abutment in N_AB_UN-2 is considered as entirely weightless to compare the effect of inertia force. Whereas, the density of the footing and the vertical wall in N_AB_UN-1 is estimated as 2.54 Mg/m^3 and 5.43 Mg/m^3, respectively. The density of the footing and the vertical wall is estimated in such a way that the total weight of the footing, vertical wall and the soil column on top of the footing remain the same as it is used in the centrifuge experiment.

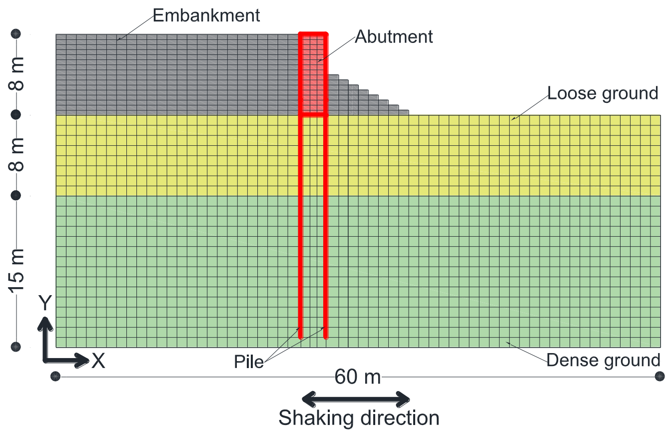

Fig. 5.29: Discretized mesh for two-dimensional finite element analysis to observe the effect of inertia force.

Table 5-6: Analysis conditions to study the effect of the inertia force of the abutment.

Case ID	Thickness of liquefiable layer (m)	Height of the abutment (m)	Existence of sheet pile	Density of the abutment (Mg/m^3)
N_AB_UN-1	8	8	No	2.54 (vertical wall) 5.43 (footing)
N_AB_UN-2	8	8	No	0

A comparison of the maximum bending moment near the head of Pile-1 and Pile-2 in N_AB_UN-1 and N_AB_UN-2 is shown in Fig. 5.30. The graph shows that the weightless abutment imposes 32% and 28% reduction of the bending moment to Pile-1 and Pile-2, respectively. It implies that the contribution of the inertia force to the maximum bending moment of the piles is significantly large. The purpose of using sheet pile is to reduce the lateral spreading of the liquefied ground, thus, reduce the bending moment of the piles. However, the bending moment originated from the inertia force of the abutment cannot be prevented by the installation of the sheet pile.

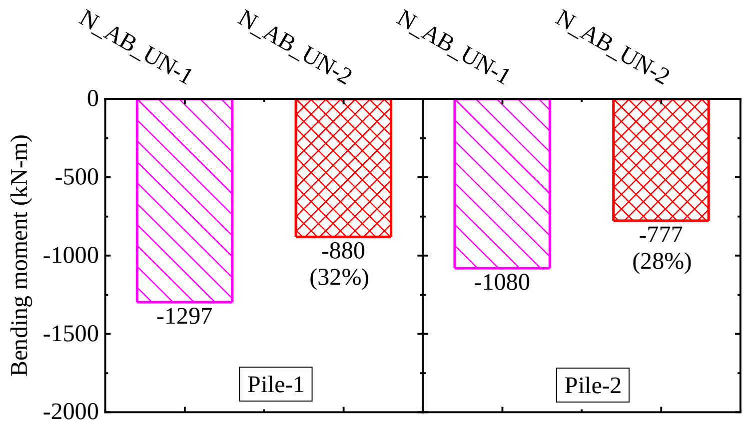

Fig. 5.30: Contribution of the inertia force of the abutment to the bending moment of Pile-1 and Pile-2.

5.7 Effect of the stiffness of sheet pile

It is observed that the increase in the stiffness of sheet pile increases its performance to reduce lateral spreading. Therefore, an attempt is made to observe the effect of sheet pile stiffness to reduce the bending moment of the abutment piles. Two finite element analyses are carried out in this regard. The ground geometry and the discretized mesh are kept similar as it is described in section 5.4.1. The stiffness of the sheet pile is considered as 2*EI in the first case and 4*EI in the second case where EI is the stiffness of the sheet pile used in the centrifuge experiment. The analysis conditions are listed in Table 5-7.

Table 5-7: Analysis conditions to observe the effect of the stiffness of sheet pile on the response of abutment piles.

Case ID	Thickness of liquefiable layer (m)	Height of the abutment (m)	Existence of bridge girder	Stiffness of sheet pile
N_AB_SP_1	8	8	No	2*EI**
N_AB_SP_2	8	8	No	4*EI**

** EI (5.2×10^8 N-m^2/m) is the stiffness of the sheet pile used in the centrifuge experiment

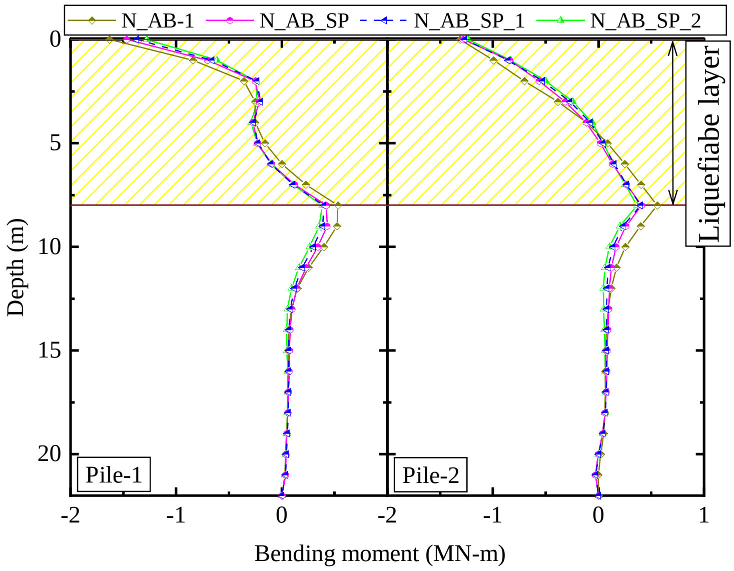

Fig. 5.31: A comparison of the bending moment profiles of the reinforced and the unreinforced cases at 81.4 s when the pile heads experience maximum bending moment.

The bending moment profiles of the abutment pile are compared between the reinforced and unreinforced cases, as shown in Fig. 5.31 at 81.4 s when the pile head experiences the maximum bending moment. The graph illustrates that the sheet pile can reduce the bending moment near the pile heads as well as near the interface of the loose and the dense layer. However, the increase in stiffness of the sheet pile does not have any remarkable change in the bending moment distribution and its magnitude. Usually, the efficiency of the sheet pile to mitigate lateral spreading largely depends on its embedment depth. The efficient embedment depth is a function of the stiffness of the sheet pile. The embedment depth needs to be increased to obtain better performance from a stiffer sheet pile. However, the embedment depth in these analyses is kept constant. Therefore, the effect of increased stiffness of the sheet pile in mitigating the bending moment of the abutment piles is not significant.

5.8 Performance of sheet pile with anchorage

The bending moment of the piles, especially near its head, is triggered by the combined action of the lateral spreading of the liquefied foundation, the channel-ward movement of the embankment and the inertia force of the abutment. The previous chapters describe that the sheet pile alone can reduce channel-ward movement of the ground up to 30 to 50%. The numerical results show that the sheet pile alone can reduce the pile bending moment up to 10% that is not so significant. In this circumstance, an anchored sheet pile can be used to achieve better performance. The numerical results in Chapter 4 show that the anchored sheet pile can reduce the lateral spreading up to 73%. Therefore, an anchored sheet pile is used in this analysis. A hollow steel pile is used here as an anchorage, as shown in Fig. 4.16. A 100 mm outer diameter steel hollow pile having the inner diameter 75 mm is used as an anchorage. The analysis conditions are listed in Table 4-5. It is to be mentioned here that the anchorage is modeled as an elastic beam element that is rigidly attached to the sheet pile at its upper end. The bottom end of the anchorage is installed 2 m deep into the dense ground where the nodes of the anchorage modeled as beam element are connected to the surrounding node of the soil element using a master and slave node technique.

The performance of the reinforcement measure is evaluated by its capability to reduce the bending moment of the piles and the channel-ward movement of the abutment. A comparison of the final horizontal displacement at the crest and the bottom of the abutment among the reinforced and unreinforced cases is shown in Fig. 4.17. The graph shows that the sheet pile reinforcement can reduce the channel-word movement of the abutment up to 23%. Whereas, the anchored sheet pile can reduce the horizontal movement of the abutment up to 50%. The results clearly show the anchored sheet pile exhibits better performance in reducing the channel-ward movement of the abutment.

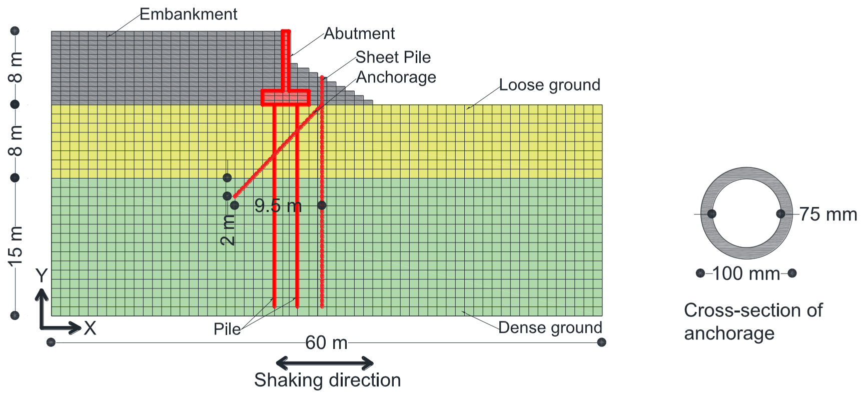

Fig. 5.32: Discretized mesh for the case of abutment reinforced with anchored sheet pile.

Table 5-8: Analysis conditions of anchored sheet pile.

Case ID	Thickness of liquefiable layer (m)	Existence of sheet pile	Description of the anchorage		
			Outer diameter (mm)	Inner diameter (mm)	Axial stiffness (N)
N_AB_SP_AN	8	yes	100	75	7.22×10^8

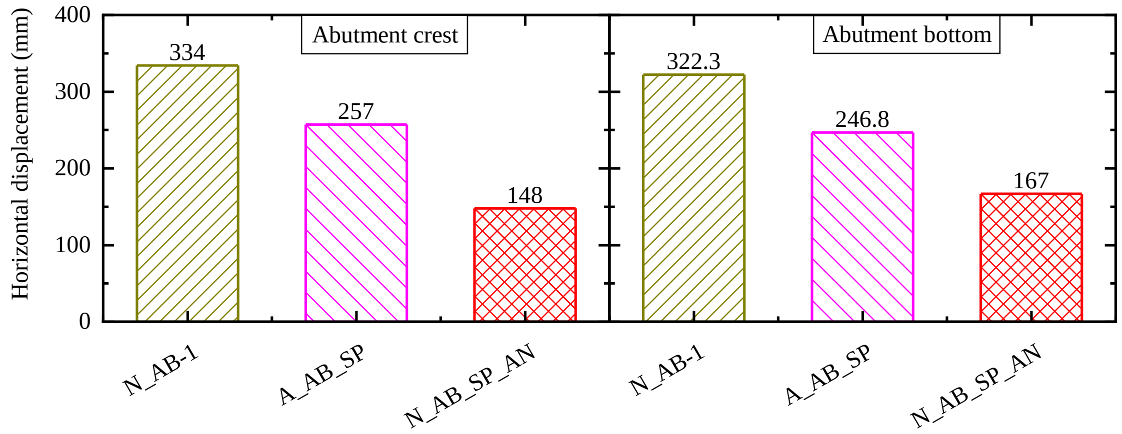

Fig. 5.33: Final horizontal displacements at the crest and the bottom of the abutment with different reinforcement measures.

A comparison of the maximum bending moment near the head of Pile-1 and Pile-2 with different reinforcement measures is shown in Fig. 4.18. The figure shows that sheet pile can reduce the maximum bending moment of Pile-1 up to 10%. Whereas, the anchored sheet pile can reduce the bending moment of the same pile up to 47%. The response is similar to Pile-2 as well. The sheet pile causes a minor reduction of the bending moment in Pile-2, whereas the anchored sheet pile can reduce the bending moment up to 32%. A plot of bending moment profiles of Pile-1 and Pile-2 when the piles experience the maximum bending moment with different reinforcement measures is shown in Fig. 5.35. The graph shows that the reinforcement measure effectively reduces the bending moment near the pile head as well as at the interface of the liquefiable and non-liquefiable soil.

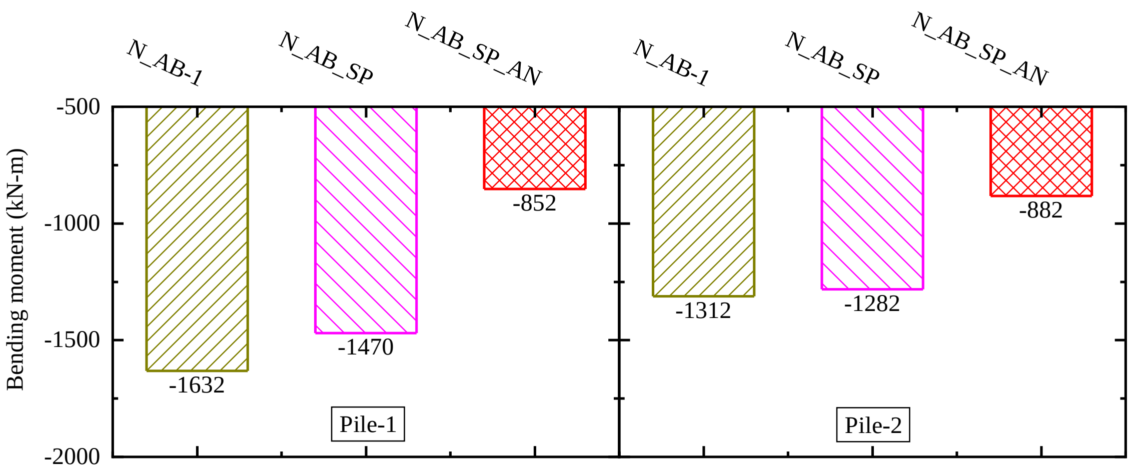

Fig. 5.34: Maximum bending moments of Pile-1 and Pile-2 with different reinforcement measures.

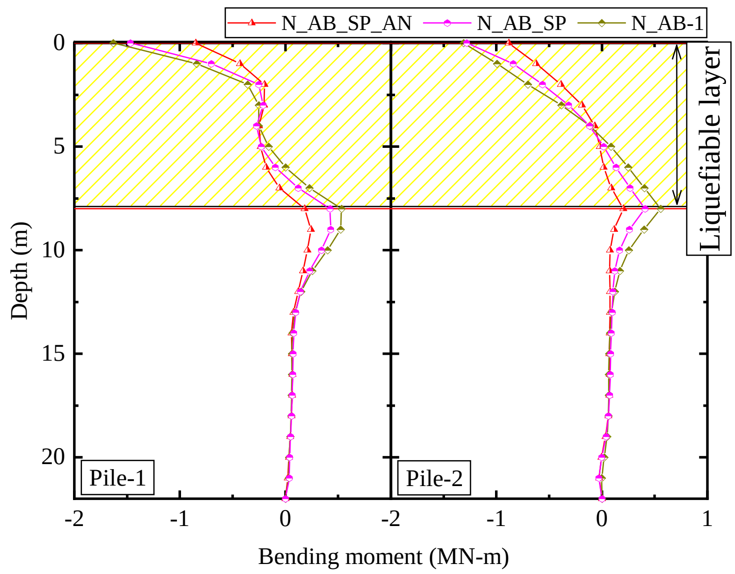

Fig. 5.35: A comparison of bending moment profiles of Pile-1 and Pile-2 when piles experience maximum bending moment with different reinforcement measures.

5.9 Summary

Two dynamic centrifuge experiments are conducted to investigate (1) the deformation pattern of the old piled abutment subjected to liquefaction-induced lateral spreading and (2) the performance of the sheet pile to mitigate the damage of the abutment piles due to lateral spreading. The experimental results are also compared with the cases without abutment having similar geometric configurations to study the pinning effect of the piled abutment against the lateral spreading of the ground. The centrifuge experiment is simulated by two-dimensional finite element analysis to observe the capability of the finite element model to reproduce the dynamic response of the bridge abutment. Several two-dimensional finite element analyses have been carried out to study the strut effect of the bridge girder to prevent the channel-ward movement of the abutment. The effect of the inertia force of the abutment is also studied here. Finally, the chapter describes the performance of the anchored sheet pile to reduce the bending moment of the pile as well as the channel-ward movement of the abutment.

The experimental results reveal that the piles experience the large bending moment around the pile head and the interface between the loose and dense layers due to the lateral spreading of the ground as expected. The sheet pile with sufficient embedment depth can reduce the channel-ward movement of the abutment up to 40% thus helps to minimize the bending stress on the supporting piles. The sheet pile is found effective in mitigating the channel-ward movement of the abutment under moderate to strong ground motion, thus mitigate the bending moment demand of the piles.

Since the old piled abutments are comparatively flexible, it exhibits minor pinning effect against the lateral spreading and consequently flows with the liquefied ground. The lateral spreading of the ground predominantly guides the maximum bending moment of the piles. Because of this, the bending moment is observed to increase with the increasing channel-ward movement of the embankment slope even after the principal shock. Therefore, simultaneous application of the inertia force using peak acceleration and the kinematic effect induced by the lateral spreading in the design calculation for piled abutment might yield a rather conservative result.

The numerical results, though there exists some anomaly with the experimental results in the unreinforced case, can capture the overall response of the piled abutment subjected to liquefaction-induced lateral spreading. The parametric study shows that the bridge abutment carries a considerable amount of lateral load from the backfill soil, thus reduce the bending moment near the pile head up to 57%. The contribution of the inertia force of the abutment to the maximum bending moment near the pile heads is nearly around 30%. Finally, the performance of the sheet pile can be improved with the installation of anchorage. The anchored sheet pile can reduce the horizontal displacement of the abutment up to 50% and the bending moment of the pile head up to 47%.

Chapter 6
Conclusions and recommendations

Liquefaction-induced lateral spreading has caused massive damage to the embankments and the water-front structures, for example, the bridge abutments in the previous earthquakes. The lateral spreading of the foundation ground is typically responsible for damage of the embankments and the structures near the water body. Extensive research has been conducted to find out a viable solution to treat the liquefaction-induced lateral spreading. The remedial measures are broadly classified into two types, i.e., ground improvement and ground reinforcement. Ground improvement technique is found effective in the laboratory experiments as well as in the previous earthquakes. However, ground improvement techniques are challenging to implement in the existing structures. Therefore, the reinforcement technique is considered in this study.

This study focuses on the seismic retrofitting technique for the existing bridge abutment designed according to the old Japanese standard for highway bridges without considering the effects. The installation of sheet pile is considered as the potential remedial measure against lateral spreading because of its handiness to implement in the existing structures. The dynamic centrifuge experiment, as well as the finite element analysis, is used in this study to observe the seismic response of the bridge abutment and the approach embankment of a river spanning bridge. The factors that may affect the performance of the sheet pile, for example, the thickness of liquefiable foundation ground and embedment depth of sheet pile are emphasized here. This study provides a guideline about the thickness of the liquefiable foundation, where the sheet pile can be effectively used. The effect of the sheet pile width to reduce the seismic damages of a target area is also described in this study. This study also shows how the anchorage improves the efficiency of the sheet pile to reduce the damage associated with lateral spreading.

6.1 Conclusions

Chapter 2: Seismic response of the piled abutment subjected to liquefaction-induced lateral spreading

A fully-coupled three-dimensional finite element analysis is used in this chapter to observe the seismic response of piled abutment resting on the liquefiable ground. A large-scale shake table test of a model abutment designed based on the current Japanese standard is simulated. Two model abutments designed based on the old Japanese standard with the different geometrical shapes of the embankment are also analyzed to observe the strut effect of bridge girder and the influence of the width of the embankment on the failure mechanism of the bridge abutment. Besides, the two-dimensional finite element analysis is used here to simulate a shake table test to observe the performance of sheet pile as a seismic retrofit. The embankment and the liquefiable foundation layer in all the experimental cases are made of loose sand. The numerical results show that the accumulation of displacement of both soil and abutment starts with the generation of excess pore water pressure. The liquefaction of the foundation soil triggers a significant permanent displacement of soil and as well as a structural system towards the channel. Consequently, the abutment pile near its head experiences an excessive bending moment in all types of model abutment. The existence of a bridge girder prevents the channel-ward movement of the abutment crest that causes a backward rotation of the abutment. The bending moment of the piles can be reduced by limiting the width of the approach road. Besides, the installation of a fixed end sheet pile can also reduce the bending moment to some extent in a 10 m thick liquefiable foundation. Although the performance of sheet pile in 10 m thick liquefiable layer is not up to the mark. It urges further study to find out the geometric condition where the sheet pile can be effectively used.

Chapter 3: Performance of sheet pile to mitigate liquefaction-induced lateral spreading of loose soil layer under the embankment

This chapter describes the thickness of a liquefiable foundation where the sheet pile can be effectively used to mitigate lateral spreading. A series of dynamic centrifuge tests were performed. The capability of sheet pile to mitigate lateral spreading was investigated for both thin (4 m) and thick (8 m) liquefiable foundations under the 8 m high embankment. Besides, the effect of the sheet pile width on its performance as a seismic retrofit is also investigated. Centrifuge test results recommend that the installation of sheet pile can effectively mitigate the liquefaction-induced lateral spreading during the moderate to strong ground motions and equally effective in various thickness of liquefiable foundation ranging from 4 m to 8 m. The sheet pile was observed to reduce the channel-ward ground movement up to 30 to 50% at its closer vicinity. The extension of the width of sheet pile beyond the target area doesn't have any additional advantage. The performance of limited width (5 m) sheet pile in terms of mitigating lateral spreading was found similar to that of the full-width sheet piles. The dense layer immediately below the loose layer is observed to liquefy. The liquefaction of the dense layer is observed to have a significant influence on the overall response of the sheet pile.

Chapter 4: Effect of thickness of liquefiable layer and embedment depth on the performance of sheet pile as a seismic retrofit.

The thickness of the liquefiable foundation and the corresponding embedment depth significantly affect the performance of the sheet pile. Two-dimensional finite element analysis is used here to observe the effect of thickness of the liquefiable layer and the embedment depth of sheet pile. The numerical model is first validated with the experimental results for further parametric study. The numerical results come up with the conclusion that the sheet pile installed in a thick liquefiable layer (nearly 10 m) has less efficiency to mitigate lateral spreading probably because of the excessive rotation. Long embedment depth is required to mitigate rotational displacement in the thick liquefiable foundations. It may make the use of sheet pile uneconomic in a thick liquefiable layer. It is also found that the maximum efficiency of the sheet pile in mitigating lateral spreading can be achieved with an embedment depth $4/\beta$ for the bearing stratum having the average SPT (N) value of 37. The softening of the bearing stratum due to the generation of excess pore water pressure increases the embedment depth. Moreover, a properly designed anchorage pile attached to the sheet pile can significantly reduce the channel-ward movement of the ground, which is about 73% near the sheet pile.

Chapter 5: Performance of sheet pile as a seismic retrofit for piled abutment subjected to lateral spreading

The efficiency of the sheet pile to mitigate the lateral spreading of the foundation soil under an embankment is described in the previous two chapters. This chapter focuses on the performance of the sheet pile to reduce the damage of the piled abutment subjected to lateral spreading. Two dynamic centrifuge experiments and several two-dimensional finite element analyses are carried out. The half-width of an abutment designed according to the old design standard is modeled in the centrifuge experiment. The piled abutment passes through an 8 m thick liquefiable layer. The experimental and numerical results show the fact that the pile head and the interface of the liquefiable and non-liquefiable layer are found vulnerable to be damaged during an earthquake. Those locations are observed to experience large bending moment. The old piled abutment where the piles are mostly slender is observed to have a minor pinning effect on the lateral spreading in the centrifuge experiment. Therefore, the sheet pile mostly controls the channel-ward movement of the liquefied soil. The installation of sheet pile can reduce the channel-ward movement of the abutment up to 40% where there is no influence of bridge girder, thus reduces the bending moment near the pile head. Numerical results show the contribution of the inertia force of the abutment is about 30% of the total bending moment near the pile head. Besides, the existence of the bridge girder has a positive effect on reducing the bending moment of piles. The bridge girder reduces the bending moment (nearly 57%) of the pile by sharing a considerable amount of lateral load from the backfill soil. However, the collision between the abutment and the girder may cause damage to the abutment. It may cause the unseating of the bridge girder. The performance of the sheet pile can be improved with the installation of anchorage. The anchored sheet pile can reduce the horizontal displacement of the abutment up to 50% and the bending moment of the pile head up to 47% according to the numerical results.

The experimental and numerical results consolidated the fact that the sheet pile itself or combined with the appropriate anchorage, provides considerable remediation against liquefaction-induced lateral spreading. The dynamic responses of the ground and the structures are affected by their physical and geometrical properties. Therefore, the quantitative value obtained in this analysis might vary with the properties and the geometry of the ground and the structures. However, the results obtained in this study provide an insight into the performance of sheet pile as a seismic retrofit.

6.2 Recommendations

The sheet pile having sufficient embedment depth is found effective in this study to mitigate the lateral spreading of the soil under the embankment. All the observation in this study is made on a very uniform layered soil. The natural soil profile is more complex, having localized non-uniformity. The existence of a less impermeable soil immediately above the liquefiable layer resting on a gently slope ground may make the scenario more catastrophic. Further research is recommended to justify the applicability of sheet pile at that extreme geometric configuration of the foundation ground. The embankment in this study is made of loose soil to avoid unexpected densification of the loose foundation layer. However, the embankment in practice is compacted up to some desired density. The seismic response of the compacted embankment on the liquefiable layer might differ from the observation found in this study that can be a scope of future research. The installation of the driven pile or the sheet pile densifies the surrounding ground that may improve the seismic performance of the structures. The soil densification due to pile driving is not taken into consideration in this study. Finally, the anchored sheet pile recommended in this study as an effective seismic retrofit. A further experimental study is required to provide a proper guideline regarding the design of the anchored sheet pile.

References

Abdoun, T., Dobry, R., O'Rourke, T. D., & Goh, S. H. (2003). Pile response to lateral spreads: Centrifuge modeling. *Journal of Geotechnical and Geoenvironmental Engineering*, *129*(10), 869–878. http://doi.org/10.1061/(ASCE)1090-0241(2003)129:10(869)

Adalier, K., & Aydingun, O. (2003). Numerical analysis of seismically induced liquefaction in earth embankment foundations. Part II. Application of remedial measures. *Canadian Geotechnical Journal*, *40*(4), 766–779. http://doi.org/10.1139/t03-026

Adalier, K., & Elgamal, A. (2004). Mitigation of liquefaction and associated ground deformations by stone columns. *Engineering Geology*, *72*(3–4), 275–291. http://doi.org/10.1016/j.enggeo.2003.11.001

Adalier, K., Elgamal, A. W., & Martin, G. R. (1998). Foundation liquefaction countermeasures for earth embankments. *Journal of Geotechnical and Geoenvironmental Engineering*, *124*(6), 500–517. http://doi.org/10.1061/(ASCE)1090-0241(1998)124:6(500)

Adalier, K., Pamuk, A., & Zimmie, T. F. (2004). Earthquake retrofit of highway/railway embankments by sheet-pile walls. *Geotechnical and Geological Engineering*, *22*(1), 73–88. http://doi.org/10.1023/B:GEGE.0000014000.27895.5d

Adamidis, O., & Madabhushi, G. S. P. (2015). Use of viscous pore fluids in dynamic centrifuge modelling. *International Journal of Physical Modelling in Geotechnics*, *15*(3), 141–149. http://doi.org/10.1680/ijpmg.14.00022

Amiri, S. K. (2008). The earthquake response of bridge pile foundations to liquefaction induced lateral spread displacement demands. *Doctoral Dissertation, University of Southern California*.

Antoniou, S., & Pinho, R. (2016). SeismoSignal. Seismosoft srl.

Arias, A. (1970). A measure of earthquake intensity. In *Seismic Design for Nuclear Power Plants* (pp. 438–483). MIT Press.

Armstrong, R. J., Boulanger, R. W., & Beaty, M. H. (2013). Liquefaction effects on piled bridge abutments: Centrifuge tests and numerical analyses. *Journal of Geotechnical and Geoenvironmental Engineering*, *139*(3), 433–443. http://doi.org/10.1061/(ASCE)GT.1943-5606.0000780

Asaoka, A., Toshihiro, N., Eiji, Y., Kazuhiro, K., & Masaki, N. (2002). An elasto-plastic description of two distinct volume change mechanisms of soils. *Soils and Foundations*, *42*(5), 47–57. http://doi.org/10.3208/sandf.42.5_47

Asgari, A., Oliaei, M., & Bagheri, M. (2013). Numerical simulation of improvement of a liquefiable soil layer using stone column and pile-pinning techniques. *Soil Dynamics and Earthquake Engineering*, *51*, 77–96. http://doi.org/10.1016/j.soildyn.2013.04.006

Aydingun, O., & Adalier, K. (2003a). Numerical analysis of seismically induced liquefaction in earth embankment foundations. Part I. Benchmark model. *Canadian Geotechnical Journal*, *40*(4), 753–765. http://doi.org/10.1139/t03-025

Aydingun, O., & Adalier, K. (2003b). Numerical analysis of seismically induced liquefaction in earth embankment foundations. Part I. Benchmark model. *Canadian Geotechnical Journal*, *40*(4), 753–765. http://doi.org/10.1139/t03-025

Bartlett, S. F. (2014). Liquefaction-induced ground failure and bridge damage to the alaskan railroad and highway in South Central Alaska during the 1964 Alaskan Earthquake. In *Proceedings of the 10th National Conference on Earthquake Engineering, Anchorage, AK*. Earthquake Engineering Research Institute.

Bartlett, S. F., & Youd, T. L. (1992). *Case histories of lateral spreads caused by the 1964 Alaska earthquake*. in Case Studies of Liquefaction and Lifeline Performance During Past Earthquakes: U.S. National Center for Earthquake Engineering Research Technical Report NCEER-92-0002, v. 2.

Berrill, J. B., Christensen, S. A., Keenan, R. P., Okada, W., & Pettinga, J. R. (2001). Case study of lateral spreading forces on a piled foundation. *Geotechnique*, *51*(6), 501–517. http://doi.org/10.1680/geot.2001.51.6.501

Bhatnagar, S., Kumari, S., & Sawant, V. A. (2016). Numerical analysis of earth embankment resting on liquefiable soil and remedial measures. *International Journal of Geomechanics*, *16*(1). http://doi.org/10.1061/(ASCE)GM.1943-5622.0000501

Bhattacharya, S., Madabhushi, S. P. G., & Bolton, M. D. (2004). An alternative mechanism of pile failure in liquefiable deposits during earthquakes. *Géotechnique*, *54*(3), 203–213. http://doi.org/10.1680/geot.2004.54.3.203

Boulanger, R. W., Khosravi, M., Khosravi, A., & Wilson, D. W. (2018). Remediation of liquefaction effects for an embankment using soil-cement walls: Centrifuge and numerical modeling. *Soil Dynamics and Earthquake Engineering*, *114*, 38–50. http://doi.org/10.1016/j.soildyn.2018.07.001

Bowles, J. E. (1996). *Foundation analysis and design* (5th ed.). McGraw-Hill.

Brandenberg, S. J., Asce, a M., Boulanger, R. W., Asce, M., Kutter, B. L., Chang, D., & Asce, S. M. (2005). Behavior of pile foundations in laterally spreading ground during centrifuge tests. *Journal of Geotechnical and Geoenvironmental Engineering*, *131(11)*, 1378–1391. http://doi.org/10.1061/(ASCE)1090-0241(2005)131:11(1378)

Brandenberg, S. J., Wilson, D. W., & Rashid, M. M. (2010). Weighted Residual Numerical Differentiation Algorithm Applied to Experimental Bending Moment Data. *Journal of Geotechnical and Geoenvironmental Engineering*, *136*(6), 854–863. http://doi.org/10.1061/(asce)gt.1943-5606.0000277

Chang, D., Boulanger, R., Brandenberg, S., & Kutter, B. (2014). FEM analysis of dynamic soil-pile-structure interaction in liquefied and laterally spreading ground. *Earthquake Spectra*, *29*(3), 733–755. http://doi.org/10.1193/1.4000156

Chopra, A. K. (2012). *Dynamics of Structures: Theory and Applications to Earthquake Engineering* (Fourth). Pearson Education.

Conlee, C. T., Gallagher, P. M., Boulanger, R. W., & Kamai, R. (2012). Centrifuge modeling for liquefaction mitigation using colloidal silica stabilizer. *Journal of Geotechnical and Geoenvironmental Engineering*, *138*(11), 1334–1345. http://doi.org/10.1061/(ASCE)GT.1943-5606.0000703

Elgamal, A. W., Zeghal, M., Taboada, V., & Dobry, R. (1996). Analysis of Site Liquefaction and Lateral Spreading Using Centrifuge Testing Records. *Soils and Foundations*, *36*(2), 111–121. http://doi.org/10.3208/sandf.36.2_111

Finn, W. D. L., & Fujita, N. (2002). Piles in liquefiable soils: seismic analysis and design issues. *Soil Dynamics and Earthquake Engineering*, *22*(9–12), 731–742. http://doi.org/10.1016/S0267-7261(02)00094-5

Gallagher, P. M., Conlee, C. T., & Rollins, K. M. (2007). Full-scale field testing of colloidal silica grouting for mitigation of liquefaction risk. *Journal of Geotechnical and Geoenvironmental Engineering*, *133*(2), 186–196. http://doi.org/10.1061/(ASCE)1090-0241(2007)133:2(186)

Haeri, S. M., Kavand, A., Rahmani, I., & Torabi, H. (2012). Response of a group of piles to liquefaction-induced lateral spreading by large scale shake table testing. *Soil Dynamics and Earthquake Engineering*, *38*, 25–45. http://doi.org/10.1016/j.soildyn.2012.02.002

Hamada, M. (2000). Performances of foundations against liquefaction-induced permanent ground displacements. In *Proceedings of the 12th World Conference on earthquake engineering, Auckland, New Zealand, paper (no 1754)*.

Hamada, M., & O'Rourke, T. D. (1992). Case studies of liquefaction and lifeline performance during past earthquakes, Vol. 1 Japanese case studies. *National Center for Earthquake Engineering Research, Technical Report*.

Hamada, M., Yasuda, S., Isoyama, R., & Emoto, K. (1986). Study on liquefaction-induced permanent ground displacements and earthquake damage. In *Proc. of JSCE Vol. 376* (pp. 221–229).

Hansen, W. R., Eckel, E. B., Schaem, W. E., Lyle, R. E., George, W., & Chance, G. (1966). *The Alaska earthquake, March 27, 1964: field investigations and reconstruction effort*. *USGS Professional Paper 541*. USGS Professional Paper 541, Government Printing Office, Washington, D.C.

Haskell, J. J. M., Madabhushi, S. P. G., Cubrinovski, M., & Winkley, A. (2013). Lateral spreading-induced abutment rotation in the 2011 Christchurch earthquake: Observations and analysis. *Geotechnique*, *63*(15), 1310–1327. http://doi.org/10.1680/geot.12.P.174

Iai, S., Tobita, T., & Nakahara, T. (2005). Generalised scaling relations for dynamic centrifuge tests. *Geotechnique*, *55*(5), 355–362. http://doi.org/10.1680/geot.2005.55.5.355

Idriss, I. M., & Boulanger, R. W. (2003). Estimating Kα for use in evaluating cyclic resistance of sloping ground. In *The 8th US–Japan Workshop on Earthquake Resistant Design of Lifeline Facilities and Countermeasures against Liquefaction* (pp. 449–468).

Ishihara, K., Kawase, Y., & Nakajima, M. (1980). Liquefaction Characteristics of Sand Deposits at an Oil Tank Site During The 1978 Miyagiken-Oki Earthquake. *Soils and Foundations*, *20*(2), 97–111. http://doi.org/10.3208/sandf1972.20.2_97

Japan Road Association. (1964). Design guideline of substructures for highway bridges (Design of pile foundations).

Japan Road Association. (2002). Specifications for highway bridges-Part V seismic design, Tokyo, Japan.

Japan Road Association. (2014). Specifications for highway bridges-Part V seismic design, Tokyo, Japan.

Kachadoorian, R. (1968). *Effects of the earthquake of March 27, 1964, on the Alaska Highway System*. US Government Printing Office.

Kavand, A., Haeri, S. M., Asefzadeh, A., Rahmani, I., Ghalandarzadeh, A., & Bakhshi, A. (2014). Study of the behavior of pile groups during lateral spreading in medium dense sands by large scale shake table test. *International Journal of Civil Engineering*, *12*(3), 374–391.

Kawashima, K., & Buckle, I. (2013). Structural performance of bridges in the Tohoku-Oki Earthquake. *Earthquake Spectra*, *29*(S1), S315–S338. http://doi.org/10.1193/1.4000129

Keenan, R. P. (1996). Foundation loads due to lateral spreading at the Landing Road Bridge, Whakatane. *Master of Engineering Thesis, University of Canterbury, Christchurch, New Zealand*.

Knappett, J. A., Mohammadi, S., & Griffin, C. (2010). Lateral spreading forces on bridge piers and pile caps in laterally spreading soil: Effect of angle of incidence. *Journal of Geotechnical and Geoenvironmental Engineering*, *136*(12), 1589–1599. http://doi.org/10.1061/(ASCE)GT.1943-5606.0000387

Kogai, Y., Towhata, I., Amimoto, K., & Putra, H. G. (2000). Use of embedded walls for mitigation of liquefaction-induced displacement in slopes and embankments. *Soils and Foundations*, *40*(4), 75–93. http://doi.org/10.3208/sandf.40.4_75

Kokusho, T. (1999). Water film in liquefied sand and its effect on lateral spread. *Journal of Geotechnical and Geoenvironmental Engineering*, *125*(10), 817–826. http://doi.org/10.1061/(ASCE)1090-0241(1999)125:10(817)

Kramer, S. L. (1996). *Geotechnical Earthquake Engineering*. *Engineering* (Vol. 6). Pearson Education India. http://doi.org/10.1007/978-3-540-35783-4

Li, G., & Motamed, R. (2017). Finite element modeling of soil-pile response subjected to liquefaction-induced lateral spreading in a large-scale shake table experiment. *Soil Dynamics and Earthquake Engineering*, *92*, 573–584. http://doi.org/10.1016/j.soildyn.2016.11.001

Liu, L., & Dobry, R. (1997). Seismic response of shallow foundation on liquefiable sand. *Journal of Geotechnical Engineering*, *123*(6), 557–566. http://doi.org/10.1061/(asce)1090-0241(1997)123:6(557)

Maharjan, M., & Takahashi, A. (2014). Liquefaction-induced deformation of earthen embankments on non-homogeneous soil deposits under sequential ground motions. *Soil Dynamics and Earthquake Engineering*, *66*, 113–124. http://doi.org/10.1016/j.soildyn.2014.06.024

Matsuo, O. (1996). Damage to river dikes. *Soils and Foundations*, *36*(Special), 235–240. http://doi.org/10.3208/sandf.36.Special_235

McCulloch, D. S., & Bonilla, M. G. (1970). *Effects of the earthquake of March 27, 1964, on the Alaska Railroad*. US Government Printing Office.

Mizutani, T., & Towhata, I. (2001). Model tests on mitigation of liquefaction-induced subsidence of dike by using embedded sheet-pile walls. In *International Conferences on Recent Advances in Geotechnical Earthquake Engineering and Soil Dynamics. 17*. San Diego, California: University of Missouri--Rolla.

Mohanty, P., & Bhattacharya, S. (2019). Case Studies of Liquefaction-Induced Damages to Two Pile-Supported River Bridges in China. *Journal of Performance of Constructed Facilities*, *33*(5). http://doi.org/10.1061/(ASCE)CF.1943-5509.0001306

Motamed, R., & Towhata, I. (2010). Mitigation measures for pile groups behind quay walls subjected to lateral flow of liquefied soil: Shake table model tests. *Soil Dynamics and Earthquake Engineering*, *30*(10), 1043–1060. http://doi.org/10.1016/j.soildyn.2010.04.016

Motamed, R., Towhata, I., Honda, T., Tabata, K., & Abe, A. (2013). Pile group response to liquefaction-induced lateral spreading: E-Defense large shake table test. *Soil Dynamics and Earthquake Engineering*, *51*, 35–46. http://doi.org/10.1016/j.soildyn.2013.04.007

Motohashi, Y., Yasuhara, K., Komine, H., & Murakami, S. (2011). Mitigation of existing structure settlement by sheet pile walls when liquefaction. In *Geotechnical Special Publication* (pp. 1815–1820). http://doi.org/10.1061/41165(397)185

Mukunoki, T., Kasama, K., Murakami, S., Ikemi, H., Ishikura, R., Fujikawa, T., … Kitazono, Y. (2016). Reconnaissance report on geotechnical damage caused by an earthquake with JMA seismic intensity 7 twice in 28 h, Kumamoto, Japan. *Soils and Foundations*, *56*(6), 947–964. http://doi.org/10.1016/j.sandf.2016.11.001

National Research Council. (1985). *Liquefaction of Soils During Earthquakes,*. National Academy Press, Washington D. C.

National Research Council (US). Committee on the Alaska Earthquake. (1972). *The great Alaska earthquake of 1964. Vol. 5*. National Academies.

Oka, F., Tsai, P., Kimoto, S., & Kato, R. (2012). Damage patterns of river embankments due to the 2011 off the Pacific Coast of Tohoku Earthquake and a numerical modeling of the deformation of river embankments with a clayey subsoil layer. *Soils and Foundations, 52*(5), 890–909. http://doi.org/10.1016/j.sandf.2012.11.010

Okamura, M., & Matsuo, O. (2002). Effects of remedial measures for mitigating embankment settlement due to foundation liquefaction. *International Journal of Physical Modelling in Geotechnics, 2*(2), 01–12. http://doi.org/10.1680/ijpmg.2002.020201

Okamura, M., & Tamura, K. (2004). Prediction method for liquefaction-induced settlement of embankment with remedial measure by deep mixing method. *Soils and Foundations*, *44*(4), 53–65. http://doi.org/10.3208/sandf.44.4_53

Pamuk, A., Gallagher, P. M., & Zimmie, T. F. (2007). Remediation of piled foundations against lateral spreading by passive site stabilization technique. *Soil Dynamics and Earthquake Engineering*, *27*(9), 864–874. http://doi.org/10.1016/j.soildyn.2007.01.011

PWRI. (2016). *Design manual of sheet piling as a countermeasure against liquefaction-induced river dike failure*. Public Works Research Institute, Ministry of Construction, Japan.

Rasouli, R., Towhata, I., & Rattez, H. (2017). Shaking Table Model Tests on Mitigation of Liquefaction-Induced Distortion of Shallow Foundation. In *Geotechnical Hazards from Large Earthquakes and Heavy Rainfalls* (pp. 463–477). http://doi.org/10.1007/978-4-431-56205-4_43

Saha, P., Horikoshi, K., & Takahashi, A. (2018). 3D Numerical simulation of old pile-supported bridge abutment subjected to lateral spreading. In *53rd Japan National Conference on Geotechnical Engineering, Paper ID: 930*.

Saha, P., Horikoshi, K., & Takahashi, A. (2019). Effectiveness of sheet pile as a seismic retrofit for piled abutment subjected to liquefaction-induced lateral spreading. In *Earthquake Geotechnical Engineering for Protection and Development of Environment and Constructions- Proceedings of the 7th International Conference on Earthquake Geotechnical Engineering* (pp. 4784–4791).

Saha, P., & Takahashi, A. (2017). Seismic performance of pile-supported bridge abutment resting on a liquefiable soil layer. In *3rd International Conference on Performance-based Design in*

Earthquake Geotechnical Engineering, Paper ID: 504.

Sasaki, Y., Towhata, I., Miyamoto, K., Shirato, M., Narita, A., Sasaki, T., & Sako, S. (2012). Reconnaissance report on damage in and around river levees caused by the 2011 off the Pacific coast of Tohoku Earthquake. *Soils and Foundations*, *52*(5), 1016–1032. http://doi.org/10.1016/j.sandf.2012.11.018

Shibata, T., Oka, F., & Ozawa, Y. (1996). Characteristics of ground deformation due to liquefaction. *Soils and Foundations*, (Special Issue), 65–79.

Su, L., Tang, L., Ling, X., Liu, C., & Zhang, X. (2016). Pile response to liquefaction-induced lateral spreading: A shake-table investigation. *Soil Dynamics and Earthquake Engineering*, *82*, 196–204. http://doi.org/10.1016/j.soildyn.2015.12.013

Takahashi, A. (2002). Soil – pile interaction in liquefaction-induced lateral spreading of soils. *DEng. Dissertation, Tokyo Institute of Technology*.

Takahashi, A., Sugita, H., & Tanimoto, S. (2007). Centrifuge model tests on abutments of river-crossing bridge on liquefiable soils. In *4th International Conference on Earthquake Geotechnical Engineering, Paper ID :1618*.

Takahashi, A., Sugita, H., & Tanimoto, S. (2010). Forces acting on bridge abutments over liquefied ground. *Soil Dynamics and Earthquake Engineering*, *30*(3), 146–156. http://doi.org/10.1016/j.soildyn.2009.10.007

Takemura, J., Kondoh, M., Esaki, T., Kouda, M., & Kusakabe, O. (1999). Centrifuge model tests on double propped wall excavation in soft clay. *Soils and Foundations*, *39*(3), 75–87. http://doi.org/10.3208/sandf.39.3_75

Tanaka, H., Kita, H., Iida, T., & Saimura, Y. (1996). Countermeasure for liquefaction using steel sheet pile with drain capability. In *11th World Conference on Earthquake Engineering, Paper No. 1052*. Acapulco, Mexico: Elsevier Science.

Tanaka, H., Murata, H., Kita, H., & Okamoto, M. (2000). Study on sheet pile wall method as a remediation against liquefaction. In *12th world conference on earthquake engineering. Paper No. 535*. New Zealand.

Tokimatsu, K., & Asaka, Y. (1998). Effects of liquefaction-induced ground displacements on pile performance in the 1995 Hyogoken-Nambu earthquake. *Soils and Foundations*, *38*(Special), 163–177. http://doi.org/10.3208/sandf.38.special_163

Tokimatsu, K., Mizuno, H., & Kakurai, M. (1996). Building damage associated with geotechnical problems. *Soils and Foundations*, (Special), 219–234. http://doi.org/10.3208/sandf.36.special_219

Travasarou, T., Bray, J. D., & Abrahamson, N. A. (2003). Empirical attenuation relationship for Arias Intensity. *Earthquake Engineering and Structural Dynamics*, *32*(7), 1133–1155. http://doi.org/10.1002/eqe.270

Waldin, J., Jennings, J., & Routledge, P. (2012). Critically damaged bridges & concepts for earthquake recovery. In *Proceedings of the New Zealand Society for Earthquake Engineering annual conference* (pp. 1–8).

Watanabe, T. (1966). Damage to oil refinery plants and a building on compacted ground by the niigata earthquake and their restoration. *Soils and Foundations*, *6*(2), 86–99. http://doi.org/10.3208/sandf1960.6.2_86

White, D. J., & Take, W. a. (2002). GeoPIV: Particle Image Velocimetry (PIV) software for use in geotechnical testing. *Cambridge University Engineering Department Technical Report*.

Wood, D. M. (2004). *Geotechnical modelling* (Vol. 1). Taylor & Francis.

Yakut, A., & Ylmaz, H. (2008). Correlation of deformation demands with ground motion intensity. *Journal of Structural Engineering*, *134*(12), 1818–1828. http://doi.org/10.1061/(ASCE)0733-9445(2008)134:12(1818)

Yasuda, S., Harada, K., Ishikawa, K., & Kanemaru, Y. (2012). Characteristics of liquefaction in Tokyo Bay area by the 2011 Great East Japan Earthquake. *Soils and Foundations*, *52*(5), 793–810. http://doi.org/10.1016/j.sandf.2012.11.004

Yasuda, S., Ishihara, K., Morimoto, I., Orense, R., Ikeda, M., & Tamura, S. (2000). Large-scale shaking table tests on pile foundations in liquefied ground. *12th World Conference on Earthquake Engineering*, Paper No. 1474.

Yasuda, S., & Ishikawa, K. (2018). Appropriate measures to prevent the liquefaction-induced inclination of existing houses. *Soil Dynamics and Earthquake Engineering*, *115*, 652–662. http://doi.org/10.1016/j.soildyn.2018.07.019

Yegian, M. K., Ghahraman, V. G., & Harutiunyan, R. N. (1994). Liquefaction and embankment failure case histories, 1988 armenia earthquake. *Journal of Geotechnical Engineering*, *120*(3), 581–596. http://doi.org/10.1061/(ASCE)0733-9410(1994)120:3(581)

Yoshimi, Y., Keizo, T., & Tokimatsu, K. (1989). Liquefaction resistance of a partially saturated sand. *Soils and Foundations*, *29*(3), 157–162.

Youd, T. L. (1993). Liquefaction-induced damage to bridges. *Transportation Research Record*.

Zekri, A., Ghalandarzadeh, A., Ghasemi, P., & Aminfar, M. H. (2015). Experimental study of remediation measures of anchored sheet pile quay walls using soil compaction. *Ocean Engineering*, *93*, 45–63. http://doi.org/10.1016/j.oceaneng.2014.11.002

Zeng, X., & Liu, G. (2012). Liquefaction of dense sand under earthquake loading. In *Geotechnical Special Publication* (pp. 1670–1679). http://doi.org/10.1061/9780784412121.172